CHEMICAL REVIEWS

Review

Cite This: *Chem. Rev.* XXXX, XXX, XXX−XXX

pubs.acs.org/CR

Alkaline Anion-Exchange Membrane Fuel Cells: Challenges in Electrocatalysis and Interfacial Charge Transfer

Nagappan Ramaswamy[†] and Sanjeev Mukerjee*

Northeastern University Center for Renewable Energy Technology, Department of Chemistry and Chemical Biology, Northeastern University, 317 Egan Research Center, 360 Huntington Avenue, Boston, Massachusetts 02115, United States

ABSTRACT: Alkaline anion-exchange membrane (AAEM) fuel cells have attracted significant interest in the past decade, thanks to the recent developments in hydroxide-anion conductive membranes. In this article, we compare the performance of current state of the art AAEM fuel cells to proton-exchange membrane (PEM) fuel cells and elucidate the sources of various overpotentials. While the continued development of highly conductive and thermally stable anion-exchange membranes is unambiguously a principal requirement, we attempt to put the focus on the challenges in electrocatalysis and interfacial charge transfer at an alkaline electrode/electrolyte interface. Specifically, a critical analysis presented here details the (i) fundamental causes for higher overpotential in hydrogen oxidation reaction, (ii) mechanistic aspects of oxygen reduction reaction, (iii) carbonate anion poisoning, (iv) unique challenges arising from the specific adsorption of alkaline ionomer cation-exchange head groups on electrocatalysts surfaces, and (v) the potential of alternative small molecule fuel oxidation. This review and analysis encompasses both the precious and nonprecious group metal based electrocatalysts from the perspective of various interfacial charge-transfer phenomena and reaction mechanisms. Finally, a research roadmap for further improvement in AAEM fuel cell performance is delineated here within the purview of electrocatalysis and interfacial charge transfer.

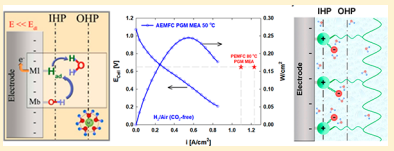

CONTENTS

1. Introduction A
2. Current Status of AAEM Fuel Cell Performance D
   2.1. PEM vs AEM Electrolyte Bulk Properties F
   2.2. General Context of Alkaline Electrocatalytic Interfaces H
3. Hydrogen Oxidation Reaction in Alkaline Media H
4. Oxygen Reduction Reaction in Alkaline Electrolyte N
   4.1. Nature of the First Electron Transfer Step to O_2 N
   4.2. Base Catalysis of the Hydrogen Peroxide Intermediate P
5. Effect of Carbonate Poisoning of Alkaline Membranes on Fuel Cell Performance U
6. Effect of Ammonium Cation Poisoning on Interfacial Charge Transfer W
7. Alternate Small Molecule Oxidation X
8. Conclusions Y
Author Information Z
   Corresponding Author Z
   ORCID Z
   Present Address Z
   Funding Z
   Notes Z
   Biographies Z
References Z

1. INTRODUCTION

Proton-exchange membrane (PEM) fuel cell performance has witnessed enormous progress due to decades of developmental research in electrocatalysts, perfluorinated sulfonic acid (PFSA), membrane electrolytes and interfacial ionomer solutions, as well as effective integration of these individual components to fabricate a membrane electrode assembly (MEA).[1,2] State of the art PEM fuel cell performance operating on H_2/air gas feeds using high surface area carbon-supported Pt/Pt-alloy-based catalysts yield power densities ranging roughly 900 to 1000 mW/cm^2_{MEA} at cell voltages ≥ 0.65 V (80 °C, 100% RH, 150 kPaa outlet pressure).[2−4] This is typically achieved with total MEA precious metal loading of 0.20 to 0.25 mg_{pgm}/cm^2 leading to platinum specific power density values of roughly 0.20 to 0.25 g_{Pt}/kW or alternately 4 to 5 kW/g_{Pt}. Recent studies using PtCoMn/PtNi nanostructured thin film (NSTF) cathode catalysts of total MEA loading 0.15 to 0.25 mg_{PGM}/cm^2 have enabled power densities of 800 mW/cm^2_{MEA} at cell voltages ≥ 0.65 V leading to Pt-specific power densities of roughly 0.3 g_{Pt}/kW or alternately 3.3 kW/g_{Pt}.[3,5] While this represents a tremendous progress in performance achieved via both decrease in mass transport induced voltage losses and increase in Pt/Pt-alloy catalyst activity,[2] the sustainable use of PEM fuel cell technology in large-scale applications still demands further improvements in Pt-specific power density in consideration of both the Pt supply and volatile cost. The department of Energy (DOE) has set year 2020 targets for PEMFC electrocatalysts that calls for Pt-specific power density to be improved to 0.125

Received: March 9, 2019

DOI: 10.1021/acs.chemrev.9b00157
Chem. Rev. XXXX, XXX, XXX−XXX

g_{PGM}/kW or, alternately, 8 kW/g_{Pt} (~8 to 10 g of PGM for 80 kW_{net} automotive fuel cell stack) with total MEA loading of 0.125 mg_{PGM}/cm^2.[3] Researchers in the automotive industry have stretched this target even higher up to 16 kW/g_{Pt} to reduce the total stack PGM content of ~6 g_{PGM}/vehicle.[4] This has to be accomplished without compromising on the performance (i.e., power density of at least 1.0 W/cm^2_{MEA} at operating potentials ≥ 0.65 V) and durability at low PGM loadings (5000 h of operation for automotive applications equivalent to 150000 miles, and 40000 h of reliable operation for stationary applications).[3−6] Durability issues lead to constant decrease in PEM fuel cell performance (i.e., power/current density loss with lifetime) due to the manifestation of a wide range of degrading factors related to the materials (membrane, electrocatalysts, support, ionomer, and gas diffusion media) and operating conditions (temperature, pressure, humidity, impurities, and potential excursions).[7] The projected cost target of PEM fuel cell system (stack plus balance of plant for an 80 kW_{net} system) is $30/kW by 2020 out of which ~25% of the cost arises from the use of precious metal cathode catalysts.[6] The major challenges in PEM fuel cells to be overcome prior to widespread deployment can be broadly classified as related to cost minimization without affecting performance and durability. There is significant effort related to the development of non-PGM catalysts for PEM fuel cells to mitigate the cost arising from the use of Pt in the cathode. So far, some of the leading non-PGM cathode catalyst candidates based on the metal−nitrogen coordination centers ($Fe-N_x$) have shown H_2/air MEA performance of ~0.8 A/cm^2 at 0.65 V leading to ~500 mW/cm^2_{MEA} at 80 °C and 100% RH.[8] While this represents tremendous progress, the non-PGM catalysts suffer from poor stability and still unacceptably low performance at high power.[4] Despite worldwide research effort in nonprecious catalyst developments[9] and durability improvements,[7] the chronic dependence of acidic PEM fuel cells on PGM catalysts causes significant liabilities for both cost and durability targets. This strongly predicates widespread commercialization on retrenching component costs and striking an optimum balance between performance and durability.

Alkaline electrolyte provides a paradigm shift with the possibility of complete elimination of precious metal catalysts and potentially enhanced material stability. The advantages of traditional alkaline fuel cells (AFC) operating on concentrated aqueous alkali metal hydroxide (30−45% KOH) electrolyte to enable nonprecious metal catalysts has been far outweighed by the difficulties of working with a liquid electrolyte, high system-level complexity, as well as poor CO_2 tolerance (reaction of atmospheric CO_2 in the cathode gas feed with the aqueous base to form insoluble alkali metal carbonate precipitates). This chronic CO_2 syndrome (i.e., effect of carbonate precipitation on electrolyte properties, reactant transport, porous electrode structure, and the need for complex balance of plant such as electrolyte circulation, CO_2 scrubbers, etc.) forced the tradiational AFCs as a niche product for extra-terrestial applications where pure hydrogen and oxygen gas feeds are used.[10−12]

Alkaline anion exchange membrane (AAEM) fuel cell technology mitigates the shortcomings of both PEM fuel cells and traditional AFCs and provides a more sophisticated, robust, and cost-effective alternative approach by enabling nonprecious electrocatalysts with acceptable performance, durability, and minimized system-level complexity. While catalysis in high pH electrolytes has been of long-standing interest, recent developments in highly conducting hydroxide anion-exchange membrane (AEM) electrolytes have triggered a renaissance of the alkaline electrolyte based fuel cells.[13−15] Energy conversion in AAEM fuel cell involves the hydrogen oxidation reaction (HOR) at the anode ($H_2 + 2OH^- \rightarrow 2H_2O + 2\bar{e}$) with hydroxide anions that are produced as a result of oxygen reduction reaction (ORR) at the cathode ($O_2 + 2H_2O + 4e^- \rightarrow 4OH^-$) leading to the formation of final product water on the anode side. The primary function of AAEM polymeric electrolyte is to spatially separate the electrodes and enable the selective transport of hydroxide anions from cathode to anode and transport of water from anode to cathode without reactant/oxidant gas crossover. Water produced as a byproduct on the anode is consumed as a stoichiometric reactant in the ORR process at the cathode presumably leading to better water management and decreased cathode flooding at high current densities. To date, a majority of the AAEM polymer chemistry investigated typically involves a hydrocarbon membrane backbone (polysulfone,[16,17] polyphenylene,[18] and polyethylene[19]) covalently functionalized with positively charged benzyltrimethyl quaternary ammonium (QA) cation headgroup side-chains for hydroxide-anion transport.[14,20−27] Use of solid state AAEM electrolytes free of mobile alkali metal cations implies that the carbonate precipitation found in liquid electrolyte AFC is also largely mitigated (vide infra). Typical AAEM solid electrolytes exhibit ~20−40 mS cm^{-1} hydroxide anion conductivity with ion-exchange capacities of ~1.5 to 2.0 mmol g^{-1} at room temperature and well-hydrated conditions to enable moderate current densities during fuel cell operation.[14] For applications in the watts to a few kilowatts scale, AMFC technology has the potential to capture the early market in applications such as auxiliary power sources in automotive applications, critical backup power, material handling equipment, and micro-CHP applications.[28]

In the first part of this treatise, we will establish the current state of the art AAEM fuel cell performance operating on PGM and non-PGM catalysts in comparison to PEM fuel cells. For this purpose, we utilize Tokuyama A201 anion-exchange membrane along with commercially available Pt/C and in-house developed non-PGM electrocatalysts. It should be noted that arguments in the PEM fuel cell literature has shifted to Pt-specific power densities due to the pertinent requirement of reduced Pt-loading, whereas AAEM fuel cell is in an early stage of development and the arguments here are made based on MEA area-specific power density. Further, the poor thermal stability of the currently available AAEM electrolytes limits the fuel cell operating temperature ~50 to 60 °C. While the development of highly conductive and thermo-chemically stable AAEM chemistry remains the central requirement of the technology, it will be shown that significantly unique challenges arise in electrocatalysis and interfacial charge transfer processes in AAEM fuel cells. These challenges primarily relate to the (i) high overpotential for hydrogen oxidation reaction, (ii) mechanistic aspects of ORR, (iii) implications of carbonate-anion exchange of the cation head-groups on MEA performance, (iv) effect of the specific-adsorption of quaternary ammonium cations on catalyst surface which will be dealt with here in the context of alcohol oxidation, and (v) complications arising due to inefficient water distribution across the cell.

HOR in PEM fuel cells requires only small loadings of <0.05 mg_{Pt}/cm^2, thanks to the rapid kinetics and high exchange current densities on the order of a few mA/cm^2 in acidic electrolytes.[29−31] Contrarily, it has become increasingly realized that HOR kinetics in alkaline media is roughly 2 orders of magnitude lower than acidic conditions.[30,32] It is predicted that

DOI: 10.1021/acs.chemrev.9b00157
Chem. Rev. XXXX, XXX, XXX−XXX

HOR overpotential of 130−150 mV would be expected in the AAEM fuel cell operating at 80 °C cell temperature and 1.5 A/cm^2 current density with anode catalyst loading of 0.05 mg_{Pt}/cm^2_{anode}.[32] This clearly indicates that the application of Pt anode catalysts in AAEM fuel cells would require loadings much greater than 0.05 mg_{Pt}/cm^2, thereby contributing to the cost factor and causing major impediment to AAEM fuel cell commercialization. Recent studies have shown that the high HOR overpotential is related to either stronger hydrogen reaction intermediate bond strength to the catalyst surface or the higher activation energy required for the arrival of hydroxide anion intermediate at the catalyst surface in alkaline electrolyte.[33−37]

Contrarily, ORR in alkaline media on Pt surfaces exhibit roughly similar activity, if not better, compared to acidic conditions.[32,38,39] In addition, non-pgm catalysts exhibit very high ORR activities due to their higher turnover number in liquid alkaline electrolytes compared to acid.[40,41] Several unique aspects of ORR that arise due to changes in reaction mechanisms in alkaline electrolytes need to be addressed. These are due to the existence of both inner- and outer-sphere electron transfer mechanisms during ORR in alkaline electrolyte and the nature of alkaline hydroperoxide intermediate (HO_2^- at high pH versus H_2O_2 at low pH).[38,42,43] The underlying ORR mechanisms on both Pt and non-pgm surfaces (Fe−N_x−C-type, MnO_x and perovskite-type catalysts) are reviewed here along with an exposition on the causes of higher ORR turnover numbers on non-pgm catalysts in alkaline electrolyte. Further, it is also emphasized that major challenges remain not in developing new non-pgm ORR catalysts (a vast number of which has been reported in the recent past in alkaline electrolytes) but in translating the observed high ORR activities on existing non-pgm surfaces from liquid alkaline electrolytes to AAEM based membrane-electrode assembly (MEA). This needs to be achieved by fabricating better electrode structures with enhanced three-phase boundaries and minimizing mass transport losses. ORR literature is a vast subject, and an excellent review in alkaline electrocatalysis was provided by Spendelow et al.,[42] and our section on ORR in this article here recapitulates only the recent advances since then particularly focusing on those with a more mechanistic understanding of the reaction.

As mentioned above, traditional AFCs have been largely relegated to extra-terrestrial applications due to its poor CO_2 tolerance. The prospects of AAEM fuel cells operating under terrestrial atmospheric conditions strongly hinges on immunizing the CO_2-syndrome of AAEM fuel cells without adding to the cost and system complexity. Specifically, while the use of AAEM electrolyte negates the precipitation of insoluble carbonates due to the absence of free alkali metal cations, the ion-exchange of carbonate anions leads to serious loss of anion conductivity. Further, the interplay of carbonate anion diffusion and migration currents leads to its accumulation on the anode side leading to the formation of a pH gradient across the MEA and significantly affecting electrocatalysis via a thermodynamic effect.[44,45] Recent developments and existing strategies in mitigating the effect of carbonate anions on AAEM fuel cells are reviewed.

A more chronic problem in the development of the AAEM fuel cell has been the very poor performance of direct alcohol (KOH-free) anode feed systems.[46] In particular, alkali metal free, direct methanol AAEM fuel cells have shown meager power densities on the order of a few tens of mW cm^{-2}, in spite of the generous use of platinum in the electrode structures.[47−50] While the addition of excess aqueous-KOH to the anode feed improves the short-term performance via increase in alcohol oxidation kinetics at the anode, this is not acceptable in a practical fuel cell because CO_2 from the atmospheric air cathode and complete alcohol oxidation leads to insoluble carbonate precipitation that catastrophically affects operation lifetime. There are several factors that can limit the AAEM fuel cell performance in the absence of excess KOH, including low anode pH, poor catalyst utilization, and fuel crossover to the cathode, lower interfacial/bulk ionic conductivity, and poor fuel transport in the anode/ionomer interface. Some latest developments in this field are reviewed here which point to the deleterious effect of specific adsorption of the quaternary ammonium cation functional groups in alkaline ionomer side chains on the electrocatalyst surface and its influence on disrupting the potential distribution profile at the anode/electrolyte double-layer interface.[51] In the absence of excess KOH in the anode feed, efficient fuel oxidation is dependent on the establishment of the three-phase boundary at the active site between ionomer, carbon support, and reactant. The presence of excess KOH in the anode feed discredits the use of ionomer solutions in the catalyst layer by establishing the so-called "flooded electrolyte" system. Most electrocatalyst developmental studies are carried out in aqueous KOH electrolytes, where the excess amount of free hydroxide anions hides the true interfacial effect of quaternary ammonium cation headgroup adsorption. The importance of more fundamental investigation of the electrocatalytic and charge transfer processes at excess KOH-free alkaline electrode/electrolyte interfaces are emphasized here. One common theme that will be emphasized in this treatise is the difference between studying electrocatalysis in liquid alkaline electrolyte versus liquid-free alkaline ionomer environments (i.e., the so-called "flooded-electrolyte" vs three-phase boundary conditions). Given the potential fuel flexibility of AAEM fuel cells, and the necessity to develop alternative nonalcoholic anodic fuel (to avoid the presence of CO_2 from complete oxidation of alcohols), the developments in the field of hydrazine oxidation are briefly reported here. Further, water management in an AAEM fuel cell MEA is critical since ineffective operating conditions is suggested to lead to anode flooding where water is generated and cathode dry-out where water is stoichiometrically consumed.[52,53] In the cathode, poor water management leads to increases in both charge transfer resistance and hydroxide-anion transport.[54−58] The subject of water management in AAEM fuel cells is beyond the scope of this review.

Rapid progress has been made in recent years in AAEM fuel cell performance leading to a significant set of new materials, concepts, and scientific phenomena. The major objective of this review article is to provide a coherent and unified picture of the current state of AAEM fuel cell performance, critically evaluate the scientific merits of this technology, and delineate a strategy for future research within the perspective of electrocatalysis and interfacial charge transfer. While the continued development of highly conductive and thermally stable anion-exchange membranes is unambiguously the principal requirement, we attempt to put the focus on the challenges in electrocatalysis and interfacial charge transfer at an alkaline electrode/electrolyte interface. To achieve these objectives, a mechanistic and phenomenological discussion is carried out here to fundamentally understand (i) electrocatalysis of hydrogen oxidation, (ii) mechanisms of oxygen reduction, (iii) consequences of carbonate anion exchange, (iv) effect of specific adsorption of quaternary ammonium cation head-groups on catalyst surface, and (v) alternative anodic nonalcohol fuel oxidation. Literature

DOI: 10.1021/acs.chemrev.9b00157
Chem. Rev. XXXX, XXX, XXX−XXX

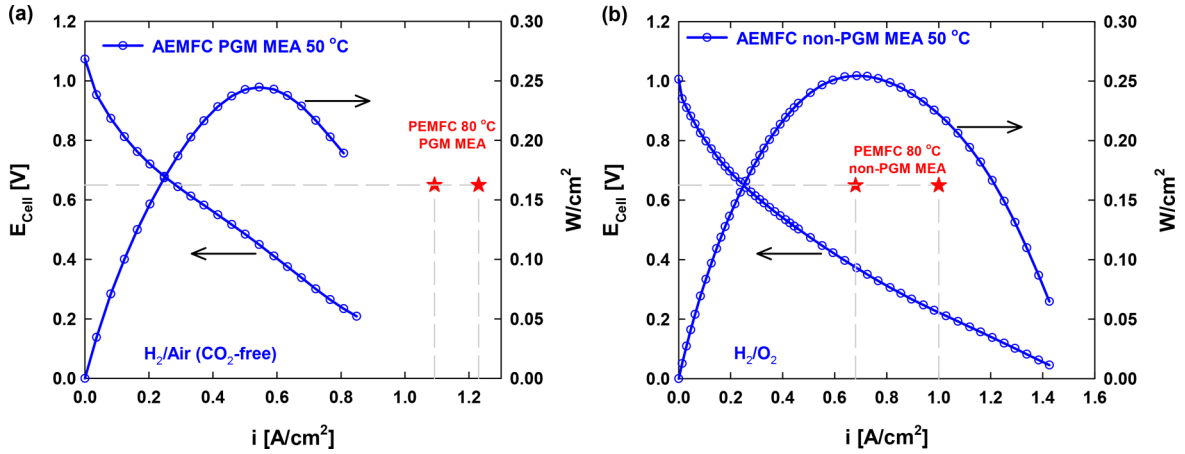

Figure 1. Representative AAEM fuel cell performance measured using Tokuyama A201 AEM electrolyte in a 5 cm^2 single-cell at T_{cell} = 50 °C, 100% RH. (a) Performance of PGM cathode consisting of 46% Pt/C catalyst sprayed to a loading of 0.5 mg_{Pt}/cm^2 on a gas diffusion layer with Tokuyama AS4 alkaline ionomer to carbon ratio 0.6:1. Interfacial ionomer layer of 1 mg_{AS4}/cm^2 was sprayed on top of the cathode. Measurements were made using H_2/air (CO_2-free) gas feeds at 200/600 sccm flow rates, respectively, with a mild back-pressure of 10 psig. (b) Performance of non-PGM cathode consisting of in-house prepared Fe−N_x−C type catalyst sprayed to a loading of 3 $mg_{non\text{-}pgm}/cm^2$ on a gas diffusion layer with AS4 ionomer in the ratio 0.2:1. Interfacial ionomer layer of 1 mg_{AS4}/cm^2 was sprayed on top of the cathode. Measurements were made using H_2/O_2 gas feeds at 200/400 sccm flow rates, respectively, with a gauge back-pressure of 28/28 psi. All MEA's consisted of a commercially available Pt-based gas diffusion electrode (0.5 mg_{Pt}/cm^2) directly used as the anode after spraying an alkaline ionomer layer of 1 mg_{AS4}/cm^2 on top. MEA's were fabricated by hot pressing the anode and cathode with Tokuyama A201 AEM at 100 psig pressure and 80 °C for 4 min. (Asterisk symbols: The analogous PEM fuel cell performance from literature at T_{cell} = 80 °C is shown for comparison. See text for references).

in AAEM fuel cell development has witnessed rapid growth in the past few years, and several excellent review articles have been published on this subject.[59−61] It is not the intention of this article to provide an exhaustive repertoire of all the work. Rather, this review centers around the recent developments in AAEM fuel cells from our laboratory interspersed with a literature review to provide a comprehensive summary on the scientific aspects of the reaction mechanisms and charge transfer phenomena.

2. CURRENT STATUS OF AAEM FUEL CELL PERFORMANCE

Figure 1a shows a representative of H_2/air (CO_2-free) AAEM fuel cell performance at 50 °C cell temperature, 100% RH conditions employing commercially available Tokuyama A201 AEM electrolyte (OH-form, 28 μm thick, 1.7 mmol/g). A cathode comprised of a 0.5 mg_{Pt}/cm^2 catalyst (using 46% Pt/C TKK) sprayed on a gas diffusion layer along with a Tokuyama AS4 alkaline ionomer at an ionomer:carbon ratio of 0.6:1. Prefabricated BASF Pt-based gas diffusion electrode was used as the anode (Pt-loading 0.5 mg_{Pt}/cm^2). Interfacial alkaline ionomer layer of 1 mg_{AS4}/cm^2 was sprayed on top of both the electrodes. The AAEM fuel cell polarization curve shown in Figure 1a is characterized by a current density of 0.28 A/cm^2 at 0.65 V leading to a power density of 180 mW/cm^2. In PEM fuel cell literature, MEA performance comparisons are typically carried out at 0.65 V based on considerations of heat rejection requirements.[62] On the contrary, in AAEM fuel cell literature performance at peak power is typically reported which is achieved at cell voltages much lower than 0.65 V, and this does not have much practical relevance due to the high heat generated at lower cell voltages; further, this is exacerbated by the low operating cell temperature of AAEM fuel cells (50−60 °C for AAEM vs 80−90° for PEM fuel cells). So, we avoid making comparisons at peak power and rather use performance at 0.65 V as a point of comparison between PEM and AAEM fuel cell MEAs. A brief survey of the literature shows that under roughly similar conditions (H_2/CO_2-free air gas feeds at 50 °C cell temperature) of AAEM fuel cell performance, (i) Tokuyama Corporation demonstrated ∼190 mW/cm^2 of power density (0.29 A/cm^2 at 0.65 V) using a similar set of materials,[63] (ii) acta S.p.A showed a marginally higher performance of roughly 225 mW/cm^2 [∼340 mA/cm^2 at 0.65 V (proprietary alkaline ionomer 'I2' developed at Acta S.p.A was utilized in their study)],[64] and (iii) CellEra reported H_2/air (CO_2-free) short-term performance at 80 °C of 0.58 A/cm^2 at 0.65 V, leading to ∼375 mW/cm^2 power density using a back pressure of 2/2 bar (utilizing an undisclosed amount of anode/cathode catalysts loading).[65] A summary of the AAEM fuel cell performance has been recently compiled by Dekel et al., although a vast majority of them are with H_2/O_2 gas feeds.[60]

One major advantage of operating the fuel cell at alkaline pH is to eliminate the use of Pt and enable the application of non-pgm materials as the cathode catalyst. Figure 1b shows an AAEM fuel cell MEA performance incorporating a PGM anode (0.5 mg_{Pt}/cm^2) and a non-PGM cathode (3 $mg_{non\text{-}PGM}/cm^2$ of a pyrolyzed Fe−N_x−C type catalyst) at 50 °C, 100% RH using H_2/O_2 gas feeds at 28/28 psi back pressure, Tokuyama A201 AEM, AS4 alkaline ionomer. Non-PGM cathode performance in Figure 1b is characterized by a current density of 240 mA/cm^2 at 0.65 V leading to a power density of 155 mW/cm^2. Similar results were also shown recently utilizing composite cobalt oxide with nitrogen-doped graphene cathode electrocatalysts (undisclosed non-pgm cathode loading) for AAEM fuel cells[66] at a cell temperature of 60 °C, H_2/O_2 gas feeds leading to a current density of ∼250 mA/cm^2 (160 mW/cm^2) at 0.65 V. While these non-pgm cathode performances were measured with humidified pure-O_2 cathode feed, it has been demonstrated recently using proprietary nonplatinum-based catalysts (Hypermex 4020, Acta S.p.A.) and alkaline ionomer (I2 developed at Acta S.p.A) that high fuel cell performance can be achieved with air (CO_2-free) cathode feed. Acta S.p.A demonstrated fuel cell performance using 0.45 mg_{Pt}/cm^2 anode and 0.8 $mg_{non\text{-}PGM}/cm^2$ cathode

DOI: 10.1021/acs.chemrev.9b00157
Chem. Rev. XXXX, XXX, XXX−XXX

Table 1. Select Literature Data Showing AAEM Fuel Cells Performance[a]

institution	catalyst (anode and cathode)	loading (anode/cathode) (mg/cm^2)	reactant gases	membrane	T (°C), P_{cell} (kPaa), RH (%)	i (A/cm^2) /P.D. (mW/cm^2)[a]	HFR (mΩ cm^2)	ref
Northeastern University[a]	46% Pt/C	0.5	H_2/air (CO_2-free)	Tokuyama A201	50, 165, 100	0.28/180	~180	this work
Tokuyama	46% Pt/C	0.5		Tokuyama A901	50, n/a, 95	0.29/190	~150	63
Acta S.p.A	40% Pt/C	0.45		n/a	50, n/a, 85	0.34/225	n/a	64
CellEra Corp.	n/a	n/a		Tokuyama	80, 200, n/a	0.58/375	200	65
Technion, LANL et al	Pt and Ag	n/a		n/a (30 μm AEM)	75, 200, 100	~1.0/650	n/a	59
Bar Ilan Univ.	Pd/Ni and Ag-alloy	1.5/3.0		QA functionalized Hydrocarbon membrane	73, 200, 100	0.29/200	n/a	72
Univ. New Mexico	Pt black	2	H_2/air	aminated tetramethyl poly(phenylene)	80, 200, 100	0.05/33	n/a	18
Korea Institute of Technology	40% Pt/C	0.5		cross-linked QA polysulfone	60, 101, 100	0.04/26	n/a	73
LANL, RPI	PtRu and Pt	0.5/0.6		alkylammonium tethered poly(fluorene)	80, 285, 100	~1.0/650	~60	74
Univ. Surrey	20% Pt/C	0.5	H_2/O_2	80 μm QA radiation grafted ETFE	50, 101, 100	0.25/160	n/a	75
Univ. Surrey	20% Pt/C	0.4		20 μm QA radiation-grafted ETFE	50, 101, 100	0.28/182	n/a	76
LANL, RPI	PtRu and Pt	0.5/0.6		alkylammonium tethered poly(fluorene)	80, 285, 100	~2.0/1300	~60	74
US Army Research Lab	Pt/C	0.4		quaternized PMMA-*co*-butyl acrylate-*co*-VBC	70, 200, 80	0.18/117	n/a	77 and 78
Univ. New Castle	60% Pt/C	0.8		cross-linked QA methylated melamine grafted pVBC	15, 101, 100	0.2/130	n/a	79
Univ. California Riverside	Pt black	0.5		FumaTech GmbH	80, 350, n/a	0.275/180	n/a	80
Chinese Academy of Sciences	Pt/C	0.4		cross-linked QA pVBC (PTFE reinforced)	60, n/a, 100	0.4/260	n/a	81
Los Alamos National Lab	Pt black	3.0		Aminated poly(phenylene)	60, n/a, n/a	0.225/146	n/a	82
Los Alamos National Lab	Pt black	3.0			60, n/a, 100	0.38/247	n/a	82
Univ. of Connecticut	PtRu and Pt	0.71/0.53		ETFE-benzyltrimethyl ammonium headgroup	60, 101, 62	~2.0/1300	n/a	52
non-PGM cathodes								
Northeastern University[a]	Pt/C and Fe−N_x−C	0.5/3.0	H_2/O_2	Tokuyama A201	50, 290, 100	0.24/155	180	this work
Acta S.p.A	40% Pt/C and Acta HYPERMEC 4020	0.45/0.8	H_2/air (CO_2-free)	commercial membrane	50, n/a, 85	0.2/130	n/a	64
Univ. of Connecticut	PtRu and N−C−CoO_x	0.10/2.4		LDPE-benzyltrimethyl ammonium headgroup	65, 100, n/a	~0.5/325	n/a	52
UCLA and LANL	Pt/C and CoO/rGO (N)	1.5 and n/a	H_2/O_2	Tokuyama A201	60, 101, 57/100	0.25/160	n/a	66
Wuhan University	NiCr and Ag	1.0/5.0		QA polysulfone	60, 132, 100	0.06/40	n/a	83
Univ. of Delaware	Ni/C and Ag	5.0/0.5	H_2/O_2	phosphonium-based ionomer	70, 250, ~ 100	0.11/70	n/a	84

[a]Current density (i) and power density (P.D.) values are tabulated here at 0.65 V. Peak power density is not reported here since it is typically observed at cell voltages < 0.45 V, which is irrelevant for practical applications based on considerations of heat rejection.

loadings with H_2/air (CO_2-free) gas feeds reach current density of 200 mA/cm^2 at 0.65 V amounting to 130 mW/cm^2 at 50 °C, 85% RH conditions.[64] Analogous PEM fuel cell performance incorporating similar Fe−N_x−C type non-PGM cathode catalysts (4 $mg_{non\text{-}pgm}$/cm^2 cathode loading and 0.25 mg_{Pt}/cm^2 anode loading) such as PANI FeCo−C yield 440 mW/cm^2 at 0.65 V (~0.68 A/cm^2) using H_2/O_2 gas feeds at 80 °C, 2.8/2.8 bar.[67] Also, other non-PGM cathode catalyst systems (5.3 mg/cm^2 cathode non-pgm loadings) have been shown to yield 195 mW/cm^2 at 0.65 V (~0.3 A/cm^2) using H_2/O_2 gas feeds at 80 °C, 1.5/1.5 bar absolute leading to a volumetric current density of 99 A/cm^3 at 0.8 $V_{iR\text{-}free}$ (H_2/O_2, 1 bar absolute pressure, 80 °C).[68] Other high power density non-PGM cathode catalyst (3.9 mg/cm^2 cathode NPMC loadings) have been shown to yield ~650 mW/cm^2 @ 0.65 V (~1 A/cm^2) using H_2/O_2 gas feeds at 80 °C, 1.5/1.5 bar absolute with volumetric current density of 230 A/cm^3 at 0.8 $V_{iR\text{-}free}$ (H_2/O_2, 1 bar absolute pressure, 80 °C).[69] DOE PEMFC non-PGM volumetric activity target has been set at 300 A/cm^3 at 0.8 $V_{iR\text{-}free}$ at 80 °C, H_2/O_2, 100% RH, total outlet pressure of 150 kPa (1.5 bar total pressure), anode/cathode stoichiometry of 2/9.5.[28] Translation of volumetric activity to geometric current density equates to

DOI: 10.1021/acs.chemrev.9b00157
Chem. Rev. XXXX, XXX, XXX−XXX

100 mA/cm^2 at 0.8 $V_{iR\text{-free}}$ at the above conditions of H_2/O_2, 80 °C, 100% RH, 1.5 bar total pressure. Recently concluded AAEM fuel cell workshop suggested a H_2/O_2 performance target of 0.044 A/cm^2 at 0.9 $V_{iR\text{-free}}$ for non-pgm cathodes (at 60 °C, H_2/O_2, 100% RH).[70] Analysis of non-PGM AAEM fuel cell performance in Figure 1b and in Table 1 clearly shows that they do pass these criteria of 0.044 A/cm^2 and 100 mA/cm^2 at 0.9 $V_{iR\text{-free}}$ and 0.8 $V_{iR\text{-free}}$, respectively, under H_2/O_2 gas feeds.

Fuel cell performance results from several research groups utilizing various alkaline membranes and ionomers along with Pt-containing cathodes are briefly summarized in Table 1. As shown in Figure 1a, AAEM fuel cell performance measured using commercially available PGM catalysts and membrane materials is characterized by 0.28 A/cm^2 at 0.65 V at 50 °C cell temperature. Applying the correction for cell voltage drop arising from membrane Ohmic resistance of 180 mΩ cm^2 (measured via the high frequency intercept) yields a marginal improvement current density to 0.37 A/cm^2 at 0.65 $V_{iR\text{-free}}$. This performance is still roughly three to four folds lower than that measured in current PEM fuel cells at 80 °C (asterisk symbols in Figure 1a).[2,5] This performance gap could be closed to some extent by operating the AAEM fuel cell at higher temperatures of 80 °C such as that shown by CellEra Corporation (~0.58 A/cm^2 at 0.65 V)[65] and/or using thinner AEM electrolytes as shown by Kim et al. (~1.0 A/cm^2 at 0.65 V).[59] Further, PEM fuel cells have witnessed several decades of empirical but very significant developments in fabricating catalyst layer structures comprising highly dispersed Pt/C catalysts heterogeneously mixed with colloidal ionomer solutions.[71] These developments in PEM fuel cell literature are nontrivial and these findings are only in the nascent stage for AAEM fuel cell catalyst layer fabrication. While the above comparison across various laboratories inherently carries with it inconsistencies arising from usage of wide range of materials, MEA designs, fabrication procedures and operating conditions, it clearly shows that this significant performance gap cannot be closed by only developing highly conductive anion-exchange membranes and their corresponding solubilized ionomer dispersions; particular attention has to be put on understanding the nonmembrane components in the AAEM fuel cell MEA.

2.1. PEM vs AEM Electrolyte Bulk Properties

Ideal AAEM electrolyte for good performance under fuel cell operating conditions would feature ionic conductivity high enough to support large current densities (1.5 A/cm^2 at ≥ 0.65 V), high thermo-chemical stability at elevated temperature and high pH, sufficient ion-exchange capacity with optimal water uptake/swelling and mechanical stability, amenability to fabrication at smaller thickness (≤10 μm) to minimize resistance and facilitate water transport from anode to cathode, and low fuel/oxidant crossover. In general, conductivity in ionomer membranes is dependent on the nature of the mobile charge carrier (hydrated ion-size, charge, concentration, and mobility), membrane properties (structure, chemistry, basicity of cationic-headgroup, phase separation, pore structure, IEC, and water uptake), the ion-transport mechanism (Grotthus mechanism or structure diffusion versus vehicular transport), and other external factors such as temperature. In this section, we provide a phenomenological review of the current status of AAEM electrolytes by considering the following aspects: (i) factors controlling the hydroxide anion conductivity, (ii) thermo-chemical stability of cationic head-groups, and (iii) the need for solubilized or colloidal dispersions of alkaline ionomers. Following this, we provide a brief comparison of AAEM electrolyte OH^- conductivity in comparison to H^+ conductivity in Nafion. For a more extensive review of membrane chemistry and its applications, interested readers are directed to a detailed treatise on this subject by Varcoe et al.,[85] Zhang et al.,[86] and an excellent repertoire by Merle et al.[14]

Hydroxide anion transport in AAEM electrolytes is typically considered to experience some fundamental thermodynamic limitations in comparison to proton transport in acidic conditions. Ionic transport in AAEM electrolytes is controlled by various factors such as (i) mobility of hydroxide anions, (ii) concentration of mobile charge carriers, (iii) state of membrane hydration, (iv) contamination by HCO_3^-/CO_3^{2-} species, and (v) ion transport mechanisms. Ionic mobility of H^+ is 36.23 × 10^{-4} cm^2 V^{-1} s^{-1} compared to 20.64 × 10^{-4} cm^2 V^{-1} s^{-1} for OH^- anions in aqueous solutions at 298 K,[15] or alternatively the diffusion coefficient of H^+ and OH^- anions at infinite dilution are 9.3 × 10^{-9} m^2/s and 5.3 × 10^{-9} m^2/s, respectively, in liquid water.[87] This clearly indicates that the mobility and diffusion coefficients of hydroxide anions are roughly lower than that of protons by a factor of 1.75 in aqueous solutions. While lower mobility of OH^- anions is a fundamental thermodynamic limitation, the concentration of mobile charge carriers are dependent on both the membrane IEC and the dissociation constant of the cationic-headgroup. The acid dissociation constant (pK_a) of Nafion type membranes is typically represented by small molecules such as trifluoromethanesulfonic acid (CF_3SO_3H), which exhibits a superacidic behavior with a pK_a value of −12.[88,89] In comparison, while small molecules such as ammonium hydroxide (NH_4OH) has modest pK_b values of 4.75, recent studies show that molecules such as benzyltrimethylammonium hydroxide that more closely resembles AAEM electrolytes are actually strong bases with pK_b < 1.[85] At least under fully hydrated conditions, AAEMs appear to be fully dissociated.[19,90] One conventional strategy to increase hydroxide anion conductivity and mobile charge carrier concentration is to maximize IEC without compromising on the dimensional and mechanical stability of the membrane (due to excessive water uptake/swelling at high IEC values).[14,91] AAEM electrolytes typically feature high IEC values of >1.5 mmol g^{-1} compared to ~1.0 mmol g^{-1} for Nafion which leads to mobile OH^- anion concentrations that are equal to or greater than H^+ concentrations in acidic membranes.[19] In AAEM electrolytes, for IEC < 1.5 mequiv g^{-1}, conductivity is limited due to isolation of ionic domains from each other, whereas for IEC > 1.5 mequiv g^{-1}, conductivity increases as the volume fraction of water and concentration of ionic groups in the membrane increases.[17] In such cases of very high IEC values >1.5 mequiv g^{-1}, a combination of strategies such as membrane cross-linking and reinforcement appear useful to overcome challenges of mechanical stability.[81]

Another major strategy currently being utilized to improve hydroxide anion conductivity is to synthesize AAEM electrolytes with proper phase separation between the polymer membrane backbone and the ion-conducting head groups.[17,87,90] The current state of the art AEM synthesis primarily involves chloromethylation-quaternization of aromatic hydrocarbon polymer backbones (such as polystyrenes,[92] polysulfones,[16] polyphenylenes,[18,93,94] and polyethylenes[95]) followed by hydroxide exchange wherein the driving force for phase separation and ion-cluster formation is absent. Such a lack of morphological organization and phase separation lead to AEM's behaving more like swollen gels rather than featuring

DOI: 10.1021/acs.chemrev.9b00157
Chem. Rev. XXXX, XXX, XXX−XXX

interconnected hydrophilic ion-conducting channels as distinct from the hydrophobic polymer backbone.[17,87] Microphase segregation between hydrophobic polymer backbone and hydrophilic ionic channels lead to improvements in the effective mobility of OH^- anions, leading to appreciable ionic conductivity even at moderate IEC levels of 1.0 mmol g^{-1}.[96] For a given degree of swelling, phase-separated hydrated domains give faster transport rates.[17]

This strategy of synthesizing membranes with proper phase separation is important not only to improve ionic conductivity at full hydration levels of the membrane but also because recent studies have shown a strong dependence of conductivity on membrane state of hydration. Kreuer et al.[90] showed that at full hydration OH^- anion transport in AAEM electrolytes can reach conductivity values within a factor of 2 compared to that of H^+ transport in Nafion 117, which corresponds to the difference in ion transport mobility as discussed above. With decreasing water content in membrane, the effective OH^- mobility fell far below the water diffusion coefficient, thereby significantly limiting the OH^- anion conductivity. Such a behavior was attributed to arise from the poor degree of dissociation of the quaternary ammonium hydroxide functional groups at low water contents which appears to be a significant difference between OH^- and H^+ exchange membranes.[90] It has become increasingly realized that the strong dependence of dissociation constant and conductivity of OH^- anions on membrane water content is related to the lack of proper phase separation between the polymer membrane backbone and the ion-conducting head groups in AAEM.[17,87,90] Grew et al.[87] used a dusty fluid model to develop an improved understanding of the transport mechanisms and conductivity limitations in AAEM electrolytes. Although both H^+ and OH^- transport involved structural diffusion via Grotthuss mechanism under fully hydrated conditions, OH^- anion transport involve higher activation energy due to significant solvent reorganization. Further, the OH^- anion transport mechanism is dependent on the state of hydration. At low humidity, vehicular or en masse diffusion was found to be dominant, which changed to the Grotthuss mechanism at high water contents. This suggests that the membrane structure, morphology, and phase separation strongly determines the OH^- solvation/dissociation processes, transport mechanisms, and hence the conductivity.[17,87,90] This clearly indicates that in order to achieve high conductivity, besides trying to maximize IEC, it is equally important to design the appropriate polymer morphology, structure, and chemistry. The strong dependence of dissociation constant and subsequently the hydroxide conductivity on the membrane state of hydration appears to be a major limiting factor.[19,90]

Another aspect of major concern in AAEM electrolyte development is the thermochemical stability in strongly alkaline environments.[13,97] While acidic PFSA membrane degradation is largely related to the radical induced (•OH, •OOH) stability issues,[98] AAEM electrolyte degradation is understood to be induced by the highly nucleophilic OH^- anions. Particularly, OH^- anions attack the cationic-head groups (> $C-N^+Me_3$) via nucleophilic substitution and/or Hoffmann elimination mechanisms leading to significant losses in IEC and conductivity. These degradation pathways are dependent on the cation type and are further exacerbated at elevated temperatures and/or lower states of membrane hydration since the OH^- anions are bereft of their solvation shell.[99] This is particularly important on the cathode side of an operating AAEM fuel cell since water is stoichiometrically consumed during ORR. This causes the cathode to exist in a relatively subsaturated condition and more prone to hydroxide attack of the ionomer in the catalyst layer. It has also been recently suggested that the radical-initiated (•OH, •OOH) and hydroxide-initiated attack of the polymer backbone cannot be completely excluded.[85] The lack of chemical stability of benzyltrimethyl quaternary ammonium cationic headgroup and the need for cationic functional groups with high basicity has led to the search for alternative head groups such as imidazolium,[100−105] phosphonium,[106,107] guanidinium,[108] sulfonium,[109] and metal−organic cationic functionalities.[110,111] While a brief survey of these alternative cationic headgroup chemistry-based AAEMs indicate appreciable conductivity of ∼30 mS cm^{-1} at close to room temperatures, the claims of improved stability largely remains controversial and needs further investigations with cross-laboratory comparisons.[112,113] Further, in most cases the AAEM fuel cell performances incorporating non-QA type AAEMs are very modest at best, most often due to either nonoptimized MEA preparation conditions or the nonavailability of compatible ionomer solutions.[80,100,103,107,113]

Another aspect of very critical importance is the need for alkaline ionomer solutions or colloidal dispersions for electrode fabrication.[114] Conventional wisdom in PEM fuel cell literature suggests that ionomer solutions are needed to maximize catalyst utilization efficiency and minimize ion transport resistance in the catalyst layer by maximizing the three-phase boundary between the catalyst, reactant, and ionomer. In the recent past, catalyst layer design has become a nontrivial subject leading to more focus on ionomer distribution in the catalyst layer.[71] Most results indicate that the ionomer film in the catalyst layer exists in a confined space distributed on the surface of the carbon support with thicknesses of ∼2−4 nm.[4] Under such conditions of spatial confinement, the physicochemical properties of few nanometers thick ionomer films are observed to deviate from that of micrometers thick bulk membranes. Particularly, the O_2 permeability of ionomer thin films are found to be much lower than bulk membranes, leading to significant overpotentials arising from O_2 transport resistance in the catalyst layer at high current densities.[115−117] While the development of alkaline ionomer solutions is still in the nascent stage, the focus needed on this subject cannot be overemphasized. Some recent studies provide encouraging results such as the phosphonium-based ionomer dispersion exhibiting 27 mS cm^{-1} OH^- conductivity at a moderate IEC of 1.1 mmol g^{-1}.[80,107]

Despite the various liabilities related to conductivity and stability, benzyltrimethyl quaternary ammonium cation based AAEM electrolytes appear to be the benchmark material.[85] A brief comparison of the OH^- anion conductivity and H^+ conductivity is performed here. Nafion membranes exhibit a room temperature through plane H^+ conductivity of ∼70−80 mS cm^{-1} at 100% RH conditions at an IEC value of ∼0.9 mmol g^{-1}.[19,87] In comparison, benchmark AAEM electrolytes from Tokuyama corporation namely A201 (28 μm thick) and A901 (10 μm thick) exhibit OH^- conductivity of 42 and 38 mS cm^{-1} at 90% RH and room temperature.[63,118,119] Although these AAEM electrolytes feature a higher IEC of 1.7 mmol g^{-1}, their OH^- anion conductivity values are essentially within a factor of 2 as expected based on the thermodynamic mobility limitations as explained below. This shows that the current state of the art AAEM electrolytes could have very well reached their empirical upper limit in terms of their OH^- conductivities with respect to Nafion. This is also true for the AAEM electrolytes with proper phase-segregated morphologies which exhibit room temper-

DOI: 10.1021/acs.chemrev.9b00157
Chem. Rev. XXXX, XXX, XXX−XXX

ature OH^- anion conductivity values of ~35 mS cm^{-1} at a moderate IEC of 1.0 mmol g^{-1}.[96] Brief survey of the literature shows that the OH^- conductivity of QA-headgroup-based AAEM electrolyte ranges from 20 to 35 mS cm^{-1} at 100% RH and close to room temperature conditions.[14,77,79,81,104,120,121] Given the above thermodynamic limitations, currently available AEM membranes do exhibit reasonable hydroxide anion conductivity at fully hydrated conditions to support fuel cell operation at modest current densities. The primary limitation of the current state of the art AAEM electrolytes is related to the sharp drop in ionic conductivity and the lack of thermo-chemical stability when operated at less than fully hydrated conditions.[16,103,113] As mentioned above in the previous section, the low OH^- anion conductivity cannot fully substantiate the lower AAEM fuel cell performances (Figure 1 and Table 1), and hence, significant attention is needed on other components such as the electrocatalytic charge transfer reactions and electrode materials at high pH conditions.

2.2. General Context of Alkaline Electrocatalytic Interfaces

While alkaline electrocatalysis is a vast subject by itself, we would like to point out a few of its generic aspects in comparison to acidic electrolytes that are of relevance here in this article. They are related to the (i) working electrode potential range,[42] (ii) abundance of protons versus hydroxide anions, (iii) structural and stoichiometric role of water in electrode reactions, (iv) electrode/electrolyte double-layer structure, and (v) general thermodynamic stability of non-noble metals. While all these factors have their own direct effects, the most crucial aspect is the confluence of all these factors toward impacting the electron transfer and electrocatalytic reaction mechanisms. These aspects are described here briefly and are taken up in more detail at the relevant place later in the article.

The Nernstian potential dependence of −59 mV/pH causes the working electrode potential range to nominally decrease by −0.83 V vs the standard hydrogen electrode (SHE) potential scale as the pH increases from 0 to 14.[42] For instance, the standard thermodynamic reduction potential of the hydrogen electrode (H^+/H_2) is 0 V versus SHE at pH = 0 which shifts to −0.83 V versus SHE at pH = 14. The first-order impact of this is on the excess surface charge on the electrode surface at alkaline pH. For instance, the electrode surface is suggested to carry an excess negative charge under alkaline conditions in comparison to acid which affects the adsorption of spectator and intermediate cationic or anionic species.[122,123] While this cannot be applied to all ionic species, one striking example of this aspect is the adsorption of chloride anions which are known to significantly poison the catalyst surface under acidic conditions via specific adsorption. Contrarily, it is less of a poison under alkaline conditions since the excess negative charge on the electrode surface tends to repel the anions away from the surface. Further, the change in working electrode potential range also directly affects the overpotentials of reactions that are pH-independent. For instance, the thermodynamic standard electrode potential of one-electron reduction of O_2 to form superoxide anion ($O_2^{\bullet-}$) is $E^0 = -0.3 \pm 0.03$ V versus SHE.[124,125] Given the pH independence of this redox couple $(O_2/O_2^{\bullet-})_{aq}$, the potential of this reaction does not change as the pH is varied from zero to 14.[126] Due to the occurrence of four proton-transfer steps in O_2 reduction to H_2O/OH^-, its standard reduction potential changes by 0.828 V from 1.229 to 0.401 V versus SHE as the pH increases from zero to 14 (i.e., 59 mV/pH). This causes the overpotential for the first electron transfer step ($O_2/O_2^{\bullet-}$) to decrease from 1.53 V at pH = 0 to 0.7 V at pH = 14, indicating a sharp decrease in overpotential at alkaline pH conditions. Electrode/electrolyte double-layer structure under alkaline conditions experiences an abundance of hydroxide anions, which is further complicated by the water molecules now acting as the source of protons besides their primary function as solvent molecules.

Besides the above-mentioned effects of the various factors, the most crucial change is related to how all these factors impact the electron transfer and electrocatalytic reaction mechanisms at high pH conditions. The dependence of electrocatalysis on reactant intermediates adsorbed/localized in the outer-Helmholtz plane (OHP) of the electrode/electrolyte double-layer structure is more prominent under alkaline conditions. For instance, (i) ORR can be conducted via an outer-sphere electron transfer mechanism on hydroxide-covered active sites that precludes the necessity for direct adsorption of O_2 on the active site thus enabling a wide range of non-noble electrode materials; (ii) the direct interaction of adsorbed hydroxide with the solvated alkali metal cations localized in the OHP influences the reaction kinetics; (iii) the drop in alkaline HOR activity on Pt is related to the overpotential required for the arrival of hydroxide anions in the OHP; (iv) contrarily, oxidation of CO on Pt in acid is dependent on the coadsorption of $Pt-CO_{ad}$ and $Pt-OH_{ad}$ on the electrode surface according to the Langmuir−Hinshelwood mechanism which involves a high overpotential. In alkaline media, the adsorbed CO_{ad} can now access the OH^- anions localized in the OHP which enables a decrease in the overpotential for CO oxidation on Pt according to the Eley−Rideal mechanism.

3. HYDROGEN OXIDATION REACTION IN ALKALINE MEDIA

Electrocatalysis of hydrogen oxidation reaction on platinum surface in alkaline electrolyte is a kinetically sluggish process and a major source of cell voltage loss in AAEM fuel cell performance.[30,127,128] HOR kinetics is characterized by at least 2 orders of magnitude lower exchange current density in alkaline electrolyte on Pt/C catalyst (ranging from 0.57 mA/cm^2_{Pt} in 0.1 M KOH to 2 mA/cm^2_{Pt} in solid alkaline electrolytes) compared to acid.[32,129] This translates to a cell voltage loss of ~130−150 mV in an AAEM fuel cell operating with an anode loading of 0.05 mg_{Pt}/cm^2 at 1.5 A/cm^2 current density and 80 °C cell temperature.[32] Figure 2 summarizes the magnitude of HOR kinetic losses in alkaline electrolyte. At a kinetic current density of 1 A/mg_{Pt}, higher overpotential of ~170 mV is observed in 0.1 M NaOH compared to 0.1 M $HClO_4$. In this section, we first discuss the fundamental mechanistic reasons for the higher alkaline HOR overpotential on Pt surfaces followed by a discussion on the improved HOR activity on Pt-alloys. In doing so, we attempt to clarify some of the controversies in the literature related to the alkaline HOR process, i.e., electronic/ligand versus bifunctional effects. A brief summary on the current status of non-Pt and non-PGM catalyst materials is also provided.

In acid, HOR is a simple and a kinetically rapid two electron process that involves the dissociative adsorption of molecular hydrogen on the catalyst surface as described below.

Acidic HOR reactions steps:

$$\text{Tafel:} \quad H_2 + 2M \rightarrow 2M{-}H_{ad} \quad \text{(rate determining step)} \quad (1)$$

$$\text{Heyrovsky:} \quad H_2 + M \rightarrow M{-}H_{ad} + H^+e^- \quad \text{(or)} \quad (2)$$

DOI: 10.1021/acs.chemrev.9b00157
Chem. Rev. XXXX, XXX, XXX−XXX

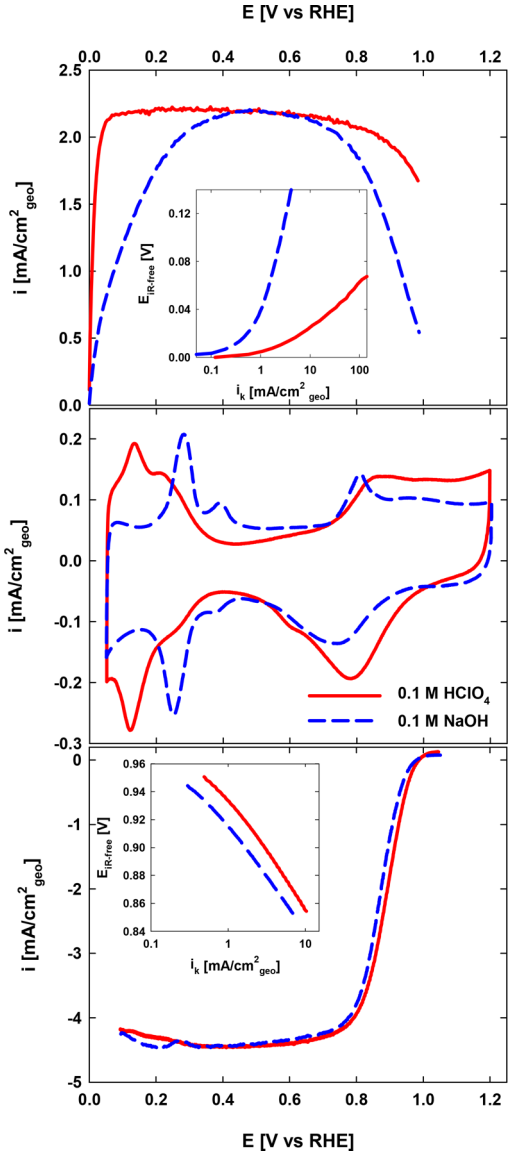

Figure 2. Comparison of Pt/C catalyst in 0.1 M $HClO_4$ and 0.1 M NaOH electrolytes. (Top) HOR curves in H_2 saturated electrolytes; (inset) mass-transport corrected Tafel plots. (Middle) Cyclic voltammetry in Ar saturated electrolytes. (Bottom) ORR curves at 900 rpm in O_2 saturated electrolytes; (inset) mass transport corrected Tafel plots. All experiments were carried out at room temperature using 15 $\mu g/cm^2$ Pt loading.

$$\text{Volmer:} \quad M{-}H_{ad} \rightarrow H^{+}e^{-} \tag{3}$$

At low to moderate overpotentials on Pt, HOR in acid proceeds via the Tafel-Volmer pathway involving the dissociative adsorption of molecular hydrogen to form $M{-}H_{ad}$ species as the rate-determining step followed by its oxidation to protons. HOR kinetics is primarily governed by the adsorption energy of the $M{-}H_{ad}$ reaction intermediate. Catalytic activity of HOR in acid represented as the exchange current density on various metal surfaces versus $M{-}H_{ad}$ bond energy exhibits a volcano-shaped curve. Highly active Pt surfaces lie at the top of the volcano curve and typically provide binding energies neither too strong nor too weak for the H_{ad} adsorption.[130−133]

In alkaline media, the adsorbed hydrogen intermediate (H_{ad}) formed in the Tafel step subsequently reacts with hydroxide anions to form water according to the following steps.[132,134]

Alkaline HOR reaction steps:

$$\text{Tafel:} \quad \rightarrow H_2 + 2M \rightarrow 2M{-}H_{ad} \tag{4}$$

$$\text{Heyrovsky:} \quad H_2 + OH^{-} + M \rightarrow M{-}H_{ad} + H_2O + e^{-} \quad \text{(or)} \tag{5}$$

$$\text{Volmer:} \quad M{-}H_{ad} + OH^{-} \rightarrow H_2O + e^{-} \quad \text{(rate determining)} \tag{6}$$

HOR in alkaline media on Pt is also understood to proceed largely via the Tafel-Volmer pathway but with the Volmer reaction as the rate-determining step.[135,136] The primary difference between acid and alkaline HOR is the involvement of OH^{-} anions in the Heyrovsk and Volmer steps. Hence at high pH, HOR kinetics is dependent not only on the $M{-}H_{ad}$ bond strength but also on the relevant processes furnishing reactive-hydroxide species.[35,134,137] The activation barrier for the Volmer reaction was found to increase from 17.1 to 34.0 kJ mol^{-1} in transitioning from acid to base.[135] While the Volmer step is largely agreed to be rate-limiting in alkaline electrolyte, there is some controversy on whether the $M{-}H_{ad}$ bond strength or the need for "reactive$-OH_{ad}$" species is the primary descriptor of the reaction. Correspondingly, there are two schools-of-thought to explain the slower alkaline HOR kinetics, namely the (i) hydrogen binding energy (HBE) theory[33,34,36,138] and (ii) "reactive$-OH_{ad}$" species theory.[35,37,72,139]

Proponents of the former theory suggest that the metal−hydrogen ($M{-}H_{ad}$) bond strength is the sole descriptor of HOR kinetics in alkaline media.[33,34,36,137,138,140,141] Accordingly, for any given catalyst surface, $M{-}H_{ad}$ (M = Pt, Pd, and Ir) bond strength is suggested to be stronger in the alkaline electrolyte than in acid which leads to HOR kinetics being slower at high pH conditions. For instance, Yan et al. studied the HOR kinetics on Pt in dilute electrolytes as a function of pH from 0.2 to 12.8. They suggested that the increasing overpotential for alkaline HOR process correlates linearly with the calculated "H-binding energy" values on Pt.[33] This was interpreted as an increase in the $M{-}H_{ad}$ binding energy with increasing pH that leads to a corresponding linear drop in the kinetic activity of Pt for alkaline HOR. Similar suggestions were also made by Durst et al., who calculated the "H-binding energy" of Pt to be ∼12.5−13.5 kJ mol^{-1} higher as the pH increases from 0 to 13.[34] Zhuang et al. took this hydrogen-binding energy theory one step further and suggested that alloying Pt with elements such as Ru would weaken the $Pt{-}H_{ad}$ binding energy, thereby increasing the alkaline HOR kinetics.[36] DFT calculations were also used in their study to suggest that "H-binding energy" on $Pt_3Ru(111)$ is −0.19 eV which is weaker than that of −0.33 eV calculated on the Pt(111) surface.

Proponents of the "reactive$-OH_{ad}$" theory suggest that the nonavailability of reactive$-OH_{ad}$ species at the reaction interface is the major cause for slower alkaline HOR kinetics.[35,139] For instance, Pt is known to be a very good catalyst for the dissociative adsorption of H_2 to form $Pt{-}H_{ad}$ but is not a good surface to form adsorbed hydroxide species ($Pt{-}OH_{ad}$) at potentials relevant for HOR reactions.[37] Since alkaline HOR depends not only on the formation of dissociatively adsorbed H_{ad} reaction intermediate but also on the availability of OH^{-} anions in a suitably reactive form at the reaction interface, it was suggested that HOR kinetics can be significantly improved by promoting hydroxyl ($M{-}OH_{ad}$) adsorption on the catalyst surface. This is referred to as the bifuncational effect of the alloys, wherein the H_{ad} species formed on the primary active site such as Pt in combination with more "oxophilic" alloying metals

DOI: 10.1021/acs.chemrev.9b00157
Chem. Rev. XXXX, XXX, XXX−XXX

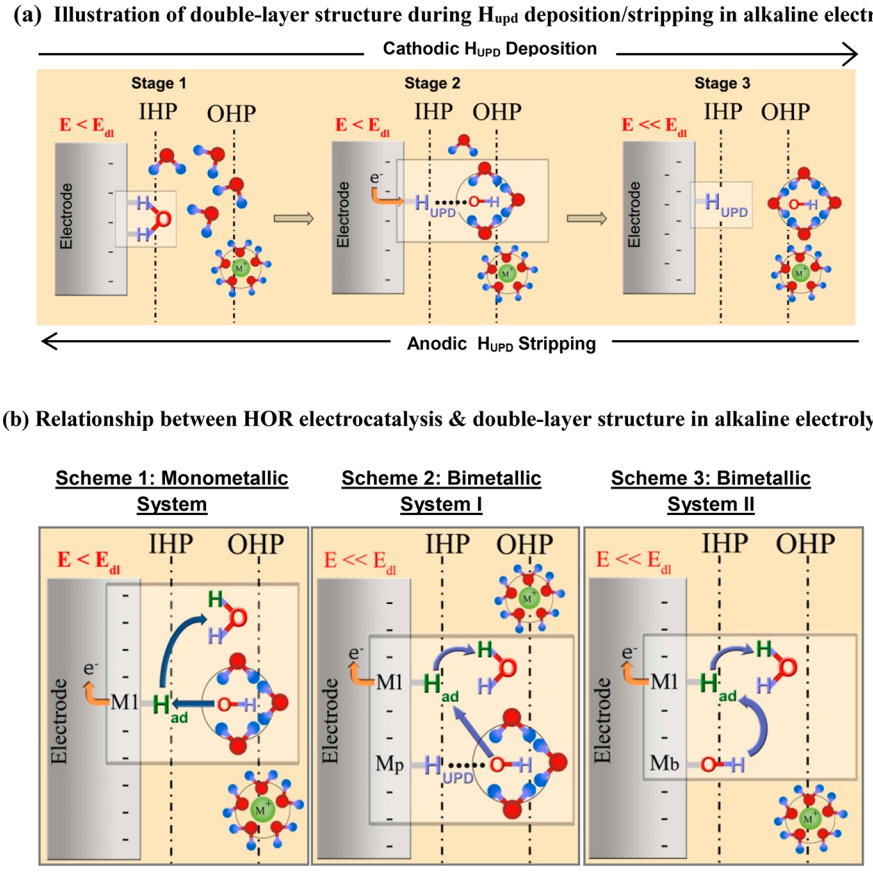

Figure 3. (Top) Schematic illustration of electrochemical double-layer structure during H_{UPD} deposition/stripping process in dilute alkaline electrolytes at various potentials with respect to the potential of the double-layer region (E_{dl}). (Bottom) Generic mechanistic reaction schemes for HOR in dilute alkaline electrolytes on mono- and bimetallic catalyst systems. M1 represents a metal site capable of dissociatively adsorbing molecular hydrogen. In scheme 2, alloy element M_p represents a precious metal site capable of forming H_{upd} in alkaline electrolyte. In scheme 3, alloy element M_b represents a base-metal site passivated with adsorbed (hydr)oxide species in dilute alkaline electrolytes.

(e.g., Ru or Ni) increases HOR activity significantly due to the enhanced formation of hydroxide species on the alloying element.[35]

One common limitation with the HBE theory is the way in which H-binding energy values are calculated. For instance, the H_{upd} peak potentials (E_{peak}) from cyclic voltammetry are simply multiplied by the Faraday constant (F) to arrive at an enthalpic number ($E_{M\text{-}H} = -E_{peak}F$) which is suggested to represent the strength of H-binding energy to the catalyst surface.[33,34] We would like to point out that the validity of such elementary methods needs to be revisited. Per se, such a method is indeed technically correct to calculate binding energies when applied on various catalyst surfaces in one single electrolyte pH. The validity of such an approach is questionable when applied on a single catalyst surface across electrolytes of varying pH. From basic principles of catalysis, it is reasonable to understand that the M−H_{ad} bond strength is different for various metal surfaces in any given electrolyte pH.[131] However, it is intriguing and quite unproven to note that for any given metal surface, the M−H_{ad} bond strength of a neutral atomic adsorbate such as H_{ad} becomes stronger with increasing pH. Such elementary H-binding energy calculation seriously overlooks some of the profound changes to the reaction mechanisms occurring at the alkaline electrode/electrolyte double layer. Such a method would be valid only if the responsible reactions and the accompanying mechanisms in the Pt−H_{UPD} process do not change as the pH traverses from acid to alkaline regime. We would like to point out that none of the proponents of the HBE theory has attempted to explain why H-adsorption on a given catalyst surface is stronger in alkaline electrolyte compared to acid. DFT studies that have been used to calculate atomic H-binding energies rarely account for the effect of changing pH.[33,36] Some recent DFT calculations by Rossmeisl et al. and theoretical studies by Anderson et al. that do include the pH effect in their calculations did not take into consideration the effect of changing reaction mechanisms as the pH is traversed from acid to alkaline conditions.[134,142−144] Rossmeisl et al. have made some important strides in incorporating the effect of pH via change in proton free energy and electron work function.[142] On the basis of this, pH has been found to affect adsorbate coverage and water dipole orientation and also pointed out that in activation energy calculations, the reaction barriers are highly dependent on the structure of water at the interface. The effect of these changes on the activation energies of various alkaline HOR reaction steps remain unexplored using DFT calculations. In this context, while the proponents of the HBE theory claim that the H-adsorption energy is higher in alkaline media on a given catalyst surface, some authors have also DFT calculations to show that there is actually a decrease in hydrogen-adsorption energy in going from acid to base on bulk Pt surface.[135] This seriously puts into question that validity of the HBE theory to convincingly explain the reasons behind the increase in HOR overpotentials on monometallic Pt surface under alkaline conditions.

DOI: 10.1021/acs.chemrev.9b00157
Chem. Rev. XXXX, XXX, XXX−XXX

On the contrary, while there are certain merits to the "reactive−OH_{ad}" theory in its existing format proposed by Markovic et al.,[35] there is a need to better understand the exact nature of the "reactive−OH_{ad}" species that is involved in the Volmer step of the alkaline HOR process. On monometallic Pt surfaces, it was suggested that reactive−OH_{ad} species are formed via specific adsorption of hydroxide anions on "Pt-defect sites" of the form Pt−OH_{ad}.[35] The authors proposed that such reactive species are formed even in the H_{upd} region at potentials well below the potential of zero charge (pzc). Electrocatalytic processes proceed via the reaction between adsorbed intermediates, and the hydroxide species (OH^-) in the second elementary reaction (Volmer step) should exist on the surface in an adsorbed state as OH_{ad} or in an analogous reactive form. One route for the formation of Pt−OH_{ad} species is via direct specific adsorption of hydroxide anions ($Pt + O\bar{H} \rightarrow Pt{-}OH_{ad} + e^-$). Further, Pt−$OH_{ad}$ species formation implies that the plane of closest approach of negatively charged OH^- anions is the inner-Helmholtz plane (IHP) where the hydroxide anions are largely desolvated and form the loci of specifically adsorbed species via a covalent bond on the positively charged Pt surface. It should be noted that H_{upd} formation and H_2-oxidation reaction occurs on Pt surfaces at potentials well below pzc where the surface is negatively charged. Invocation of "defect-sites" on Pt surface as a host for Pt−OH_{ad} in the H_{upd} region does not convincingly answer the problem; further it was clearly shown recently that Pt−OH_{ad} formation via specific adsorption of hydroxide anions occurs only at potentials ≥ 0.7 V versus RHE in 0.1 M NaOH; no evidence for the presence of Pt−OH_{ad} was observed in the H_{upd} potential region (≤0.45 V) via surface-sensitive X-ray absorption spectroscopic measurements.[37] This brings into question the exact nature of the reactive−OH_{ad} species responsible for the enhancement of alkaline HOR kinetics. It is important to clearly define the plane of closest approach of OH^- anions in the electrochemical double layer. The nature of this hydroxide species, its conditions, and source of formation requires detailed attention as this is a key elementary step during HOR in alkaline media causing higher overpotentials.

In order to understand the mechanistic changes involved during HOR reaction in alkaline media, it is pertinent to take a closer look at the H_{upd} deposition/stripping processes and identify the commonality between the H_{upd} stripping mechanism and the alkaline HOR process.[37] In acid electrolyte, Pt−H_{upd} formation simply involves the direct discharge of protons ($Pt + H^+ + e^- \rightarrow Pt{-}H_{upd}$). H_{upd} in alkaline media is formed via the one electron reduction of solvent water molecule on the electrode surface ($Pt + H_2O + e^- \rightarrow Pt{-}H_{UPD} + OH^-$). As a result of this reaction, OH^- anions are formed as a conjugate base in the compact part of the double layer. Classically, this hydroxide anion would be expected to diffuse away into the electrolyte bulk. Given the complexity of the electrochemical events in this process, we performed a series of thought experiments to sequentially visualize the elementary reaction steps in the H_{upd} deposition/stripping process with detailed attention to the double-layer structure. The process of H_{upd} formation upon cathodic potential sweep is illustrated in Figure 3a (stages 1−3) with respect to the double-layer potential region (E_{dl}). Ideally, in stage 1 ($E < E_{dl}$), the adsorbed water molecule could be imagined to be oriented with the hydrogen end toward the electrode surface (flip-down state of water molecule) prior to any electron transfer. After the one electron transfer process (stage 2, $E < E_{dl}$), hydroxide anion is not completely cleaved from the water molecule but rather is only partially cleaved to form the cluster Pt−H_{upd}···$OH_{q\text{-}ad}$, wherein the hydroxide species is represented to be in a quasi-adsorbed state stabilized in the outer-Helmholtz plane via hydrogen (H_{upd})-bond formation. Only upon further drop in electrode potential (stage 3, $E \ll E_{dl}$), hydroxide anion could be considered to be completely cleaved from the H_{upd} adsorbate. The reverse of this process essentially occurs during the anodic H_{upd} stripping (Figure 3a, stages 3 through 1). In such a case, the approach of the negatively charged hydroxide anions would essentially be limited to the outer-Helmholtz plane, thereby forming the cluster Pt−H_{upd}···$OH_{q\text{-}ad}$ followed by water molecule formation. In this process, the larger overpotential required for the H_{upd} stripping process arises due to the voltage penalty required to draw the negatively charged hydroxide anions to the plane of closest approach (i.e., OHP) of a negatively charged electrode surface. This modern rendition of the H_{upd} deposition/stripping mechanism takes into account the critical role of the electrochemical double-layer structure at an alkaline electrode/electrolyte interface. The most critical aspect of this proposition in the H_{upd} deposition and stripping mechanism is the bond breaking and bond formation of the water molecule, respectively, that involves the formation of a unique transition state structure of the form Pt−H_{upd}···$OH_{q\text{-}ad}$, which requires higher activation energy.[37,135] Such processes simply do not occur in acid electrolyte.

The above rendition can be extended to explain the higher overpotentials required for alkaline HOR kinetics on monometallic Pt surfaces as depicted in Figure 3 (scheme 1).[37] In the HOR process, the reaction intermediate is represented by the dissociatively adsorbed H_2 on Pt active sites of the form Pt−H_{ad}. There is a voltage penalty involved in the process of drawing the negatively charged OH^- anions to the plane of closest approach of a negatively charge Pt surface covered with H_{ad} reaction intermediate. This leads to the formation of a transition state cluster Pt−H_{ad}···$OH_{q\text{-}ad}$ prior to the formation of the water molecule. The bond formation of the final product water molecule involves the assemblage of an exclusive transition state structure of the form Pt−$H_{upd/ad}$···$OH_{q\text{-}ad}$, which requires additional activation energy to draw OH^- anions to the plane of closest approach (i.e., OHP and not IHP) of a negatively charged electrode surface. On monometallic Pt surfaces, the nature of the "reactive−OH_{ad}" species is the quasi-specifically adsorbed ($OH_{q\text{-}ad}$) hydroxide anions located in the outer-Helmholtz plane.

Interestingly, the above findings of alkaline HOR mechanisms on monometallic Pt surfaces being limited by the bond-formation process of the product water molecule are in excellent agreement with the recent development in alkaline H_2-evolution reaction mechanisms where the bond breaking of H_2O molecules was shown to be the major limitation for the sluggish HER kinetics.[37,135,145] In the context of the alkaline HER process, Subbaraman et al. showed that while Pt is a good catalyst for adsorption and recombination of the reactive hydrogen intermediate (H_{ad}), it is generally inefficient in the prior step of water dissociation.[145] Similarly, while Pt is an excellent catalyst surface for the dissociative adsorption of H_2 to form H_{ad}, it is an inefficient material by itself to enable the formation of water molecules during alkaline HOR. Further, this is also in agreement with Wang et al., who suggested that the intrinsically low mobility of OH^- may cause an increase in activation barrier for the Volmer reaction in the alkaline HOR process.[135]

DOI: 10.1021/acs.chemrev.9b00157
Chem. Rev. XXXX, XXX, XXX−XXX

Given the limitations of pure Pt surface as a sluggish catalyst for alkaline HOR, several authors have suggested bimetallic or composite catalyst materials such as PtRu, PtCu, PtNb, PtNi, PdNi, PdIr, Pd/C−CeO_2, etc.[35−37,135,137,139,141,146−149] Typically, these alloy catalysts provide HOR activity much higher than that of pure Pt. For instance, Figure 4 shows that the HOR

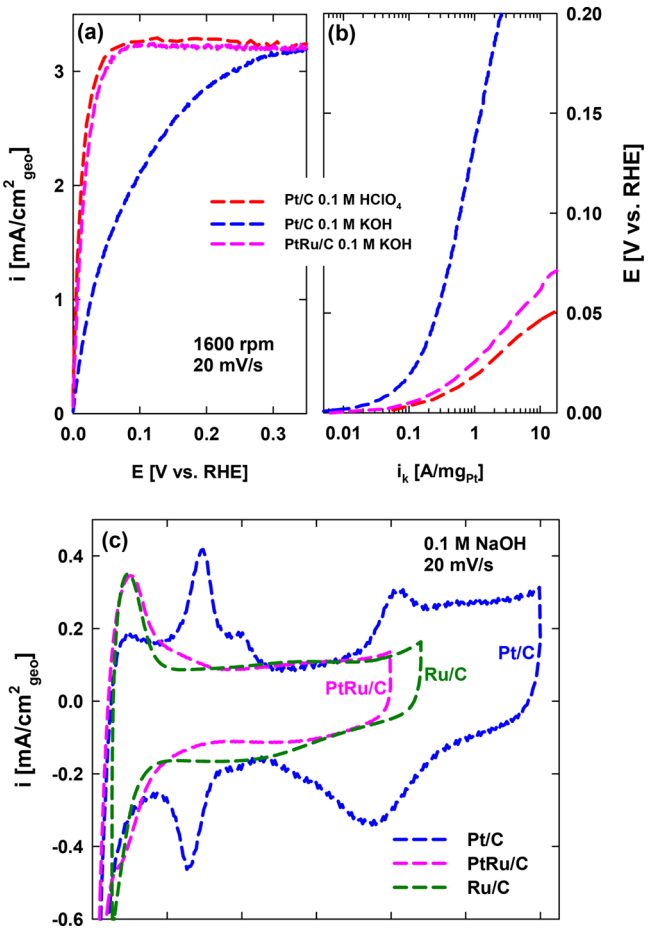

Figure 4. HOR electrocatalysis on bimetallic catalysts in alkaline electrolyte. (a) HOR curves, (b) Ohmic and mass transport corrected Tafel plots in H_2 saturated electrolytes, and (c) cyclic voltammetry in argon-saturated electrolyte. All measurements carried out at 40 °C.

activity of PtRu/C bimetallic catalysts in 0.1 M NaOH is very comparable to pure Pt/C catalyst in dilute acidic electrolyte. For instance, at i_k = 1 A/mg$_{Pt}$ HOR overpotential on PtRu/C is minimized by 110 mV in comparison to Pt/C in alkaline electrolyte. This is in good agreement with the HOR activity improvements demonstrated across various laboratories. Exchange current densities of PtRu alloys have been demonstrated to be roughly 3 to 4-fold higher (1.42 mA/cm$^2_{PtRu}$ for $Ru_{0.2}Pt_{0.8}$ vs 0.49 mA/cm$^2_{Pt}$ for Pt) than that of Pt in dilute alkaline electrolytes.[35,37,135,139,141] This represents a significant set of results because it shows that use of Pt-alloys can provide a pathway for the decrease in Pt loading at the AAEM fuel cell anode comparable to that of PEM fuel cell anode loading levels (~0.025 to 0.05 mg$_{Pt}$/cm^2).

Proponents of the H-binding energy theory suggest that PtRu shows an improvement in HOR activity due to an electronic effect wherein the Ru alloy weakens the Pt−H_{ad} bond strength.[36,141] Contrarily, proponents of the "reactive−OH_{ad}" theory suggest that Ru being very "oxophilic" promotes HOR activity in alkaline media via formation of specifically adsorbed Ru−OH_{ad} species.[35,139] According to the latter schemes in literature, Pt−H_{ad} intermediate is proposed to directly react with Ru−OH_{ad} (formed via $O\bar{H}$ specific adsorption) thereby enhancing HOR activity. However, our recent studies have clearly shown that at potentials less than 0.2 V vs RHE, there is no spectroscopic evidence for the formation of Ru−OH_{ad}.[37] It should be noted that HOR on PtRu reaches limiting current densities well below 0.2 V thereby questioning the mechanism of HOR on PtRu that leads to the significant improvement.

We have recently extended on our double-layer structural model to explain the phenomenon of improved HOR activity on Pt-alloy surfaces.[37] In accordance with this scheme, Ru was shown to enable the formation of H_{upd} at potentials below 0.2 V via one electron reduction of water molecules (Ru + H_2O + e^- → Ru−H_{upd} + OH^-). This is evidenced by the Ru−H_{upd} deposition/stripping peak centered at 0.10 V versus RHE in dilute alkaline solutions. On the basis of our modern rendition of the electrochemical double-layer structure discussed above, this suggests the formation of quasi-specifically adsorbed hydroxide species on Ru in the outer-Helmholtz plane of the form Ru−H_{upd}···$OH_{q\text{-}ad}$. Accordingly, Pt−H_{ad} intermediate reacts with the quasi-specifically adsorbed hydroxide species ($OH_{q\text{-}ad}$) on Ru to enable the bond formation of the final product water molecule. In essence, the Ru alloy accelerates alkaline HOR kinetics on Pt by enabling the bond formation of the final product water molecule by furnishing the quasi-specifically adsorbed reactive hydroxide species. It should be noted that the reactive hydroxide species furnished by Ru is formed via 1e$^-$ reduction of water molecules to form H_{upd}. As depicted in Figure 3b (xcheme 2), in the cases of alloying elements such as Ru, Ir, or Pd, where H_{upd} formation is possible, the nature of the "reactive−OH_{ad}" corresponds to the quasi-specifically adsorbed hydroxide species localized in the outer-Helmholtz plane formed via 1e$^-$ reduction of water molecules of the form Ru−H_{upd}···$OH_{q\text{-}ad}$.

In the cases of alloying elements such as Cu, Ni, Co, Nb, etc., where the transition alloying element does not show H_{upd} formation but rather are passivated by layers of oxide/hydroxide film on its surface, the following simple bifunctional mechanism could be proposed to occur.[35,37,137] This is depicted in Figure 3b (scheme 3). Pt−H_{ad} intermediate reacts with specifically adsorbed (M−OH_{ad}) reactive species formed on an adjacent base alloy metal in the fashion of $NbO_x(OH_y)$/Cu−OH_{ad}/Ni−OH_{ad} to enhance the alkaline HOR process. Only in such cases, the "reactive−OH_{ad}" species can be attributed to the simple specifically adsorbed hydroxide species on the base alloying element. It should be noted while the availability of "reactive−OH_{ad}" is rate limiting for alkaline HOR processes, an optimal adsorption of hydrogen binding to the primary active site is still required on the primary catalytic metal site. It is only suggested that the binding energy of Pt−H_{ad} for a given catalyst does not change significantly with varying pH and is no more important than what it already is in acidic electrolytes.

Recently, several studies have been carried out to investigate the alkaline HOR kinetics of PtRu catalyst and deduce the reasons for its improved activity over Pt. Given the importance of PtRu as a catalyst for the alkaline HOR process, we provide a case study of this material and attempt to draw some generalized conclusions on its activity and reaction mechanisms. Wang et al. argued that the HOR kinetics on PtRu is better than Pt because of the electronic effect of Ru on decreasing the binding energy of Pt−H_{ad}.[36] On the basis of cyclic voltammetry of Pt and PtRu in 0.1 M KOH electrolyte, they suggested that the Pt−H_{upd} peak

DOI: 10.1021/acs.chemrev.9b00157
Chem. Rev. XXXX, XXX, XXX−XXX

observed at ~0.3 V on pure Pt ("strong H_{ad}") is cathodically shifted to ~0.1 V ("weak H_{ad}") on PtRu catalyst, indicating a weakening of Pt−H binding energy upon alloying Pt with Ru. The authors claimed that the weakening of binding energy was also apparently corroborated by their DFT calculations. We would like to point out that first of all the H_{upd} at 0.1 V on the PtRu catalyst is related to Ru−H_{upd} stripping and is not due to the "weakened Pt−H_{upd}" stripping process. A simple comparison of a cyclic voltammetry between PtRu and pure Ru would have avoided such confusions, and the results of Wang et al. cannot be used as evidence of electronic effect of Ru on Pt. In a recent study, St. John et al. have investigated the alkaline HOR kinetics on Pt-rich $Pt_{0.8}Ru_{0.2}$ and Ru-rich $Ru_{0.8}Pt_{0.2}$ nanocatalyst alloys.[139] While the cyclic voltammetry of their Ru-rich alloy is inevitably reflective of the surface Ru content (as evidence by the Ru−H_{upd} formation below 0.2 V in their publication), a Pt-rich alloy yields interesting results that help deconvolute the electronic versus bifunctional effects of the alloy catalyst. For instance, it is observed from their publication that while the Pt−H_{upd} peak in $Pt_{0.8}Ru_{0.2}$ catalyst cathodically shifted only a few mV (~5 mV) in the 0.1 M KOH electrolyte, the HOR activity on the same catalyst showed improvements on the order of several tens of mVs (~40 to 50 mV) at 2 mA/cm^2 current density along with a 3-fold increase in exchange current density compared to pure Pt (0.49 mA/cm^2_{metal} for Pt vs 1.42 mA/cm^2_{metal} for $Pt_{0.8}Ru_{0.2}$). This clearly indicates that the ligand effect of Ru on Pt cannot be completely rejected, but it only confers a very small effect on the HOR activity improvement in comparison to the dominant bifunctional effects. On the basis of a Tafel slope analysis, it was suggested that for a pure Pt catalyst, the Volmer step is rate-determining in an alkaline electrolyte, whereas on PtRu surfaces dissociative adsorption of molecular H_2 (Tafel rds) is rate-determining. The interplay between the ligand and bifunctional effects of Ru on Pt causes the transition of the rate-determining step from the Volmer step for pure Pt to Tafel step for PtRu alloys.[139]

One way to distinguish whether the bifunctional mechanism or the ligand effect is the dominant reason for improved HOR activity on Pt-alloys is to study them using core−shell structures such that Pt is preferentially located on the surface of a core element. In that context, two independent studies clearly suggest that the Ru@Pt core−shell structure with a Ru core and roughly two monolayer Pt shell catalysts has at least similar activity or a higher activity by a factor of 2 compared to Ru_xPt_{1-x} (x = 0.2 to 0.6) alloy nanocatalysts (based on total noble metal loading).[135,141] This suggests that placing the Pt atoms selectively on the surface of the Ru core may be beneficial in terms of the resultant catalyst activity toward the alkaline HOR process and help minimize the precious metals usage.[135,141] In one of these studies, while the authors suggested the catalyst to consist of Ru-core with two monolayers of Pt-shell, the cyclic voltammetry of this catalyst suggested that there was still a significant fraction of Ru exposed to the electrolyte (see Figure 4a in the referred article where the Ru−H_{upd} peak less than 0.2 V is still evident).[135] In the other study, HOR activity of the Ru@Pt core−shell catalyst was studied as a function of Pt monolayer coverage from 0.3 to 2.6 in alkaline electrolyte.[141] It was shown that increasing the coverage of Pt on Ru from 0.3 to 2.0 monolayer led to a smooth and continuous increase in HOR activity beyond which (>2.0 monolayer) the activity dropped since the surface was apparently covered exclusively by Pt overlayers. The authors suggested that the continuous increase in activity with no sudden drop after completion of one Pt-monolayer demonstrates the electronic/ligand effect since in a purely bifunctional mechanism a sudden drop in activity would be expected after completion of a Pt monolayer with no Ru present on the surface. While this is an interesting observation, we would like to point out that the characterization of their core−shell catalyst surfaces in an alkaline electrolyte was not shown. The surface of the catalyst was studied using cyclic voltammetry and CO-stripping measurements in acidic electrolytes to draw conclusions regarding its mechanisms for the HOR process in alkaline electrolytes.[141] Given that the HOR and CO-stripping mechanisms are considerably different in acid and alkaline electrolyte, it would be more relevant to characterize a given catalyst in the electrolyte of interest to understand its surface nature prior to drawing conclusions.

In an another independent study, Ru nanotubes with Pt overlayers were investigated wherein the surface coverage of Pt on Ru was varied from 0.24 to 0.94.[146] A plot of the HOR activity vs Pt coverage suggested a peak in performance at Pt coverage of 0.8 on Ru nanotubes followed by a drop in activity as the Pt coverage reached 0.94. This clearly suggests that the presence of surface Ru is required for improvements in HOR activity. An analysis of Pt L_3 X-ray absorption spectra indicated an electronic interaction between Ru and Pt which was evidenced by electron donation from Ru to Pt and a compression of the Pt−Pt nearest neighbor interactions. This indicates that the effect of electronic interaction between Pt and Ru cannot be completely eliminated. This is also confirmed by a Tafel slope analysis that suggests a 86−94 mV/dec for PtRu nanotubes which is intermediate between what would be expected for a pure Tafel rds (~30 mV/dec) and Volmer rds (120 mV/dec). These conclusions are in accordance with earlier studies on PtRu alloys for CO electrooxidation reaction, wherein it was found that Ru does have a minor electronic effect on Pt.[150,151] Ru was shown to alter the Pt electronic density of states near the d-orbital via electron donation to Pt and a compressive strain effect on the Pt−Pt bond distance. These earlier studies clearly suggest that the electronic/ligand effect of alloying Pt with Ru abets the bifunctional effects existent on the catalyst surface.

In summary, it is clear that for monometallic Pt catalyst the nonavailability of reactive−OH_{ad} species is the major cause of low alkaline HOR activity. On the other hand, the enhancement observed on Pt-alloy catalysts appear to be largely due to the dominant bifunctional effects, and the contributions from electronic/ligand or lattice compression (strain) effects appear to be minor.[137,146] The presence of the electronic/ligand effect versus the bifunctional mechanism should be considered depending upon the nanoparticle structure and synthesis procedure under consideration. Irrespective of the specific reasons of improved activity, the most enticing aspect is that the Pt-alloys have demonstrated enhanced alkaline HOR kinetics significantly to levels that can match Pt/C in dilute acidic electrolytes. It signifies that very low Pt loadings currently used in PEM fuel cell anodes (0.025 to 0.05 mg_{Pt}/cm^2) could be enabled in AAEM fuel cells as well.

While PtRu-based catalyst certainly provide great technological promise for the AAEM fuel cell, the application of non-Pt or non-PGM anode catalysts would be of ultimate success. The search for an alternate to Pt for HOR should likely begin with a good understanding of volcano plots based on Sabatier's principles of catalysis to find non-Pt materials that provide optimal binding of hydrogen-adsorbed reactive intermediate. It is typically observed that Pt-based surfaces exhibit hydrogen

DOI: 10.1021/acs.chemrev.9b00157
Chem. Rev. XXXX, XXX, XXX−XXX

adsorption bond strengths that are neither too strong nor too weak, thereby positioning itself at the top of the volcano plot. Other elements such as Pd, Ir, and Ru from the precious metal group fall very close to Pt near the top of the volcano plot.[132,152,153] Elements such as Ag, Au, and Cu with low hydrogen-adsorption energies are observed on the descending portion of the volcano plot, whereas base transition metals such as Ni, Co, Fe, and W fall on the ascending portion of the curve due to their high reactivity and binding energies for H_{ad}.[152,153] Few recent studies have investigated non-Pt elements from the precious metals groups such as Pd, Ru, and Ir for alkaline HOR applications.[34,138,139,146] Monometallic Pd/C shows a very low exchange current density even when compared to Pt/C in 0.1 M NaOH (~0.06 mA/cm$^2_{Pd}$ vs 1 mA/cm$^2_{Pt}$ at 313 K).[34] Studies on bimetallic PdIr[149] and Pd/Ni[72,148] materials demonstrate some improvements in their HOR activity over pure Pd. However, these improvements on bimetallic Pd materials are insufficient as they are able to match the activity of monometallic Pt in dilute alkaline electrolyte but still well below the PtRu activity. While Ru and Ir typically show low alkaline HOR exchange current densities compared to Pt, some recent studies do suggest that the activity is strongly dependent on the particle sizes. Yan et al.[138] and Ohyama et al.[154] suggested that 12 nm Ir and 3 nm Ru particle size very high HOR activities are observed as these materials expose the critical metal surface structure and crystalline facets that are responsible for the peak activity.

Non-pgm materials based typically on Raney Ni and Ni-alloys have long been used in alkaline electrolyzers for hydrogen evolution.[155,156] Taking cue from these applications, recent studies have investigated the possibility of using Ni-based catalysts for alkaline HOR. Ni tends to adsorb H_2 reaction intermediates (Ni−H_{ad}) very strongly compared to Pt and, hence, are typically found on the ascending portion of the volcano curve.[152] Studies on Ni-based catalyst have resulted in wide-ranging exchange current densities due to highly sensitive nature of the Ni-surface structure/composition that strongly depends on the electrode pretreatment and conditioning procedure. Recent studies suggest that metallic Ni electrodes conduct HOR/HER via the Heryrovsky-Volmer pathway and "activation" of the surface via oxidation to form NiO islands on the metallic Ni surface leads to an improvement in activity and a concomitant decrease in hydrogen intermediate adsorption energy.[157] However, it should be noted that the exchange current densities on these Ni/NiO nanoparticle surfaces are at best on the order of a few tens of μA/cm$^2_{Ni}$. Zhuang et al. operated AAEM fuel cell with a NiCr alloy anode catalyst that exhibited a current density of ~0.60 A/cm^2 at 0.65 V (H_2/O_2 cell operating at 60 °C, 100% RH, 130 kPaa, Ag-based cathode).[83] They suggested that alloying Ni with Cr suppresses the formation of oxides on Ni thereby potentially enhancing the adsorption of hydrogen reaction intermediate. The half-cell performance of NiCr anode in a liquid electrolyte was not shown in this study which makes the quantification of its HOR activity difficult. Encouraging results have also been recently published by Yan et al. on non-pgm HOR catalysts such as NiCoMo alloy and Ni/N-doped CNT.[158,159] In the case of NiCoMo, a 20-fold higher HOR activity was observed compared to pure Ni and claimed to outperform Pt at high enough loadings. The alloy was suggested to provide a hydrogen-binding energy similar to that of Pt which was suggested to be the reason for its high performance. Similarly, deposition of Ni on nitrogen-doped carbon nanotubes showed a significant enhancement of HOR activity compared to unsupported Ni due to the presence of both a stabilizing support material and the electronic effect of nitrogen on nickel. Ni/N−CNT catalyst exhibited an exchange current density of 0.028 mA/cm$^2_{Ni}$, which is significantly better than pure Ni but still an order of magnitude lower than Pt. More studies that demonstrate high alkaline HOR activity and elucidate reaction mechanisms on non-PGM catalyst materials are clearly warranted. Particularly, studies that demonstrate the performance of non-PGM anode catalysts in comparison to PGM systems in AAEM fuel cell MEA configuration is required. Further, while a better understanding of the reaction mechanisms in alkaline electrolyte could help design PGM catalysts for HOR, the non-PGM anode catalysts are primarily limited by the stronger binding energy H-adsorbed intermediate. Hence, the focus of non-PGM anode catalyst development should be more on strategies to improve the HBE and not necessarily on mechanistically enabling hydroxide availability at the reaction site.

4. OXYGEN REDUCTION REACTION IN ALKALINE ELECTROLYTE

The objective of this section is to provide a selective review to capture the unique mechanistic aspects of the alkaline ORR process that enables distinctive reaction pathways at high pH. The subject of ORR is too vast to compile in this section here. Interested readers are referred to articles by Spendelow et al.,[42] Ge et al.,[160] Shao et al.,[161] and He et al.[162] which provide excellent materials-based reviews on various precious and nonprecious catalysts surfaces. From the perspective of reaction mechanisms, there are two critical aspects that distinguish ORR in alkaline media from acidic conditions. They are related to the (i) nature of the first electron transfer step to molecular O_2 and (ii) base catalysis of the hydrogen peroxide intermediate.

4.1. Nature of the First Electron Transfer Step to O_2

The single biggest challenge for ORR catalysis in acidic electrolytes is in enabling the initial adsorption of molecular O_2 at an optimal binding energy with or without the electron transfer. This critical requirement narrows down the choice of catalytic materials to the precious metals group with optimal *d*-band electronic structure and geometric features that provides a sufficiently high free energy of adsorption for O_2 and other related reaction intermediates.[163−166] On the other hand, the lack of necessity for O_2 adsorption prior to the first electron transfer at high pH conditions liberates the entire ORR process from this critical requirement thus enabling a wide range of electrode materials at high pH conditions. Such a scenario arises due to the possibility of outer-sphere electron transfer mechanism under alkaline conditions, which is discussed briefly here in this section.[38,167,168]

There are two mechanisms for ORR in alkaline electrolytes. The first mechanism is the well-known electrocatalytic inner-sphere electron transfer (ISET) mechanism where molecular O_2 undergoes direct chemisorption, either dissociatively or associatively, on oxide-free Pt site leading to a direct/series 4e$^-$ pathway without the desorption of reaction intermediates such as peroxide from the surface according to the following reaction scheme.[169−174]

$$\text{initial adsorption:} \quad O_2 \rightarrow O_{2,ad} \tag{7}$$

$$\text{direct pathway:} \quad O_{2,ad} + 2H_2O + 4e^- \rightarrow 4OH^- \tag{8}$$

$$\text{series pathway:} \quad O_{2,ad} + e^- \rightarrow (O_2^{\bullet -})_{ad} \tag{9}$$

DOI: 10.1021/acs.chemrev.9b00157
Chem. Rev. XXXX, XXX, XXX−XXX

$$(O_2^{\bullet -})_{ad} + H_2O \rightarrow (\bullet OOH)_{ad} + OH^- \quad (10)$$

$$\bullet OOH_{ad} + e^- \rightarrow (HO_2^-)_{ad} \quad (11)$$

$$(HO_2^-)_{ad} + H_2O + e^- \rightarrow \bullet OH_{ad} + 2OH^- \quad (12)$$

$$\bullet OH_{ad} + e^- \rightarrow OH^- \quad (13)$$

Direct pathway involves the concerted transfer of $4e^-$ to adsorbed molecular oxygen to form OH^- anions without the formation of peroxide reaction intermediates. Series pathway involves the sequential transfer of $4e^-$ to the adsorbed molecular O_2 to form OH^- anions via the progressive formation of adsorbed reaction intermediates such as superoxide $(O_{2\ ad}^{\bullet -})$ hydroperoxyl radical $(\bullet OOH_{ad})$, hydroperoxide anion (HO_{2ad}^-), and hydroxyl radical $(\bullet OH_{ad})$. Surface-enhanced infrared spectroscopy has been used to detect the presence of adsorbed superoxide on Pt and hydroperoxide species on Au catalyst surfaces which strongly indicates that the $4e^-$ ORR process progresses via the series pathway.[174−176] In both these pathways, the rate-determining step on Pt-based surfaces is widely known to be either the initial adsorption of molecular oxygen[172] or the first electron transfer step to the adsorbed molecular O_2.[177−179] Recent DFT calculations suggest that the water molecules involved in the associative $4e^-$ transfer pathway are present at the interface in a chemisorbed state (H_2O_{ad}) and not simply in its aqueous form (H_2O_{aq}) with the reaction potential strongly determined by the conversion of adsorbed hydroxyl radical $(\bullet OH_{ad})$ to OH^-.[180]

The double-layer structure in a dilute alkaline electrolyte under ORR conditions is shown in Figure 5c.[38] Cathodic potentials of oxygen reduction in an operating fuel cell typically occur at potentials well positive of the potential of zero charge (pzc). At high pH environment water molecules act not only as solvent but also serve as the source of protons required in ORR. IHP is populated by specifically adsorbed hydroxyl species (OH_{ads} arising from OH^- anion adsorption), solvent water dipoles, and chemisorbed O_2. Presence of both OH^- and the H_2O leads to the formation of a compact H-bonding network in the double-layer that affects adsorption configuration of O_2.[181] Alkali metal ions are typically well solvated and are classically expected to populate the OHP. Figure 5c (inset a) shows the well-known electrocatalytic ISET mechanism which involves direct chemisorption of desolvated oxygen molecule on an oxide-free Pt site to form $O_{2,ads}$ followed by a direct/series $4e^-$ ORR pathway.

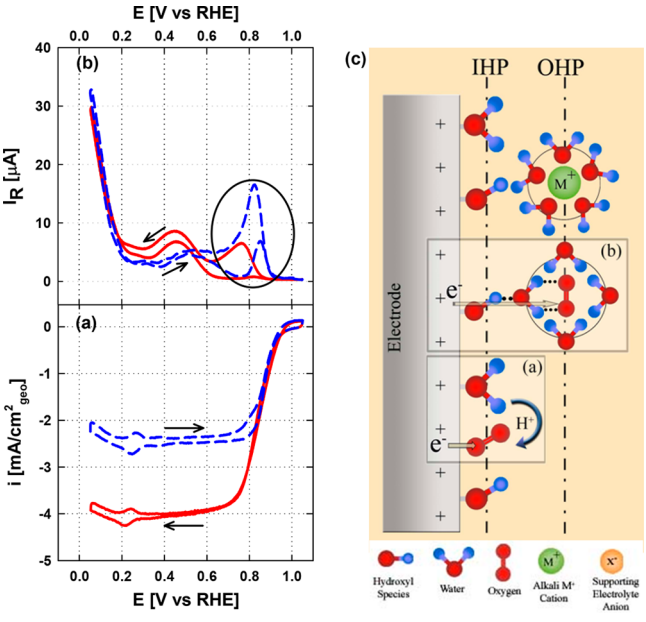

Figure 5. Comparison of electrochemical characteristics of Pt/C in 0.1 M NaOH and 1.0 M NaOH electrolytes at a loading of 15 $\mu g_{Pt}/cm^2$ on 5.61 mm Glassy Carbon disk electrode. (a) ORR polarization curves, (b) ring currents measured in O_2 saturated electrolytes at 900 rpm and 20 mV/s, and E_{ring} = 1.1 V vs RHE; (c) schematic illustration of the double-layer structure during ORR in alkaline conditions; Insets (a) and (b) illustrate the inner and outer-sphere electron transfer processes.

The second mechanism is the outer-sphere electron transfer (OSET) mechanism where the solvated molecular O_2 cluster written here as the $O_2{\cdot}(H_2O)_n$ cluster undergoes the electron transfer process without directly chemisorbing on the catalyst active site.[38] For electrocatalytic reactions, it is typically assumed that the molecular adsorption of reactant species (dissociatively or nondissociatively) is the first step.[182] Multistep, multielectron transfer processes like ORR that involves many adsorbed intermediates undoubtedly classifies as an inner-sphere electron transfer reaction. However, among the many elementary reaction steps involved in ORR there could be a surface-independent outer-sphere electron transfer component in the overall electrocatalytic $4e^-$ inner-sphere electron transfer reaction.[168] In that perspective, the standard electrode potential of one-electron reduction of O_2 to form superoxide anion $(O_2^{\bullet -})$ is thermodynamically expected at $E^0 = -0.3 \pm 0.03$ V versus SHE corresponding to $\Delta G^0 = 30 \pm 2$ kJ mol^{-1} with both O_2 and $O_2^{\bullet -}$ remaining in the aqueous phase.[124,125]

$$O_{2,aq} + e^- \rightarrow (O_2^{\bullet -})_{aq} \quad E^0 = -0.33\text{V vs SHE} \quad (14)$$

Given the pH independence of this redox couple $(O_2/O_2^{\bullet -})_{aq}$, the potential of this reaction does not change as the pH is varied from 0 to 14.[126] Due to the occurrence of four proton-transfer steps in O_2 reduction to H_2O/OH^-, its standard reduction potential changes by 0.828 V from 1.229 to 0.401 V vs SHE as the pH increases from 0 to 14 (i.e., 59 mV/pH). This causes the overpotential for the first electron transfer step $(O_2/O_2^{\bullet -})$ to decrease from 1.53 V at pH = 0 to 0.7 V at pH = 14, indicating a sharp decrease in overpotential at alkaline pH conditions. Markovic et al.[126] argued based on a modified Pourbaix diagram approach that the above-mentioned decrease in overpotential is the primary thermodynamic reason for the applicability of a wide range of non-noble materials in alkaline media. Due to the high overpotential required for $(O_2/O_2^{\bullet -})_{aq}$ redox couple in acidic media, only certain specific catalyst surfaces such as platinum that offer high free energy of adsorption for O_2 can catalyze ORR in acidic media. In alkaline media, decrease in overpotential for $O_2/O_2^{\bullet -}$ causes almost all electronically conducting electrode material to be ORR active at alkaline pH.[126] While the decrease in overpotential for the first electron transfer is certainly significant, this argument is primarily of thermodynamic origin.

The experimental kinetic evidence for the OSET mechanism is observed in the ring-electrode behavior during the alkaline ORR process.[38,183−186] Figure 5 shows the rotating disk-ring current during ORR on Pt/C catalyst in dilute alkaline solutions. The ring current due to peroxide oxidation in 0.1 M NaOH electrolyte shows a sharp peak feature in the region around 0.8 V, which is closely related to Pt−OH formation from specific adsorption of hydroxide anions as seen from the cyclic

DOI: 10.1021/acs.chemrev.9b00157
Chem. Rev. XXXX, XXX, XXX−XXX

voltammetry in the 0.1 M NaOH electrolyte (Figure 2). Oxide formation on Pt in acidic media is due to oxidation of the solvent water molecules (water activation), and in alkaline media, it is due to specific adsorption of hydroxide anions from the supporting electrolyte.[39,173,187−189] As shown in Figure 2, the onset potential of Pt−OH formation is similar in both electrolytes, although in alkaline media oxide formation current exhibits a characteristic peak shape where as in acidic media oxide formation current is relatively more flat. In the 0.1 M NaOH electrolyte, Pt−OH formation commences at ∼0.7 V versus RHE, reaches a peak current at 0.81 V, and a plateau at ∼0.9 V. On the cathodic direction, the peak potential for Pt−OH reduction is ∼0.75 V vs RHE. As seen in Figure 5, on the cathodic ORR scan, the increase in ring current commences at 0.9 V and reaches a peak potential of 0.75 V vs RHE. This clearly indicates that there is an interaction between molecular oxygen and the hydroxyl species on the surface. This interaction leads to the formation of hydrogen peroxide intermediate which is detected at the ring electrode. Detection of peroxide intermediate at the ring electrode has been observed previously on precious metal surfaces such as Pt, Pd, and Ru in the oxide/hydroxide formation region.[190−193] Further, among the various single crystal Pt surfaces, this peak peroxide production is prominently observed on the (100) and (110) surfaces.[173]

Looking back at the double layer structure in alkaline media depicted in Figure 5 (inset b), the solvated molecular O_2 cluster ($O_2{\cdot}(H_2O)_n$) is shown to interact with the surface hydroxyl species (OH_{ads}) via a hydrogen bond between H atom in OH_{ads} and O atom in the solvent water molecule. Such hydrogen bond energies (<35 kJ mol^{-1}) are typically much lower than the energy associated with covalent bond strength such as in the case of direct chemisorption of O_2 on Pt (>300 kJ mol^{-1}).[194] Such low interaction energies due to hydrogen bond formation are sufficient enough to overcome the overpotential for the first electron transfer reaction in alkaline media according to eq 14 shown above. This hydrogen bond formation stabilizes the solvated molecular oxygen $O_2{\cdot}(H_2O)$ cluster in the OHP and promotes an outer-sphere electron transfer to form the superoxide species.[38] On the contrary, in acidic media while this hydrogen bond formation could still take place, the interaction energy is not sufficient enough to allow electron transfer to the solvated molecular O_2. This reaction is formulated as shown here:

$$\mathrm{Pt{-}OH} + [\mathrm{O_2}{\cdot}(\mathrm{H_2O})_n]_{aq} + e^- \rightarrow \mathrm{Pt{-}OH} + [\mathrm{O_2^{\cdot-}}{\cdot}(\mathrm{H_2O})_n]_{aq} \quad (15)$$

$$[\mathrm{O_2^{\cdot-}}{\cdot}(\mathrm{H_2O})_n]_{aq} + e^- \rightarrow [\mathrm{HO_2^-}{\cdot}(\mathrm{H_2O})_{n-1}]_{aq} + \mathrm{OH^-} \quad (16)$$

The first step in the above reaction shown in eq 15 involves electron transfer (or tunneling) from the electrode surface across a thin oxide film and at least one layer of solvation shell to solvated O_2. Eq 16 involves proton transfer to the solvated superoxide molecule followed by a second electron transfer to form hydroperoxide anion. Thus, the OSET mechanism enables a $2e^-$ pathway to form hydroperoxide (HO_2^-) anion as the final product which is detected at the ring electrode. The rate-determining step in the $2e^-$ OSET reaction is the proton transfer process to the aqueous superoxide species.[125] Increasing alkalinity of the supporting electrolyte (pH > 12) causes the rate of proton transfer from water to decrease concomitant to the decrease in water activity. This is primarily the reason for increased stability of the superoxide radical anion $O_2^{\bullet-}$ in strongly alkaline electrolytes.[195] It is noted that while the OSET mechanism enables only a $2e^-$ pathway leading to hydroperoxide anion formation, the interaction between the $O_2{\cdot}(H2O)_n$ cluster and the surface-adsorbed hydroxide species causes certain nonspecificity to the identity of the underlying electrode metal. This nonspecificity opens the gate to use a wide-range of non-noble metals and their oxides as electrode materials for ORR in alkaline medium without necessitating the initial adsorption of molecular O_2.

On noble metals such as Pt, this nonspecificity is observed only in the oxide formation region and depending on the extent of −OH coverage both inner- and outer-sphere electron transfer mechanisms are likely to coexist. On non-noble metals such as the first row transition elements that are completely passivated by a layer of oxide/hydroxide film upon immersion into the aqueous electrolyte, this outer-sphere electron transfer process is likely to be the dominant mechanism. In acidic media, the adsorbed OH_{ads} species from water activation primarily serves only to block/inhibit the adsorption of molecular O_2 and other reaction intermediates via the well-known site-blocking effect.[166,196] However, as shown here in alkaline media the OH_{ads} species not only blocks the direct adsorption of O_2 but also serves to promote the $2e^-$ outer-sphere electron transfer reaction to form peroxide.[38]

The concept of involving the possibilities of outer-sphere electron transfer during ORR in alkaline media bears importance, and it was pointed out earlier by Bockris,[10] and Appleby[21] that the exchange current density values in alkaline media exhibit near-independence on a large number of polycrystalline electrode materials including silver, gold, manganese oxides, perovskites, and various carbon surfaces. So certain steps in the overall ORR process in alkaline media could proceed via a nonelectrocatalytic pathway.[21,168] It should be noted that while the OSET mechanism enables the use of non-pgm materials for ORR alkaline media, it leads primarily to the formation of HO_2^- intermediate as the final product. In order for the four-electron transfer process to occur, the catalyst should either be able to (i) enable the direct adsorption of O_2 on the active site followed by the $4e^-$ ISET mechanism or (ii) readsorb the HO_2^- intermediate followed by its electrochemical reduction to OH^- (discussed in the next section).

4.2. Base Catalysis of the Hydrogen Peroxide Intermediate

Another major aspect that provides a sharp contrast between acidic and alkaline ORR processes is related to the chemical nature of the hydrogen peroxide intermediate and its stability as a function of pH. Hydrogen peroxide being a weak acid ($pK_a \sim 11.7$) is represented by its protonated state as H_2O_2 under acidic conditions; but as the pH increases, it exists in its deprotonated form as the HO_2^- anion. This is ascribed to the base catalysis equilibrium reaction ($H_2O_2 + OH^- \leftrightarrow HO_2^- + H_2O$). H_2O_2 disproportionation is kinetically very sluggish and not favored under conditions of low pH, temperature, and concentrations, implying that it is a relatively more stable intermediate under dilute acid conditions. As the pH increases, the rate of hydrogen peroxide disproportionation increases and goes through a maximum between ∼11 and 13 pH.[197−199]

In this section, we first explain the distinction between the disproportionation of hydrogen peroxide under homogeneous chemical conditions and heterogeneous electrochemical conditions. Following this, we then attempt to elucidate its implications for the alkaline ORR process. Homogeneous

DOI: 10.1021/acs.chemrev.9b00157
Chem. Rev. XXXX, XXX, XXX−XXX

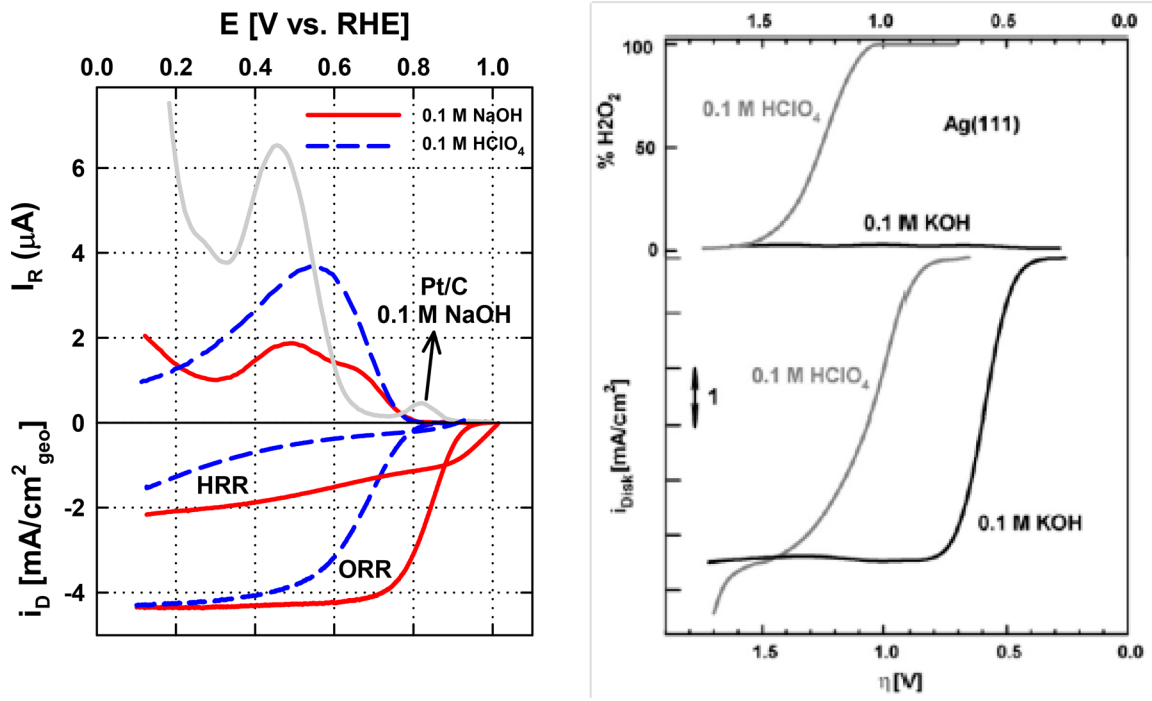

Figure 6. ORR polarization curves and the corresponding ring current profile measured in dilute acidic and alkaline electrolytes on a (left) pyrolyzed Fe−N_x−C type non-PGM catalyst and (right) Ag(111) electrode. Also shown on the left are the hydrogen peroxide reduction reaction (HRR) polarization curves measured using 3.5 mM H_2O_2 in argon saturated 0.1 M NaOH. (Figure on the right is reproduced with permission from ref 126. Copyright 2006 Elsevier Ltd.).

chemical disproportionation of H_2O_2 (or) HO_2^- is typically written as follows:[200]

$$\text{acid:}\quad 2H_2O_2 \rightarrow 2H_2O + O_2 \quad \text{(or)}$$
$$\text{alkaline:}\quad 2HO_2^- \rightarrow O_2 + 2OH^- \qquad (17)$$

Disproportionation of hydrogen peroxide molecule is a redox process that involves both its oxidation and reduction reactions by metal cations that act as a catalyst to liberate O_2. While the elementary reactions could be very complex, it is written here in a simpler form as follows:

$$M^{2+} + H_2O_2 + H^+ \rightarrow M^{3+} + H_2O + \cdot OH \quad \text{(or)}$$
$$M^{2+} + HO_2^- + H_2O \rightarrow M^{3+} + OH^- + \cdot OH \qquad (18)$$

$$\cdot OH + H_2O_2 \rightarrow \cdot OOH + H_2O \quad \text{(or)}$$
$$\cdot OH + HO_2^- \rightarrow \cdot OOH + OH^- \qquad (19)$$

$$M^{3+} + \cdot OOH \rightarrow M^{2+} + O_2 + H^+ \quad \text{(or)}$$
$$M^{3+} + \cdot OOH + OH^- \rightarrow M^{2+} + O_2 + H_2O \qquad (20)$$

The above elementary reactions represent the Haber-Weiss process, which makes use of the metal-cation-catalyzed Fenton chemistry under homogeneous chemical conditions.[201−203] The critical aspect here is that the hydrogen peroxide disproportionation reactions progress through the formation of short-lived, high-energy reaction intermediates such as the hydroxyl (•OH) and hydroperoxyl (•OOH) radicals. In the elementary reactions shown above, hydrogen peroxide is first reduced by the M^{2+} metal cation (initiation step) to generate hydroxyl radical (•OH) which oxidizes another hydrogen peroxide molecule (propogation step) forming the hydroperoxyl radical (•OOH). This chain reaction progresses until the free radicals are quenched and the cation is regenerated back to its original valence state (termination step). Catalysis of hydrogen peroxide disproportionation reaction is strongly dependent on the pH and the nature of the metal cation catalyst (i.e., its valence state and electronic structure).[204−206] While metals such as iron, copper, manganese, silver, cobalt, and nickel either in their cationic form or colloidal oxyhydroxide state are excellent catalysts for peroxide disproportionation, magnesium and calcium are known to be stabilizers for dilute hydrogen peroxide solutions.[204] Since hydrogen peroxide disproportionation is a redox process, the best catalysts are those that provide metal cation centers in its crystal lattice structure that are capable of existing in two or more oxidation states ($M^{2+/3+}$, $M^{3+/4+}$, etc.). For instance, in the cobalt−iron spinel oxide system ($Co_xFe_{3-x}O_4$, $0 \le x \le 3$), the active site for hydrogen peroxide disproportionation is known to be the Co^{2+} cations present in the octahedral sites. At a spinel composition of $x = 1.0$, the disproportionation activity goes through a maximum due to the maximization of the Co^{2+} centers present in the octahedral sites with its facile conversion to Co^{3+} that sets up a highly effective redox system.[198] Manganese oxide systems (either unsubstituted MnO_x or mixed oxides such as spinels and perovskites) that exhibit mixed valency between the $Mn^{3+/4+}$ states are known to be very active for hydrogen peroxide disproportionation reaction.[198,207−211]

Catalysis of hydrogen peroxide disproportionation reaction by metal cations is strongly accelerated at high pH. As mentioned above, this is particularly attributed to the base catalysis process that leads to the deprotonation of H_2O_2 to form HO_2^- anions.[198,200,201,204,205] Base catalysis or deprotonation initiates the disproportionation process by virtue of the high pH environment and hence critically affects the reaction pathways and mechanisms of hydrogen peroxide intermediate in alkaline

DOI: 10.1021/acs.chemrev.9b00157
Chem. Rev. XXXX, XXX, XXX−XXX

solutions.[200] While the exact reasons for the increase in the disproportionation kinetics at high pH is unknown, it is suggested that the anionic nature of the peroxide intermediate at high pH enables a favorable interaction with the cationic catalyst active sites, leading to the formation of M^{n+}-HO_2^- Lewis acid-Lewis base transition state structure. Such an adduct formation at low pH does not occur due to the neutral structure of peroxide intermediate, and hence, H_2O_2 is relatively more stable in dilute acidic solutions.

While the foregoing section primarily discusses catalytic hydrogen peroxide disproportionation under chemical conditions, the following section describes the peroxide disproportionation process under heterogeneous electrochemical conditions. Under homogeneous catalysis conditions, the catalyst and the reaction intermediates exist in their aqueous state. Under heterogeneous electrochemical conditions, the catalyst is now immobilized on the electrode surface such that the reactants and the reaction intermediates, particularly the high energy hydroxyl (•OH) and hydroperoxyl (•OOH) radicals, are adsorbed on the active sites of the electrode surface. When peroxide disproportionation occurs under heterogeneous electrochemical conditions, these high energy intermediates are now generated on the electrode surface which is poised at a potential (electrochemical) rather than held at open circuit conditions (chemical). Under such electrochemical conditions, these high energy intermediates can be electrochemically reduced since their standard reduction potentials are significantly positive. For instance, the primary reaction intermediate in peroxide reduction is the hydroxyl radical (•OH) which has a high standard reduction potential of $E^0_{\bullet OH/O\bar{H}} = 1.64$ V at a pH of 14.[124,200]

catalytic chemical disproportionation:

$$M^{2+} + HO_2^- + H_2O \rightarrow M^{3+} + \cdot OH_{ad} + 2OH^- \quad (21)$$

electrochemical reduction:

$$M^{3+} + \cdot OH_{ad} + e^- \rightarrow M^{3+} + OH^- \quad E^0 = 1.64V \quad (22)$$

regeneration of catalyst site:

$$M^{3+} + e^- \rightarrow M^{2+} \quad (23)$$

This process could be described as an electrochemical reaction (•OH_{ad} to $O\bar{H}$) promoted by a chemical catalytic process (HO_2^- to •OH). Hence, the alkaline ORR process is now determined also by the chemical disproportionation kinetics of HO_2^- on the catalyst surface. Under such electrochemical conditions, the metal cation center exists in two oxidation states with a suitable redox potential such that the lower oxidation state (M^{2+}) can be chemically oxidized by HO_2^-, and the higher oxidation state (M^{3+}) is reduced by virtue of the electrode being poised at a certain potential to regenerate the lower oxidation state.[199,212] Contrarily catalytic disproportionation of H_2O_2 in acid is very sluggish and hence does not generate the high-energy adsorbed intermediates.

Figure 6 shows the ORR polarization profile on Ag(111) disk electrode and a pyrolyzed Fe−N_x−C type non-pgm catalyst in both 0.1 M KOH and 0.1 M $HClO_4$ electrolytes.[38,126] (Note that the potential axis in Figure 6a is written as V versus RHE, whereas in Figure 6b, it is written in terms of the overpotential η). These two catalyst surfaces are used in this section as representative materials to explain the implications of hydrogen peroxide disproportionation step on the alkaline ORR process.

As observed in Figure 6a, the onset potential for ORR on Fe−N_x−C catalyst in 0.1 M NaOH is 0.95 V versus RHE, whereas in 0.1 M $HClO_4$ electrolyte it is 0.80 V vs RHE. This 150 mV lower overpotential in alkaline media is clearly reflected over the entire mixed kinetic-diffusion region. In 0.1 M NaOH electrolyte, the mixed kinetic-diffusion region is ensued by a well-defined diffusion limited region, whereas in 0.1 M $HClO_4$, no clear diffusion limited region could be discerned which is indicative of kinetic control in acidic media even at high overpotentials. Qualitatively similar behavior is also observed on the Ag(111) electrode surface as shown in Figure 6b. The performance of Ag(111) in 0.1 M KOH is characterized by a high onset potential followed by a mixed kinetic-diffusion region and then eventually by a well-defined limiting current behavior. Contrarily, in 0.1 M $HClO_4$, the ORR onset and the half-wave potentials are lower by ∼400 mV followed by a poorly defined limiting current behavior. Further, the ring electrode behavior for both the Ag(111) and Fe−N_x−C catalysts in 0.1 M $HClO_4$ suggests an immediate onset of hydrogen peroxide generation upon commencement of ORR. This indicates that at low overpotentials close to the onset of ORR, O_2 is primarily reduced to H_2O_2 in acid. Only at very high overpotentials close to the limiting current density region H_2O_2 reduction becomes feasible on both Ag(111) and Fe−N_x−C catalysts in 0.1 M $HClO_4$ as observed by the decrease in peroxide detected at the ring electrode as the disk electrode is swept close to the limiting current. On the contrary, the ring-electrode behavior of Ag(111) suggests a negligible generation of hydrogen peroxide intermediate in the alkaline electrolyte reflecting a predominantly $4e^-$ transfer. Fe−N_x−C catalysts also show very low peroxide generation in 0.1 M NaOH since the majority of the peroxide generated on this non-pgm catalyst is known to largely arise from the carbon support in base.[43] Figure 6a also shows the hydrogen peroxide reduction reaction activity of FeTPP/C catalyst (pyrolyzed at 800 °C) in both acidic and alkaline media in comparison to the corresponding ORR polarization curves. The onset potential for peroxide reduction in 0.1 M $HClO_4$ is 0.84 V versus RHE, whereas in 0.1 M NaOH it is 1.01 V versus RHE. Besides this onset potential difference, in 0.1 M NaOH electrolyte, the mixed kinetic-diffusion region for peroxide reduction is more anodic compared to that of ORR in the same electrolyte which is then followed by a reasonably discernible diffusion limited current density region. This clearly indicates that peroxide reduction in alkaline media is kinetically favored such that any peroxide intermediate formed during ORR in 0.1 M NaOH will be immediately reduced to the $4e^-$ product. On the contrary, the reduction of hydrogen peroxide in acidic media is kinetically unfavorable due to weak binding of H_2O_2 on the active site leading to its desorption into the bulk electrolyte.

For both Ag(111) and Fe−N_x−C catalysts, it is significant to note that the alkaline ORR process is anodically shifted by several hundred millivolts. Both Ag and Fe−N_x−C surfaces are known to be excellent catalysts for the chemical disproportionation of hydrogen peroxide at high pH, this enables the further progress of ORR at high pH.[213,214] The peroxide intermediate is chemically activated to form adsorbed hydroxyl radicals (•OH_{ad}) which is electrochemically reduced at high potential according to reactions 21 and 22 shown above. On the contrary, under acidic conditions ORR on these two catalysts are largely terminated at the $2e^-$ (H_2O_2) intermediate whose chemical activation kinetics is sluggish at low pH. This causes the alkaline ORR process to be dependent on the chemical disproportionation kinetics on the catalyst surfaces.

DOI: 10.1021/acs.chemrev.9b00157
Chem. Rev. XXXX, XXX, XXX−XXX

There are several references in the alkaline ORR literature that suggest the possibility of a hydrogen peroxide disproportionation reaction to regenerate O_2 and hence lead to an apparent $4e^-$ reaction pathway.[211] We would like to point out that if the peroxide anion intermediate chemically disproportionates to form O_2 then this should lead to only an increase in the limiting current density and not an anodic shift in reduction potential. In such a case, the onset and half-wave potential should be no more positive than the $E^\circ(O_2/HO_2)^-$ redox couple potential of 0.77 V versus RHE since the electrochemical process is determined by only the O_2/HO_2^- couple. This is depicted in Figure 7 where the

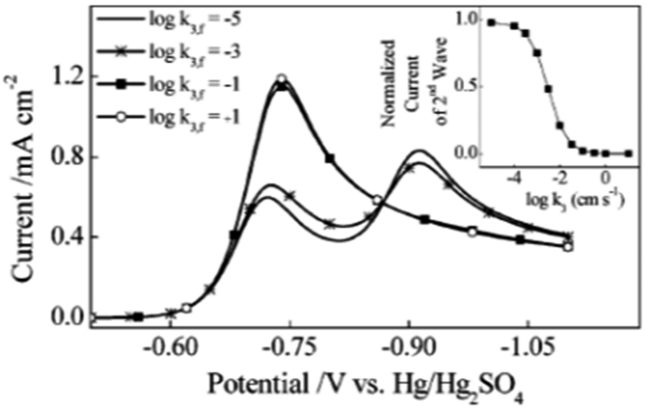

Figure 7. Simulated voltammograms of peroxide pathway reduction of O_2 with varied values for the heterogeneous hydrogen peroxide decomposition rate constant, $k_{3,f}$. The effect of $k_{3,f}$ on the normalized hydroperoxide reduction currents is shown in the inset. Scan rate = 0.1 V s^{-1}. Reproduced with permission from ref 215. Copyright 2005 American Chemical Society.

ORR behavior is simulated as a function of heterogeneous hydrogen peroxide decomposition rate constant ($k_{3,f}$).[215] For small rate constant values ($k_{3,f} \leq < 10^{-4}$ cm s^{-1}), two separate reduction peaks are observed such that the first peak corresponds to the $2e^-$ reduction of O_2 to hydrogen peroxide followed by the second peak at high overpotentials which corresponds to another $2e^-$ reduction of hydrogen peroxide to an OH^- anion. As $k_{3,f}$ increases to greater than 10^{-3} cm s^{-1}, the first reduction peak shows a significant increase in current density at the expense of the second reduction peak. The absence of the second reduction peak suggests that the electrochemically generated hydrogen peroxide chemically decomposes to O_2 at a rate faster than the rate at which it is electrochemically reduced to the OH^- anion. The critical aspect to note here is that if peroxide disproportionates to form O_2 then this leads only to an increase in the limiting current and not any shift in the reduction potential.

One common denominator of all the electrode materials [N-doped carbon,[215] various transition metal (e.g., Ag),[213,214,216] M−N_x−C type non-pgm,[217] metal oxides including manganese oxides,[207,208,210] perovskites,[218−222] and pyrochlores[223]] that have been investigated for alkaline ORR process is that they are all excellent catalysts for the heterogeneous disproportionation of hydroperoxide anion under alkaline conditions. For instance, the peroxide disproportionation rate constant of N-doped carbon is 1.8×10^{-5} cm s^{-1} for peroxide disproportionation, which is very close to that on platinum surfaces.[215,217] Ag under alkaline conditions that exists as $Ag(OH)_x$ being a very good catalyst for the chemical disproportionation of hydrogen peroxide enables the one electron reduction of HO_2^- leading to the formation of high-energy hydroxyl intermediates.[213,214]

As mentioned above, the peroxide disproportionation process involves the formation of high-energy adsorbed intermediates that are then electrochemically reduced.[198,199,224,225] The standard redox potentials of the hydroxyl intermediates are significantly positive compared to the other reactants and intermediates in the ORR process. In essence, the kinetic facility of catalytic HO_2^- anion disproportionation at high pH enables the generation of high-energy reaction intermediates that are then electrochemically reduced at high potentials. This process could be described as an electrochemical reaction (•OH to OH^-) promoted by a catalytic process (HO_2^- to •OH). This is the rationale behind the anodic shift in ORR under alkaline conditions. Under acidic conditions, catalytic disproportionation of H_2O_2 is very sluggish and hence does not generate the high-energy adsorbed intermediates.

On the basis of the above discussions, the various reaction pathways of alkaline O_2-reduction are shown in Figure 8. For the sake of illustration, the schemes are drawn out separately for metallic PGM catalyst surfaces (Pt, Pd, and Ru) and non-PGM surfaces (e.g., manganese oxides, perovskites,[226] Fe−N_x−C[41,226]). Largely, there are two main pathways on both of these catalyst groups: the noncatalytic pathway facilitated by the outer-sphere electron transfer mechanism on electrode materials that either weakly adsorb or do not adsorb O_2, and the catalytic pathway facilitated by the inner-sphere electron transfer mechanism on the active sites that adsorb O_2 with an optimal binding strength. Briefly, under conditions of oxide-covered active sites such as Pt−OH or M^{2+}−OH, the OSET mechanism enables the noncatalytic $2e^-$ reduction process of O_2 to form the HO_2^- anion in which all the reactants and products are present in the weakly adsorbed or nonadsorbed aqueous phase. This is the case where the O_2 adsorption is not strong enough or the axially coordinated hydroxide species (M^{2+}−OH) is not labile enough to be displaced by the molecular O_2. This pathway leads to the $2e^-$ HO_2^- intermediate as the primary product. In the catalytic pathway, molecular O_2 directly chemisorbs on the active site at or near the optimal binding energy. This is the case where the active site is oxide-free (e.g., Pt) or the axially coordinated hydroxide (M^{2+}−OH) is labile enough such that molecular O_2 chemisorbs at or near the optimal binding energy.[41,226] The lability is typically caused by the redox mechanism of the active site that facilitates the removal of axially coordinated hydroxide anions. Once O_2 is directly adsorbed on the active site, the reaction then proceeds via the superoxo and the hydroperoxyl states to form the adsorbed hydroperoxide anion intermediate. As mentioned above, the base catalysis equilibrium renders the hydrogen peroxide intermediate in its anionic form HO_2^- which is a very critical intermediate since its stability on the active site determines the product distribution (two vs four electron transfer) and the overall ORR electrocatalytic activity/efficiency. In other words, the chemical disproportionation kinetics of HO_2^- on a given catalyst material now begins to impact the product distribution. Qualitatively, catalysts with smaller peroxide disproportionation rate constant leads to higher peroxide formation and vice versa. By virtue of the high pH, the hydroperoxide anion intermediate involves in a chemical disproportionation step, leading to the formation of a surface-adsorbed high energy hydroxyl ($•OH_{ad}$) intermediate which is then electrochemically reduced followed by the regeneration of the active site. In acid media, on most transition metal oxide based non-pgm catalysts such as manganese oxides,

DOI: 10.1021/acs.chemrev.9b00157
Chem. Rev. XXXX, XXX, XXX−XXX

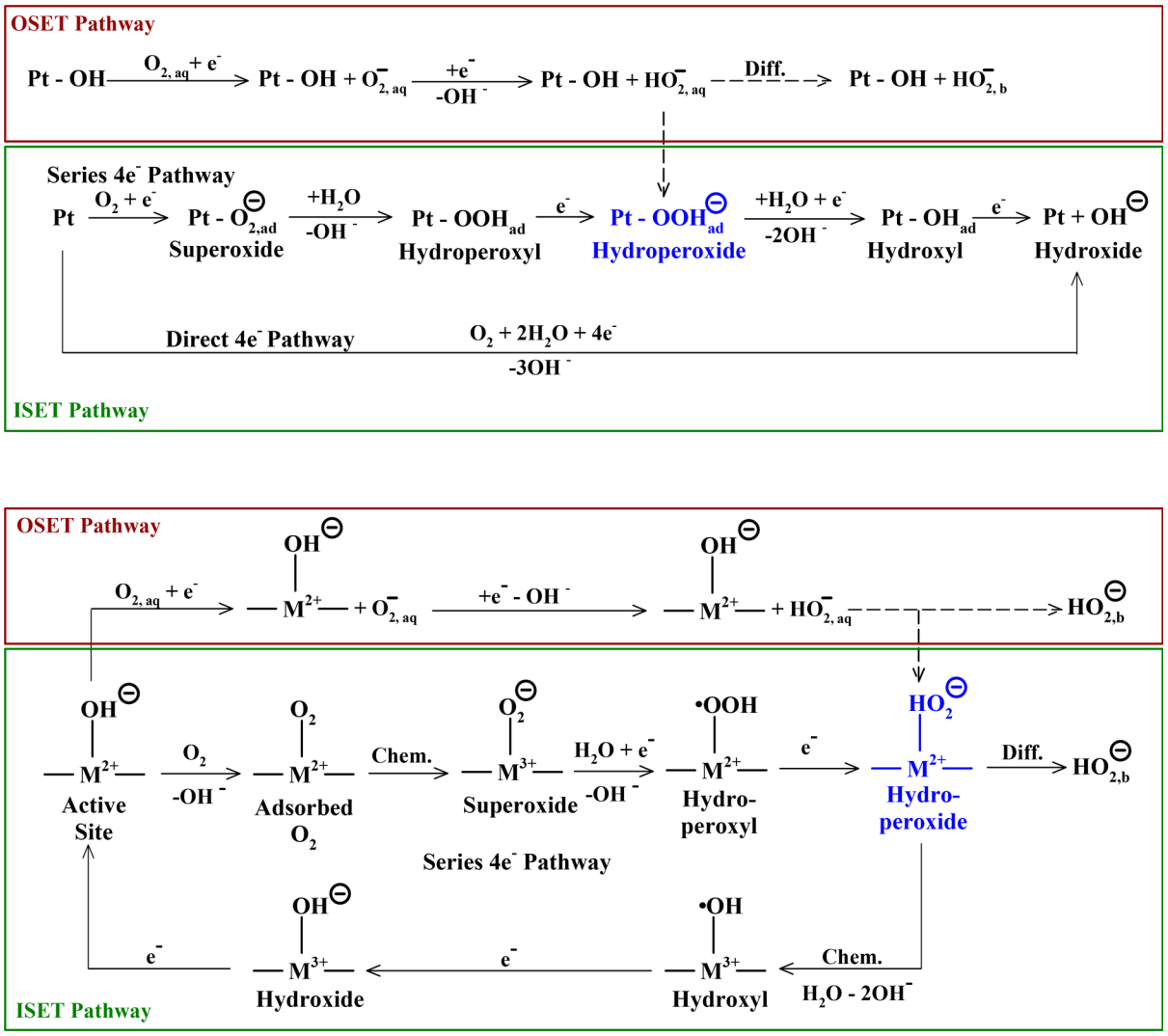

Figure 8. Generic alkaline ORR pathways on (top) PGM surfaces and (bottom) non-pgm active sites. Catalysts such as Pt and Pd are representative of PGM surfaces, whereas catalysts such as the pyrolyzed Fe−N_x−C, perovskites, and MnO_x are representative of the non-PGM active sites. The active site in the non-PGM catalysts is generically represented as M^{2+}. Subscripts aq, b, ad represent aqueous, bulk, and adsorbed species. Abbreviation "Chem." represents a chemical reaction step and "Diff." represents diffusion to bulk.

perovskites, and Fe−N_x−C surfaces, the reaction tends to be largely terminated at the hydrogen peroxide intermediate where the protonated peroxide intermediate (H_2O_2) is not easily disproportionated. In essence, the generally higher chemical disproportionation kinetics of peroxide in alkaline media enables a pathway to generate surface adsorbed hydroxyl intermediates ($\bullet OH_{ad}$). On the contrary, this is a very sluggish process at low pH conditions. One other possibility is the interactive pathway, wherein the hydrogen peroxide intermediate formed via the OSET mechanism undergoes diffusion to adsorb on another active site followed by disproportionation/reduction. This is particularly appropriate for the Fe−N_x−C type non-PGM catalysts which are well-known to exhibit significant heterogeneity in its active site. Also, these non-PGM catalysts are typically applied as thick catalyst layers that increase the probability of the interactive pathway.[227]

It would not be inappropriate to mention that the possibility of a noncatalytic first electron transfer step and/or the base catalysis initiated peroxide disproportionation process has essentially opened the flood-gates to a plethora of electrode materials being able to reduce O_2 in liquid alkaline media with remarkable activities.[228−235] A vast majority of these catalysts fall into the category of some form of heteroatom-doped (nitrogen, phosphorus, etc.) carbon allotrope with or without metal/metal oxide nanoparticles;[41,236−255] further, various transition metal surfaces [e.g., Ag,[256] Au(100)[167]] and transition metal oxides (e.g., manganese oxides[257−264] cobalt/iron/nickel oxides,[265−268] perovskites,[269−275] and spinels[276,277]) that are likely to show very low activity in acid exhibit significant activities in alkaline electrolytes. Ag(111) and Au(100) are excellent examples of catalysts that enable ORR via a weak adsorption of O_2 leading to the formation of the hydrogen peroxide anion intermediate that is rapidly disproportionated to form adsorbed hydroxyl species ($\bullet OH_{ad}$) followed by its subsequent reduction to form OH^-.[167] Gold single crystal surface such as Au(100) shows a unique $4e^-$ ORR behavior in a narrow potential range where hydroxide species are adsorbed.[278−281] The Au(100)−OH_{ad} surface was found to enable the further reduction of HO_2^- intermediate via a peroxide disproportionation step that leads to the formation of hydroxyl intermediates.[282,283] Rapid chemical kinetics of hydrogen peroxide disproportionation at high pH enables the formation of surface adsorbed hydroxyl ($\bullet OH$)

DOI: 10.1021/acs.chemrev.9b00157
Chem. Rev. XXXX, XXX, XXX−XXX

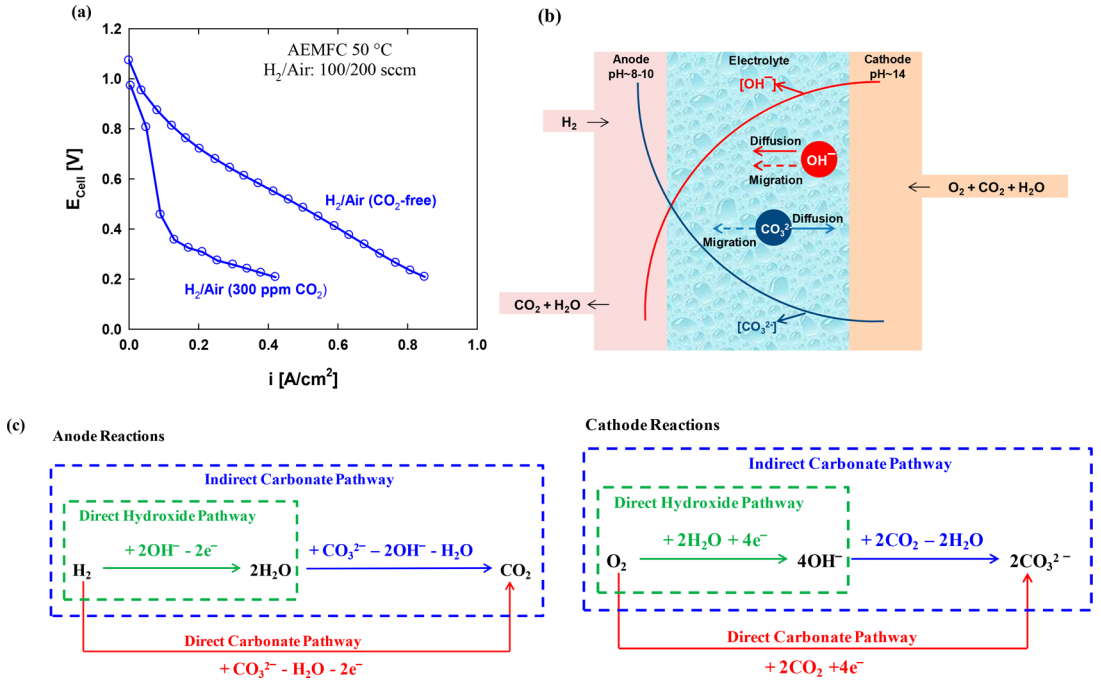

Figure 9. (a) AAEM fuel cell polarization results measured at 50 °C cell temperature using A201 membrane, AS4 alkaline ionomer, 100% RHinlet, and anode/cathode loadings of 0.5/0.5 mgPt/cm^2. (b) Schematic illustration of the effect of (bi)carbonate anion exchange of the membrane during fuel cell operation. (Illustration adapted from ref 297. Copyright 2011 The Electrochemical Society of Japan.) (c) Scheme showing the anode and cathode reactions occurring in the direct hydroxide, direct carbonate, and indirect carbonate pathways.

species which are then electrochemically reduced. Such a pathway to enable hydroxyl species formation on these metal oxides is kinetically inhibited at low pH.

Various metal oxide surfaces including manganese oxides, perovskites, pyrochlores, and spinels are all very active toward the chemical disproportionation of hydrogen peroxide at high pH which is a characteristic feature of these materials that differentiate them from low pH conditions. ORR activity on various perovskite materials such as lanthanum cobaltites and manganites was shown to follow the same activity as the chemical peroxide decomposition activity.[219] In particular, for the $LaFe_xNi_{1-x}O_3$ perovskite material, the ORR activity was found to linearly correlate with the heterogeneous peroxide decomposition activity for varying values of x. At x = 0.25 formation of solid solution of $LaFe_xNi_{1-x}O_3$ between the end members $LaFeO_3$ and $LaNiO_3$ leads to the presence of mixed valence of $Fe^{3+/4+}$ and $Ni^{2+/3+}$.[284] This was found to be the primary reason for the perovskite catalyst to act as heterogeneous catalyst for peroxide decomposition.[220,284] While $LaFeO_3$ is an insulator, 25% Ni substitution for Fe imparts metallic conductivity to the perovskite. This Ni substitution causes some fraction of the Fe^{3+} to the Fe^{4+} state along with the presence of mixed valent Ni^{2+} and Ni^{3+}. The presence of mixed valent Fe and Ni content with reduction potentials value between the O_2/HO_2^- and HO_2^-/OH^- redox couples was suggested to be the reason for fast heterogeneous peroxide decomposition.

On pristine and nondoped carbon surfaces, alkaline ORR is largely a 2e$^-$ process leading to the formation of HO_2^- as the final product with the first electron transfer mediated by the surface oxygen functionalities (quinone/hydroquinone) via an outer-sphere process.[285,286] Neither hydrogen peroxide anion disproportionation nor its adsorption is viable on pristine carbon surfaces. Recent studies show that heteroatom doping (particularly nitrogen-doping) induces a high density of edge plane defect sites on the carbon surface at which superoxide/peroxide formation occurs via the OSET mechanism.[287,288] These hydroperoxide species are subsequently adsorbed on the N-doped sites followed by further disproportionation and reduction leading to the 4e$^-$ process. N-doped carbon supports show remarkable two-orders of magnitude increase in the hydroperoxide decomposition rate constants measured from steady state polarization curves under electrochemical conditions (9×10^{-4} cm s^{-1} for doped vs 4.1×10^{-6} cm s^{-1} for nondoped carbon in 1 M KOH),[215,217] which is on the same order of magnitude as Pt black catalyst (2.9×10^{-4} cm s^{-1}).[223] Peroxide disproportionation process could either arise from the N-doped edge planes or the residual metal/metal oxide surfaces that inevitably are present in these doped materials.[217,289,290] On non-PGM surfaces that contain Fe−N_x type active sites, ORR proceeds through the series 4e$^-$ pathway with only a minor peroxide formation via OSET mechanism.[41]

5. EFFECT OF CARBONATE POISONING OF ALKALINE MEMBRANES ON FUEL CELL PERFORMANCE

The deployment of conventional liquid-electrolyte-based AFCs for terrestrial applications involving the use of atmospheric air cathode feed (~400 ppm of CO_2) has chronically suffered from the precipitation of insoluble alkali metal carbonates and its deteriorative consequences on the clogging of electrode pores, operation lifetime, and high system level complexity (such as electrolyte circulation units, CO_2 scrubbers, and removers).[291−293] The substitution of solid AAEM electrolyte with immobilized quaternary ammonium cation head-groups for hydroxide-anion transport that precludes the use of mobile alkali metal cations was originally conceived to prevent carbonate precipitation.[13] Contrarily, subsequent studies have clearly shown that the AAEM fuel cell performance is significantly

DOI: 10.1021/acs.chemrev.9b00157
Chem. Rev. XXXX, XXX, XXX−XXX

affected by the presence of CO_2 in the feed stream.[45] This is proposed to occur via the direct reaction between CO_2 and the hydroxide anion functionalized quaternary ammonium cationic-head groups in the alkaline membrane according to the equilibrium reactions represented as $CO_2 + O\bar{H} \rightarrow H\bar{CO_3}$ followed by $H\bar{CO_3} + O\bar{H} \rightarrow CO_3^{2-} + H_2O$.[119,294,295] Upon hindsight, this is rather expected since most amine-functionalized organic compounds are excellent sorbents of CO_2 for use in sequestration units.[296] Alkaline AEM membranes with the quaternary ammonium cationic-headgroup side chains rapidly absorb atmospheric CO_2 with the complete inventory of hydroxide anions being converted to an equimolar mixture of bicarbonate and carbonate anions.[118,294] Figure 9a shows the effect of CO_2 contamination in the cathode feed on AAEM fuel cell performance.[64,119] The presence of ~300 ppm of CO_2 in the cathode feed leads to a dramatic loss in cell voltage in the low current density region (<0.1 A/cm^2) of the polarization curve. At a current density of 0.2 A/cm^2, a loss in cell voltage of ~520 mV is observed in the presence of 300 ppm of CO_2 in the cathode feed.[44] The cell voltage tends to recover at high current densities (>0.2 A/cm^2), although the recovery is too late and very minimal.[64]

Recent studies by Tokuyama Corporation have comprehensively captured the negative effects of the CO_2 poisoning on AAEM fuel cell performance.[44,119,295,297−299] The major deteriorative implications of the carbonate anion exchange of the AEM electrolyte for fuel cell performance can be classified as (i) loss in membrane conductivity due to low mobility of (bi)carbonate anions,[44] (ii) thermodynamic cell voltage loss due to preferential accumulation of carbonate species on the anode side and accompanying pH gradient across the membrane,[45,297] (iii) indirect effects on electrocatalytic reaction kinetics/pathway,[44,185,300] and (iv) possible effects on O_2 mass transport.[185,301,302] The first two aspects appear to create the largest impact on fuel cell performance and are reviewed below in more detail.

Mobility of bicarbonate (4.61×10^{-8} m^2 s^{-1} V^{-1}) and carbonate anions (7.46×10^{-8} m^2 s^{-1} V^{-1}) in dilute aqueous solutions is ~1/5 and 1/3 of the hydroxide anions (20.64×10^{-8} m^2 s^{-1} V^{-1}), respectively.[298] Conversion of hydroxide anions in the membrane to a HCO_3^-/CO_3^{2-} mixture leads to roughly 4-fold loss in AEM conductivity (42 mS/cm for OH-form compared to 10 mS/cm for CO_3^{2-}-form Tokuyama A201 AEM).[118] Siroma et al.[297] recently developed a mathematical model to understand the concentration profile of carbonate anions across the AEM under steady state operation of AAEM fuel cell fed with CO_2-containing ambient air. The (bi)carbonate anions migrate to and accumulate in the vicinity of the anode interface leading to a significant pH gradient across the membrane. As shown in Figure 9b, cathode exists at a higher pH of ~14 due to the continuous generation of hydroxide anions as a result of ORR, whereas the anode is at a low pH of ~8−10 due to (bi)carbonate accumulation.[45,297] Under steady state operation, the transference number of (bi)carbonate anions (i.e., net current carried by (bi)carbonate anions) is negligible since its accumulation at the anode interface causes a balance in the diffusion and migration forces acting on the (bi)carbonate anions essentially making them stagnant and immobile in the membrane (Figure 9b). This accumulation of carbonate anions at the anode interface and the development of carbonate concentration profile across the membrane leads to (i) a concomitant pH gradient across the membrane, and (ii) concentration overvoltage due to the hydroxide concentration difference across the membrane. As long as the cathode feed contains CO_2, higher current densities and the use of thicker membranes exacerbate the problem due to an increased (bi)carbonate accumulation on the anode side with steeper concentration and pH gradients. Accumulation of (bi)carbonate anions in an operating AAEM fuel cell is analogous to cation accumulation on the cathode side of an operating PEMFC under steady state conditions.[303] The drop in cell voltages at low current densities (Figure 9a) operating with 300 ppm of CO_2 in the cathode feed largely arises due to a combination of both increase in membrane resistance and thermodynamic loss in cell voltage (for a gradient of ~6 pH across the membrane at 60 mV/pH loss would indicate ~360 mV loss).[44,45] This indicates that the drop in pH on the anode side due to carbonate accumulation leads to significant loss in cell performance. There are some reports indicating marginally better HOR and ORR reaction kinetics in liquid carbonate electrolytes;[185,300] but these kinetic benefits are largely insignificant when compared to the cell voltage losses arising from both carbonate accumulation at the anode side and membrane resistance losses during AAEM fuel cell steady state operation.

There are at least three avenues that are being pursued to mitigate (bi)carbonate anion poisoning of the membrane: (i) incorporation of CO_2 filters in the cathode feed stream, (ii) operation of AAEM fuel cells at ≥80 °C due to lower CO_2 solubility at elevated temperature, and (iii) self-purging of CO_2. The first approach is largely similar to the earlier applications in liquid alkaline fuel cells that involve the use of upstream filters to decrease the cathode CO_2 feed to less than 10 ppm.[304] Such filters are largely based on polymers containing amine functional groups that are excellent CO_2 absorbents and are also thermally regenerative.[296,305] The second strategy is related to the decrease in the solubility of CO_2 in water with increasing operating temperatures (≥80 °C).[294,306] This appears to be a useful strategy although there have not been many studies in the literature possibly due to thermal instability of membranes. More studies are warranted on the temperature effect of CO_2 solubility and its subsequent effect on AAEM fuel cell performance improvement.

Another strategy to mitigate the carbonate poisoning is to operate a carbonate-poisoned AAEM fuel cell MEA with pure O_2 or a CO_2-free air feed. In this process, carbonate anions accumulated at the anode interface can be purged out via the anode outlet in the gas phase according to the reaction $H_2 + CO_3^{2-} \rightarrow H_2O + CO_2\uparrow$ or $H_2 + HCO_3^- \rightarrow 2H_2O + 2e^- + 2CO_2\uparrow$).[119,295,307] Due to the continuous generation of pure OH^- anions as a result of ORR on the cathode in the absence CO_2 contamination, this provides an opportunity to slowly recover the performance by essentially flushing the membrane and exchanging it back to the OH-form. During the self-purging process, the carbonate anions in the AEM electrolyte are released as CO_2 in the anode outlet.[119,295] Quantity of CO_2 purged is strongly dependent on the current density and the duration of operation indicating equilibrium between carbonate anions and CO_2 release ($HCO_3^-/CO_3^{2-} \rightarrow CO_2 + OH^-$), higher current density, and longer duration favoring a more complete CO_2 purge. Purging of carbonate anions from the AEM electrolyte during fuel cell operation is observed only when the cathode is operated with pure O_2 or CO_2-free air.[118] As long as a carbonate-contaminated AEM is operated on H_2/air (~390 ppm of CO_2) gas feeds, there is always a significant drop in cell voltage at low current densities and the self-purging phenomenon is not observed.[114,307]

DOI: 10.1021/acs.chemrev.9b00157
Chem. Rev. XXXX, XXX, XXX−XXX

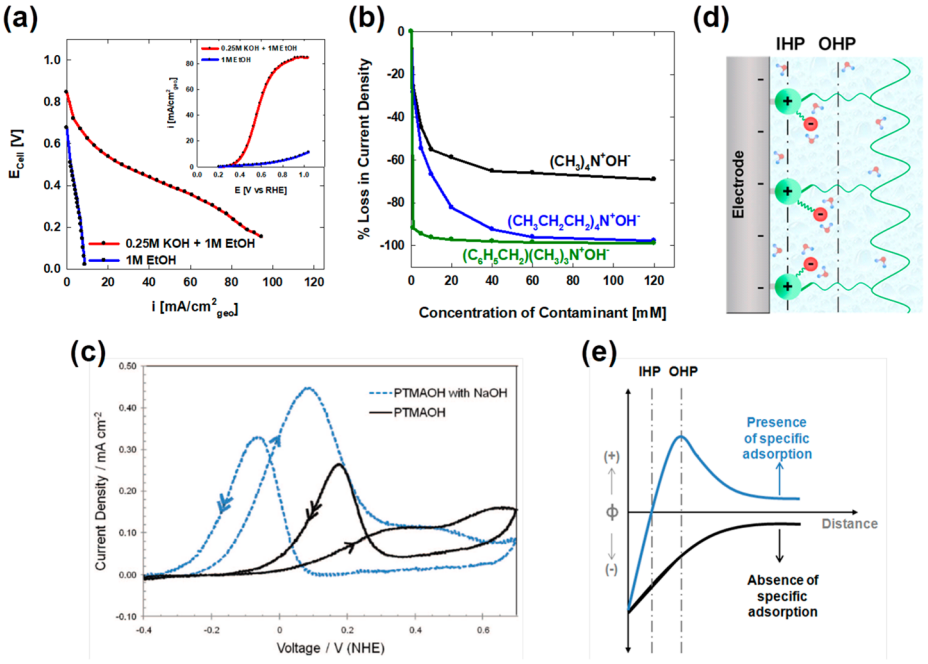

Figure 10. Polarization and power density curves for an AEM fuel cell with an anode composed of 4.0 mg_{PtRu}/cm^2 + 1.0 mg_{AS4}, cathode composed of 30% Pt/C (1.0 mg_{Pt}/cm^2 + 28 wt % AS4) + 1.0 mg_{AS4}, and Tokuyama A201 anion-exchange membrane. Anode feed: 1 M ethanol with or without 0.25 M KOH at 8 mL/min. Cathode feed: 100% RH O_2. Adapted with permission from ref 50. Copyright 2005 The Electrochemical Society.

Recent studies point to the possibility of operating AAEM fuel cells using a direct carbonate cycle, thus avoiding the formation of highly nucleophilic hydroxide anions.[300,308,309] This is essentially a low temperature alternative to the molten carbonate fuel cells. As shown in Figure 9c, a direct carbonate cycle corresponds to the case where the working anion is CO_3^{2-} and no hydroxide anions are formed during AAEM operation; rather cathodic ORR involves direct formation of CO_3^{2-} which is transported to the anode followed by direct reaction with H_2 to form H_2O. This is an ingenious design, but given the lower mobility of the carbonate anions compared to hydroxide anions, it is highly unlikely that the performance of AEM fuel cells operating on direct carbonate cycle could match those operating on direct hydroxide cycle at comparable conditions, unless the HOR and ORR reaction kinetics under the direct carbonate cycle is significantly better which appears not to be the case.[300,302,309] Further, recent studies point to the use of small concentrations of NH_3 (<7%) in the anode H_2 feed led to marginal improvements in the CO_2 tolerance.[310] This was possibly due to the ability of NH_3 to capture HCO_3^- and convert it into a weakly adsorbing anion of the form $H_2NCO_2^-$. This led to a local drop in the concentration of the HCO_3^- anion and improved the anode HOR activity. Further studies to identify complexing species that locally alleviates CO_3^{2-}/HCO_3^- species are highly warranted.

Mitigation of carbonate anion poisoning is very critical to enable terrestrial applications of AAEM fuel cells. Operation of AAEM fuel cells at elevated temperature would require thermally stable membranes, whereas the use of CO_2 filters would increase the system complexity. In reality, a combination of the above strategies involving brief excursions to high current density and elevated temperatures to enable CO_2 self-purge along with the use of upstream filters would be required. Clearly, more innovative ideas to mitigate CO_2 poisoning of the membrane are warranted. Further, studies that quantify the kinetics of HOR and ORR reactions in the presence of carbonate ions are warranted.

6. EFFECT OF AMMONIUM CATION POISONING ON INTERFACIAL CHARGE TRANSFER

A more chronic problem in the development of alkaline fuel cells has been the very poor performance of direct alcohol (KOH-free anode feed) AAEM fuel cells.[46,51] Several authors have repeatedly shown in the recent past that despite generous use of precious metal anode catalysts such as Pt/PtRu, the power density of direct alcohol-fed (excess KOH-free) alkaline AEM fuel cells is extremely low (<20 mW/cm^2).[46−50,120,311−315] Further, in all of these cases the low performance observed for the pure alcohol-fed anodes dramatically improves with the addition of excess alkali metal hydroxide to the fuel. The addition of excess alkali metal hydroxide to the fuel improves the short-term performance of the direct alcohol fuel cell, but it contradicts the whole purpose of utilizing a solid alkaline anion-exchange membrane as the electrolyte. Figure 10a depicts this typical behavior of direct ethanol-fed AAEM fuel cell with and without excess KOH in the anode fuel. Polarization curves indicate a low open circuit voltage (OCV) followed by steep drop in cell voltage at low current densities when operated in the absence of KOH. The OCV improved from 0.68 to 0.85 V in the presence of KOH along with an improvement in peak power density from 1.7 mW cm^{-2} to 22.4 mW cm^{-2}. Figure 10a (inset) also shows the anodic alcohol oxidation polarization curve measured in AAEM cell by using hydrogen-fed cathode as a reference/counter electrode. In the absence of excess KOH, alcohol oxidation exhibits very low current density and high overpotential with no clearly discernible onset potential. On the contrary, a clear onset potential of ~0.3 V is observed in the presence of KOH with a well-defined limiting current density. The rate of ethanol oxidation is significantly enhanced with excess KOH, and the half-cell result shows that the anodic oxidation of alcohol in the absence of excess KOH is a major

DOI: 10.1021/acs.chemrev.9b00157
Chem. Rev. XXXX, XXX, XXX−XXX

limiting factor in the performance of alkaline direct alcohol fuel cells.[51] The poor performance is typically attributed to the formation of carbonate anions from alcohol oxidation that accumulates on the anode side and affects performance via a drop in pH and loss in membrane conductivity. However, the alcohol oxidation current density in the absence of KOH is very low (<10 mA/cm^2) and could not account for such a drastic performance loss. There are several factors that can limit the AAEM fuel cell performance in the absence of excess KOH, including poor catalyst utilization, fuel crossover to the cathode, insufficiently lower ionic conductivity and pH gradient at the anode/ionomer interface, fuel mass transfer resistance to the anode catalyst, and carbonate formation.[47,49,51,311,314,316−319] Though each of these potential sources for the voltage drop at low current would have a negative effect on cell performance, it is unlikely that any of these could account for such a large difference in performance between alkaline direct alcohol fuel cells and their acidic counterparts. Further, given that under conventional three-electrode configuration in liquid alkaline electrolytes alcohol oxidation takes place at appreciable rates, in this study, we turn our attention to shed light on one potential issue arising at the anode double layer structure and anode catalyst/ionomer interface.[51]

In the absence of excess KOH in the anode feed, efficient fuel oxidation is dependent on the establishment of the three-phase boundary at the active site between ionomer, carbon support, and reactant. The presence of excess KOH in the anode feed discredits the use of ionomer solutions in the catalyst layer by establishing the so-called "flooded electrolyte" system. In contrast to liquid alkaline electrolytes, an operating AEM fuel cell involves the use of interfacial alkaline ionomer solution in the catalyst layer to establish the three phase boundary required for electrocatalysis. This alkaline ionomer solution consists of immobile positive charges fixed to the polymer backbone and relatively mobile negative counteranions. Quaternary ammonium cations have been categorized as weak adsorbates where the driving force is largely due to electrostatic interactions related to the solvation energy of the cations.[320] Typically, the solvation energy for alkali and alkali earth cations is much higher than that for electrostatic adsorption. In contrast, quaternary ammonium ions are weakly solvated in water so that the electrostatic attraction with an oppositely charged surface favors adsorption. Tetramethylammonium cations are likely to electrostatically adsorb on the catalyst surface at the low anode potentials along with possible covalent interactions between the side chain functionalities.

Figure 10b,c captures the effect of tetramethlammonium cation poisoning on the methanol oxidation reaction kinetics.[51] As shown in Figure 10b, the oxidation of methanol on the Pt/C catalyst was studied in the presence of various quaternary ammonium groups such as tetramethyl, tetrapropyl, and benzyltrimethylammonium hydroxide. These cationic contaminants were directly added at various concentrations to the liquid electrolyte containing 0.1 M KOH + 0.5 M methanol. In all these cases, a significant drop in methanol oxidation current density is observed even with less than 20 mM concentration of the quaternary ammonium cations. This deteriorative effect of the ammonium cations is also observed in Figure 10c which shows the cyclic voltammetry of a polycrystalline platinum disk electrode in methanol containing poly-(diallyldimethylammonium chloride) (PTMAOH) electrolyte with or without 0.1 M NaOH. In the anodic sweep of Pt in PTMAOH with excess NaOH, the cyclic voltammetry profile clearly indicates oxidation wave in both directions. In the absence of excess NaOH, the anodic sweep indicates a significant overpotential and does occur until at Pt−OH$_{ad}$ formation begins to occur.[51] On the reverse cathodic sweep, an increase in oxidation activity is observed due to the residual oxides on the Pt surface. The experiments described above involved TMA$^+$ cations because trimethyl benzyl quaternary ammonium ions bound to a polymer backbone are the most common chemical constituents of the current state of the art AEM ionomer solutions. In general, all ammonium cations showed a significant adsorption effect on the platinum surface resulting in loss of methanol oxidation activity. Particularly, the benzyltrimethylammonium cation that is prevalently used in AAEM electrolytes leads to a drastic loss of methanol oxidation activity. This observation is consistent with previous literature that showed a higher surface inhibition with the longer alkyl length on the ammonium group.[321]

These results with different quaternary ammonium cations in aqueous electrolytes show that quaternary ammonium ion adsorption on Pt surfaces lowers the rate of methanol oxidation by blockage of the active catalyst surface area. As depicted in Figure 10d,e, Kohl et al.[51] have recently proposed that the effect of methanol oxidation by the quaternary ammonium cation is likely to be 2-fold: one arising from the loss of active surface due to the cation and side chain adsorption. The second aspect is likely to be more complicated and arises due to the disruption of the potential distribution at the anode/ionomer interface that disfavors interfacial charge transfer. The specific adsorption of electro-inactive species can create significant changes in the structure of the double layer which differ from the nonadsorbing case.[322−324] A qualitative potential profile shown in Figure 10e indicates that specific adsorption of ammonium cations on the catalyst surface in the compact part of the double-layer leads to an electrochemical potential gradient at the anode/ionomer interface that inhibits hydroxide anion transport to the anode that are required for alcohol oxidation.[51] Contrarily, when excess KOH/NaOH is added, the mobile hydroxide anions essentially deluge the interface to compensate the excess positive charge at the interface and establishes a normal potential distribution. Similar results were recently shown both in the context of ORR and HOR, clearly indicating that the cationic-headgroup and the ionomer side chains significantly inhibit catalytic activity.[325−330] The inhibition of kinetic activity is also strongly dependent on the nature of the cationic-headgroup (e.g., imidazolium, guanidium) and the presence of aromatic groups on the side chain (e.g., benzyltromethylammonium). In summary, quaternary ammonium cations in solution and in the ionomer were shown to inhibit the oxidation of methanol through specific adsorption. The lower performance in polymer-bound ammonium cations relative to free ammonium cations calls into question a more quantitative understanding of the potential distribution at the alkaline ionomer electrode/electrolyte. These results clearly warrant more investigations on the effect of AEM ionomer adsorption on the catalytic activity of HOR, ORR, and alcohol oxidation. Particularly, such studies need to be performed under experimental conditions where excess KOH/NaOH is absent.

7. ALTERNATE SMALL MOLECULE OXIDATION

Among alternative small molecule fuels such as alcohols,[42,331,332] ethers,[333] sodium borohydride,[334] ammonia[335] etc., noncarbon containing hydrazine hydrate ($N_2H_4{\cdot}H_2O$) appears to be a promising small molecule fuel due to its high

DOI: 10.1021/acs.chemrev.9b00157
Chem. Rev. XXXX, XXX, XXX−XXX

energy density (3.5 Wh cm^{-3}) and a low theoretical standard electrode potential (−0.33 V vs RHE).[336,337] Hydrazine is a weak base with a pK_a of 8.1. While hydrazine is a very toxic material, recent developments at Daihatsu Motor Company show its safe fixation in the hydrazone form and on-demand generation of hydrazine could enable its practical applications.[338,339] A high theoretical standard equilibrium cell voltage of 1.56 V when paired with air cathode can be achieved in alkaline electrolytes as follows:

$$\text{anode:} \quad N_2H_4 + 4OH^- \rightarrow N_2 + 4H_2O + 4H_2O + 4e^- \qquad E^0 = -0.33V \quad \text{vs RHE} \tag{24}$$

$$\text{cathode:} \quad O_2 + 2H_2O + 4e^- \rightarrow 4OH^- \qquad E^0 = 1.23V \quad \text{vs RHE} \tag{25}$$

$$\text{overall:} \quad N_2H_4 + O_2 \rightarrow N_2 + 2H_2O \qquad E^\circ = 1.56V \tag{26}$$

N_2 is the only gaseous product formed for a purely electrocatalytic hydrazine oxidation process. Hydrazine can also undergo competitive chemical decomposition on catalytic surfaces leading to the formation of H_2 and NH_3:[340]

$$N_2H_4 \rightarrow N_2 + 2H_2 \tag{27}$$

$$3N_2H_4 \rightarrow 2N_2 + 4NH_3 \tag{28}$$

Chemical decomposition to form H_2 leads to loss of fuel efficiency and a mixed potential scenario corresponding to a combination of HER/HOR and hydrazine oxidation reactions. While electrochemical oxidation of hydrazine is plausible under both acidic and alkaline conditions, highly stable catalytic surfaces such as Pt are required in acid that are also very active for the chemical decomposition process. Alternatively, alkaline electrolytes enable the use of non-noble metal surfaces that are relatively less active for hydrazine decomposition.[336]

In acid, hydrazine oxidation involves the initial reversible adsorption of hydrazinium ions ($N_2H_5^+$) followed by three successive deprotonation steps to the final product N_2. The second deprotonation step is typically considered to be the rate-determining step (reaction scheme is shown in Figure 11).[341,342]

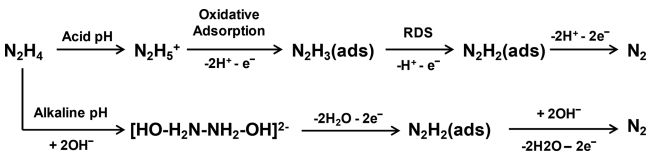

Figure 11. Electrochemical hydrazine oxidation reaction pathways in acidic and alkaline electrolytes.

The overall reaction is sensitive to the nature of the metal and its crystallographic orientations due to varying strength and mode of hydrazine adsorption on the basal planes of Pt. On Pt single crystal basal plane electrodes in alkaline electrolytes,[343] hydrazine oxidation predominantly proceeds at the N−H bond and is essentially considered as a stepwise electrochemical dehydrogenation process leading to formation of molecular nitrogen without the activation of the N−N bond (Figure 11). It is not clear what the rate-determining step is in hydrazine oxidation from this study, but it appears that N_2H_2 is a key intermediate. Online mass spectrometry studies of hydrazine oxidation on all platinum single crystal surfaces in dilute alkaline electrolyte solution indicate molecular nitrogen as the only product. Formation of molecular hydrogen and other nitrogen oxide (NO, N_2O, and NO_2) species were not observed, indicating no competitive chemical decomposition reaction of hydrazine on platinum surfaces.[343]

A range of non-pgm catalysts have been investigated such as Co, Cu, Ni, and metalloporphyrins for hydrazine oxidation in alkaline electrolyte.[340,344−348] Particularly, Ni-rich alloys such as NiCo and NiLa appear to be very active toward hydrazine oxidation.[340,347] Among the elemental catalyst surfaces, cobalt appears to provide a very low onset potential for hydrazine oxidation (−0.178 V vs RHE on Co compared to 0.062 V for Pt, −0.108 V for Ni, and 0.193 V for Cu).[344] Strasser et al.[340] have recently investigated the electrochemical oxidation of hydrazine on NiCo bimetallic alloys in alkaline media. Strong adsorption of hydrazine prior to electron transfer requires metallic surfaces free of oxides. While both monometallic surfaces such as Ni and Co exhibit low anodic onset potentials, irreversible surface passivation due to the formation of Ni/Co-$(OH)_x$ leads to a drop in catalytic activity. Interestingly, a stoichiometric $Ni_{60}Co_{40}$ alloy exhibited a 6-fold improvement in hydrazine oxidation activity with a low onset potential of −0.15 V vs RHE due to suppressed surface passivation. Despite the very high activity, hydrazine was found to undergo a parallel reaction pathway involving both electrochemical oxidation to H_2O/N_2 and also the less efficient chemical decomposition to N_2/H_2. Sakamoto et al.[347] developed carbon-supported $Ni_{1-x}La_x$ ($0.1 \leq x \leq 0.9$) binary alloy based catalysts and observed that $Ni_{0.9}La_{0.1}$ was the most active composition for hydrazine electroxidation. The high activity of $Ni_{0.9}La_{0.1}$ is ascribed to its core−shell structure exhibiting an hcp-$LaNi_5$ shell over a fcc-Ni core. $Ni_{0.9}La_{0.1}$ features an onset potential of −0.0464 V vs RHE compared to −0.0045 V for Ni. Zagal et al.[345] also demonstrated hydrazine oxidation activity on non-pgm materials such as iron metalloporphyrins and phthalocyanines with activity correlated via a volcano plot versus metal-center redox potential of which Fe-phthalocyanine is at the top.

While several catalyst materials have been demonstrated to be useful for hydrazine oxidation activity in liquid alkaline electrolyte, their performance as an anode electrode when integrated into an AAEM fuel cell has been much less explored. Some studies that do provide insights into the performance of direct hydrazine fuel based AAEM fuel cells end up utilizing excess-KOH/NaOH in the anode feed.[339,349,350] For instance, an AAEM fuel cell employing polyolefin-based electrolyte alkaline electrolyte with tatraalkyl ammonium ion-exchange groups, Ni-based anode, and Co-based cathode exhibited useful current densities of ∼300 mA/cm^2 at 0.65 V with 0.67 M hydrazine +1 M KOH anode feed and pure O_2 as the cathode feed.[339] As mentioned in previously, such operations with excess-KOH discredit the use of alkaline membrane electrolytes. Poor performance of direct-hydrazine AAEM fuel cell could be due to a range of issues arising from inefficient oxidation in anode electrode structures under three-phase boundary conditions, fuel crossover to the cathode, and specific adsorption of ammonium cations as mentioned in the previous section. We believe that ways for safe fixation of hydrazine and its application in direct-hydrazine fed AAEM fuel cell (without excess-KOH) remains a future opportunity for research.

8. CONCLUSIONS

The central requirement for the success of AAEM fuel cells lies in the development of alkaline membranes and ionomers that are thermochemically stable and conductive particularly at

DOI: 10.1021/acs.chemrev.9b00157
Chem. Rev. XXXX, XXX, XXX−XXX

elevated temperatures and subsaturated conditions. While this progress continues, complementary research in electrocatalysis and interfacial charge transfer is highly critical since significant cell voltage losses and cost are associated with it. After all, the single biggest driver of AAEM fuel cell research is the possibility to enable a PGM-free system under alkaline conditions. At present, a plethora of inexpensive PGM catalysts (e.g., Ag/C) and non-PGM catalysts have shown significantly better ORR activities at high pH due to the favorable mechanistic aspects. Future studies on ORR catalysts should focus on translating these high activities observed in liquid electrolytes to actual MEA performances. On the other hand, while some recent studies point to encouraging HOR activities on non-PGM anode catalysts (e.g., Ni based), more development is needed in this area. Fortunately, Pt alloys such as PtRu/C catalysts have demonstrated a high enough exchange current density in alkaline electrolytes to match the performance of the HOR activity on pure Pt/C in acid electrolytes. This implies that alkaline HOR anode electrodes could be developed with PtRu/C catalysts at low loadings of $\leq$0.05 mg_{Pt}/cm^2 similar to that of PEM fuel cells. So, it is possible to envision a current state of the art AAEM fuel cell electrodes to comprise of a low PtRu-loaded anode coupled with either an inexpensive PGM catalyst (such as Ag/C) or a non-PGM catalyst (such as Fe−N_x−C or perovskites) cathode.

Catalyst poisoning by ionomer functional group adsorption, membrane poisoning by carbonates, and water maldistribution are issues that tend to undermine the progress of AAEM fuel cells. These issues need to be tackled by a combination of novel materials and system engineering. Particularly, the use of upstream filters and current-density excursions are useful strategies to mitigate carbonate poisoning. Alkaline membranes/ionomers with optimal water uptake and gas diffusion layers with controlled structure/hydrophobicity are needed to maintain efficient water distribution in the cell. Improved cell designs and dynamic control of operating conditions such as inlet RH/outlet pressure are critical to enable efficient water distribution across the cell. It is clear that alkaline membranes and ionomers that maintain sufficient conductivity at high temperatures (80 to 90 °C) and subsaturated conditions would solve a host of issues related to carbonate poisoning, water management, and heat rejection capabilities of the AAEM fuel cell. On the other hand, fundamental electrochemical and spectroscopic investigations related to the catalyst-ionomer interactions are highly warranted. Particularly, studies on the adsorption of quaternary ammonium cation head groups and other side chain moieties on the catalysts surfaces and their impact on electrocatalysis are needed. There is a need to study electrochemical kinetics at alkaline interfaces containing quaternary ammonium cations in the absence of excess KOH electrolyte. This is particularly important in the context of direct alcohol/hydrazine fed AAEM fuel cells operating in the absence of excess alkali. In order to enable AAEM fuel cell technology for terrestrial applications, future studies in alkaline electrocatalysis should focus on the application and demonstration of (i) less expensive PGM or non-PGM catalysts in solid alkaline electrolytes as opposed to liquid electrolytes, (ii) MEA performances using air cathode feed (w/CO_2) instead of pure O_2, and (iii) MEA performances without excess alkali in the anode feed for direct alcohol/hydrazine anodes.

AUTHOR INFORMATION

Corresponding Author

*E-mail: s.mukerjee@northeastern.edu. Tel: +1 617 373-2382. Fax: +1 617 373-8949.

ORCID

Nagappan Ramaswamy: 0000-0002-3430-2758
Sanjeev Mukerjee: 0000-0002-2980-7655

Present Address

†General Motors Corporation, Global Fuel Cell Business, 850 N Glenwood Avenue, Pontiac, MI 48340.

Funding

We deeply appreciate financial assistance from the Army Research Office under the Single Investigator Grant 55036-CH.

Notes

The authors declare no competing financial interest.

Biographies

Dr. Nagappan Ramaswamy is currently a Research Engineer at the Global Fuel Cell Activities Division, General Motors Corporation located at Pontiac, Michigan. Dr. Ramaswamy received a Bachelor of Chemical and Electrochemical Engineering degree from Central Electrochemical Research Institute, India, in 2005 and a Ph.D. degree in Physical Chemistry from Northeastern University in 2011. His doctoral thesis involved the investigation of precious and nonprecious electrocatalyst materials in acid and alkaline electrolytes with a particular emphasis on unraveling the fundamental relationships between electrochemical double layer structure and catalytic mechanisms.

Dr. Sanjeev Mukerjee is a Professor in the Department of Chemistry and Chemical Biology (Northeastern University), where he has been since September of 1998. He also heads the newly created center for Renewable Energy Technology and its subset the Laboratory for Electrochemical Advanced Power (LEAP). He is the author of 130 peer-reviewed publications with a current H-index of 53 and is a fellow of the Electrochemical Society. He has given numerous invited and keynote presentations in various national and international meetings and holds five U.S. and international patents. He also serves on the scientific advisory boards of three companies.

REFERENCES

(1) Costamagna, P.; Srinivasan, S. Quantum jumps in the PEMFC science and technology from the 1960s to the year 2000: Part I. Fundamental scientific aspects. *J. Power Sources* **2001**, *102*, 242−252.

(2) Gasteiger, H. A.; Kocha, S. S.; Sompalli, B.; Wagner, F. T. Activity benchmarks and requirements for Pt, Pt-alloy, and non-Pt oxygen reduction catalysts for PEMFCs. *Appl. Catal., B* **2005**, *56*, 9−35.

(3) Spendelow, J. S.; Papageorgopoulos, D. C. Progress in PEMFC MEA Component R&D at the DOE Fuel Cell Technologies Program. *Fuel Cells* **2011**, *11*, 775−786.

(4) Kongkanand, A.; Mathias, M. F. The Priority and Challenge of High-Power Performance of Low-Platinum Proton-Exchange Membrane Fuel Cells. *J. Phys. Chem. Lett.* **2016**, *7*, 1127−1137.

(5) Debe, M. K. Electrocatalyst approaches and challenges for automotive fuel cells. *Nature* **2012**, *486*, 43−51.

(6) *Fuel Cell Multi-Year Research, Development and Demonstration Plan*; The US Department of Energy, Energy Efficiency and Renewable Energy: Washington, D.C., 2016.

(7) Borup, R.; Meyers, J.; Pivovar, B.; Kim, Y. S.; Mukundan, R.; Garland, N.; Myers, D.; Wilson, M.; Garzon, F.; Wood, D.; et al. Scientific Aspects of Polymer Electrolyte Fuel Cell Durability and Degradation. *Chem. Rev.* **2007**, *107*, 3904−3951.

DOI: 10.1021/acs.chemrev.9b00157
Chem. Rev. XXXX, XXX, XXX−XXX

(8) Chung, H. T.; Cullen, D. A.; Higgins, D.; Sneed, B. T.; Holby, E. F.; More, K. L.; Zelenay, P. Direct atomic-level insight into the active sites of a high-performance PGM-free ORR catalyst. *Science* **2017**, *357*, 479−484.
(9) Jaouen, F.; Proietti, E.; Lefevre, M.; Chenitz, R.; Dodelet, J.-P.; Wu, G.; Chung, H. T.; Johnston, C. M.; Zelenay, P. Recent advances in non-precious metal catalysis for oxygen-reduction reaction in polymer electrolyte fuel cells. *Energy Environ. Sci.* **2011**, *4*, 114−130.
(10) Bockris, J. O.; Appleby, J. Alkaline fuel cells (AFCs). In *Assessment of Research Needs for Advanced Fuel Cells*; Penner, S. S., Ed. 1986; Vol.*11*, pp 95−135.
(11) Cifrain, M.; Kordesch, K. Hydrogen/oxygen (air) fuel cells with alkaline electrolytes. In *Handbook of Fuel Cells*; John Wiley & Sons, Ltd, 2010.
(12) McLean, G. F.; Niet, T.; Prince-Richard, S.; Djilali, N. An assessment of alkaline fuel cell technology. *Int. J. Hydrogen Energy* **2002**, *27*, 507−526.
(13) Varcoe, J. R.; Slade, R. C. T. Prospects for Alkaline Anion Exchange Membranes in Low Temperature Fuel Cells. *Fuel Cells* **2005**, *5*, 187−200.
(14) Merle, G.; Wessling, M.; Nijmeijer, K. Anion exchange membranes for alkaline fuel cells: A review. *J. Membr. Sci.* **2011**, *377*, 1−35.
(15) Slade, R. T.; Kizewski, J.; Poynton, S.; Zeng, R.; Varcoe, J. Alkaline Membrane Fuel Cells. In *Fuel Cells*; Kreuer, K.-D., Ed.; Springer New York: 2013; pp 9−29.
(16) Yan, J.; Hickner, M. A. Anion Exchange Membranes by Bromination of Benzylmethyl-Containing Poly(sulfone)s. *Macromolecules* **2010**, *43*, 2349−2356.
(17) Hibbs, M. R.; Hickner, M. A.; Alam, T. M.; McIntyre, S. K.; Fujimoto, C. H.; Cornelius, C. J. Transport Properties of Hydroxide and Proton Conducting Membranes. *Chem. Mater.* **2008**, *20*, 2566−2573.
(18) Switzer, E. E.; Olson, T. S.; Datye, A. K.; Atanassov, P.; Hibbs, M. R.; Fujimoto, C.; Cornelius, C. J. Novel KOH-free anion-exchange membrane fuel cell: Performance comparison of alternative anion-exchange ionomers in catalyst ink. *Electrochim. Acta* **2010**, *55*, 3404−3408.
(19) Varcoe, J. R. Investigations of the ex situ ionic conductivities at 30 DegC of metal-cation-free quaternary ammonium alkaline anion-exchange membranes in static atmospheres of different relative humidities. *Phys. Chem. Chem. Phys.* **2007**, *9*, 1479−1486.
(20) Couture, G.; Alaaeddine, A.; Boschet, F.; Ameduri, B. Polymeric materials as anion-exchange membranes for alkaline fuel cells. *Prog. Polym. Sci.* **2011**, *36*, 1521−1557.
(21) Appleby, A. J., Electrocatalysis. In *Comprehensive Treatise of Electrochemistry*; Conway, B. E., Bockris, J. O. M., Yeager, E., Khan, S. U. M., White, R. E., Eds.; Springer: Boston, MA, 1983, Vol. 7, pp 173−239.
(22) Zhang, H.; Zhou, Z. Alkaline polymer electrolyte membranes from quaternized poly(phthalazinone ether ketone) for direct methanol fuel cell. *J. Appl. Polym. Sci.* **2008**, *110*, 1756−1762.
(23) Ertem, S. P.; Tsai, T.-H.; Donahue, M. M.; Zhang, W.; Sarode, H.; Liu, Y.; Seifert, S.; Herring, A. M.; Coughlin, E. B. Photo-Cross-Linked Anion Exchange Membranes with Improved Water Management and Conductivity. *Macromolecules* **2016**, *49*, 153−161.
(24) Liao, X.; Gong, Y.; Liu, Y.; Zuo, D.; Zhang, H. Blend membranes of quaternized poly(vinylbenzyl chloride-co-styrene) and quaternized polysulfone for anion-exchange membrane fuel cells. *RSC Adv.* **2015**, *5*, 99347−99355.
(25) Jeon, J. Y.; Park, S.; Han, J.; Maurya, S.; Mohanty, A. D.; Tian, D.; Saikia, N.; Hickner, M. A.; Ryu, C. Y.; Tuckerman, M. E.; et al. Synthesis of Aromatic Anion Exchange Membranes by Friedel−Crafts Bromoalkylation and Cross-Linking of Polystyrene Block Copolymers. *Macromolecules* **2019**, *52*, 2139−2147.
(26) Pan, J.; Han, J.; Zhu, L.; Hickner, M. A. Cationic Side-Chain Attachment to Poly(Phenylene Oxide) Backbones for Chemically Stable and Conductive Anion Exchange Membranes. *Chem. Mater.* **2017**, *29*, 5321−5330.
(27) Liao, X.; Ren, L.; Chen, D.; Liu, X.; Zhang, H. Nanocomposite membranes based on quaternized polysulfone and functionalized montmorillonite for anion-exchange membranes. *J. Power Sources* **2015**, *286*, 258−263.
(28) Fuel Cell Multi-Year Research, Development and Demonstration Plan. http://www.eere.energy.gov/hydrogenandfuelcells/mypp/pdfs/fuel_cells.pdf; Technical Report for The US Department of Energy, Energy Efficiency and Renewable Energy, 2012.
(29) Neyerlin, K. C.; Gu, W.; Jorne, J.; Gasteiger, H. A. Study of the Exchange Current Density for the Hydrogen Oxidation and Evolution Reactions. *J. Electrochem. Soc.* **2007**, *154*, B631−B635.
(30) Bagotzky, V.S.; Osetrova, N.V. Investigation of hydrogen ionization on platinum with the help of microelectrodes. *J. Electroanal. Chem. Interfacial Electrochem.* **1973**, *43*, 233−249.
(31) Maruyama, J.; Inaba, M.; Katakura, K.; Ogumi, Z.; Takehara, Z.-i. Influence of Nafion® film on the kinetics of anodic hydrogen oxidation. *J. Electroanal. Chem.* **1998**, *447*, 201−209.
(32) Sheng, W.; Gasteiger, H. A.; Shao-Horn, Y. Hydrogen oxidation and evolution reaction kinetics on platinum: Acid vs alkaline electrolytes. *J. Electrochem. Soc.* **2010**, *157*, B1529−B1536.
(33) Sheng, W.; Zhuang, Z.; Gao, M.; Zheng, J.; Chen, J. G.; Yan, Y. Correlating hydrogen oxidation and evolution activity on platinum at different pH with measured hydrogen binding energy. *Nat. Commun.* **2015**, *6*, DOI: 10.1038/ncomms6848.
(34) Durst, J.; Siebel, A.; Simon, C.; Hasche, F.; Herranz, J.; Gasteiger, H. A. New insights into the electrochemical hydrogen oxidation and evolution reaction mechanism. *Energy Environ. Sci.* **2014**, *7*, 2255−2260.
(35) Strmcnik, D.; Uchimura, M.; Wang, C.; Subbaraman, R.; Danilovic, N.; van der Vliet, D.; Paulikas, A. P.; Stamenkovic, V. R.; Markovic, N. M. Improving the hydrogen oxidation reaction rate by promotion of hydroxyl adsorption. *Nat. Chem.* **2013**, *5*, 300−306.
(36) Wang, Y.; Wang, G.; Li, G.; Huang, B.; Pan, J.; Liu, Q.; Han, J.; Xiao, L.; Lu, J.; Zhuang, L. Pt-Ru catalyzed hydrogen oxidation in alkaline media: oxophilic effect or electronic effect? *Energy Environ. Sci.* **2015**, *8*, 177−181.
(37) Ramaswamy, N.; Ghoshal, S.; Bates, M. K.; Jia, Q.; Li, J.; Mukerjee, S. Hydrogen oxidation reaction in alkaline media: Relationship between electrocatalysis and electrochemical double-layer structure. *Nano Energy* **2017**, *41*, 765−771.
(38) Ramaswamy, N.; Mukerjee, S. Influence of Inner- and Outer-Sphere Electron Transfer Mechanisms during Electrocatalysis of Oxygen Reduction in Alkaline Media. *J. Phys. Chem. C* **2011**, *115*, 18015−18026.
(39) Li, M. F.; Liao, L. W.; Yuan, D. F.; Mei, D.; Chen, Y.-X. pH effect on oxygen reduction reaction at Pt(1 1 1) electrode. *Electrochim. Acta* **2013**, *110*, 780−789.
(40) Gong, K.; Du, F.; Xia, Z.; Durstock, M.; Dai, L. Nitrogen-Doped Carbon Nanotube Arrays with High Electrocatalytic Activity for Oxygen Reduction. *Science* **2009**, *323*, 760−764.
(41) Ramaswamy, N.; Tylus, U.; Jia, Q.; Mukerjee, S. Activity Descriptor Identification for Oxygen Reduction on Nonprecious Electrocatalysts: Linking Surface Science to Coordination Chemistry. *J. Am. Chem. Soc.* **2013**, *135*, 15443−15449.
(42) Spendelow, J. S.; Wieckowski, A. Electrocatalysis of oxygen reduction and small alcohol oxidation in alkaline media. *Phys. Chem. Chem. Phys.* **2007**, *9*, 2654−2675.
(43) Ramaswamy, N.; Mukerjee, S. Fundamental Mechanistic Understanding of Electrocatalysis of Oxygen Reduction on Pt and Non-Pt Surfaces: Acid versus Alkaline Media. *Adv. Phys. Chem.* **2012**, *2012*, 1.
(44) Inaba, M.; Matsui, Y.; Saito, M.; Tasaka, A.; Fukuta, K.; Watanabe, S.; Yanagi, H. Effects of Carbon Dioxide on the Performance of Anion-Exchange Membrane Fuel Cells. *Electrochemistry* **2011**, *79*, 322−325.
(45) Wang, Y.; Li, L.; Hu, L.; Zhuang, L.; Lu, J.; Xu, B. A feasibility analysis for alkaline membrane direct methanol fuel cell: thermodynamic disadvantages versus kinetic advantages. *Electrochem. Commun.* **2003**, *5*, 662−666.

DOI: 10.1021/acs.chemrev.9b00157
Chem. Rev. XXXX, XXX, XXX−XXX

(46) Antolini, E.; Gonzalez, E. R. Alkaline direct alcohol fuel cells. *J. Power Sources* **2010**, *195*, 3431−3450.
(47) Bunazawa, H.; Yamazaki, Y. Influence of anion ionomer content and silver cathode catalyst on the performance of alkaline membrane electrode assemblies (MEAs) for direct methanol fuel cells (DMFCs). *J. Power Sources* **2008**, *182*, 48−51.
(48) Coutanceau, C.; Demarconnay, L.; Lamy, C.; Leger, J. M. Development of electrocatalysts for solid alkaline fuel cell (SAFC). *J. Power Sources* **2006**, *156*, 14−19.
(49) Kim, J.; Momma, T.; Osaka, T. Cell performance of Pd-Sn catalyst in passive direct methanol alkaline fuel cell using anion exchange membrane. *J. Power Sources* **2009**, *189*, 999−1002.
(50) Yu, E. H.; Scott, K. Direct methanol alkaline fuel cells with catalysed anion exchange membrane electrodes. *J. Appl. Electrochem.* **2005**, *35*, 91.
(51) Ünlü, M.; Abbott, D.; Ramaswamy, N.; Ren, X.; Mukerjee, S.; Kohl, P. A. Analysis of Double Layer and Adsorption Effects at the Alkaline Polymer Electrolyte-Electrode Interface. *J. Electrochem. Soc.* **2011**, *158*, B1423−B1431.
(52) Omasta, T. J.; Park, A. M.; LaManna, J. M.; Zhang, Y.; Peng, X.; Wang, L.; Jacobson, D. L.; Varcoe, J. R.; Hussey, D. S.; Pivovar, B. S.; et al. Beyond catalysis and membranes: visualizing and solving the challenge of electrode water accumulation and flooding in AEMFCs. *Energy Environ. Sci.* **2018**, *11*, 551−558.
(53) Zhang, H.; Ohashi, H.; Tamaki, T.; Yamaguchi, T. Direction and Management of Water Movement in Solid-State Alkaline Fuel Cells. *J. Phys. Chem. C* **2012**, *116*, 7650−7657.
(54) Peng, S.; Gong, J.; Xu, X.; Sui, P.-C.; Lu, S.; Xiang, Y. Numerical and Experimental Analyses on Deviated Concentration Loss with Alkaline Anion-Exchange Membrane Fuel Cells. *J. Phys. Chem. C* **2015**, *119*, 24276−24281.
(55) Shiau, H.-S.; Zenyuk, I. V.; Weber, A. Z. Water Management in an Alkaline-Exchange-Membrane Fuel Cell. *ECS Trans.* **2015**, *69*, 985−994.
(56) Isomura, T.; Fukuta, K.; Yanagi, H.; Ge, S.; Wang, C.-Y. Impact of Low Cathode Humidification on Alkaline Membrane Fuel Cell Performance. *ECS Meeting Abstracts* **2011**, *MA2011−01*, 221.
(57) Kaspar, R. B.; Letterio, M. P.; Wittkopf, J. A.; Gong, K.; Gu, S.; Yan, Y. Manipulating Water in High-Performance Hydroxide Exchange Membrane Fuel Cells through Asymmetric Humidification and Wetproofing. *J. Electrochem. Soc.* **2015**, *162*, F483−F488.
(58) Sohn, Y.-J.; Choi, J.-I.; Kim, K. Numerical Analysis on Water Transport in Alkaline Anion Exchange Membrane Fuel Cells. *Electrochemistry* **2015**, *83*, 80−83.
(59) Gottesfeld, S.; Dekel, D. R.; Page, M.; Bae, C.; Yan, Y.; Zelenay, P.; Kim, Y. S. Anion exchange membrane fuel cells: Current status and remaining challenges. *J. Power Sources* **2018**, *375*, 170−184.
(60) Dekel, D. R. Review of cell performance in anion exchange membrane fuel cells. *J. Power Sources* **2018**, *375*, 158−169.
(61) Pan, Z. F.; An, L.; Zhao, T. S.; Tang, Z. K. Advances and challenges in alkaline anion exchange membrane fuel cells. *Prog. Energy Combust. Sci.* **2018**, *66*, 141−175.
(62) Wagner, F. T.; Lakshmanan, B.; Mathias, M. F. Electrochemistry and the Future of the Automobile. *J. Phys. Chem. Lett.* **2010**, *1*, 2204−2219.
(63) Fukuta, K. *Electrolyte Materials for AMFCs, and AMFC Performance*, Presented at Alkaline Membrane Fuel Cell Workshop [Online], Washington, DC, May 8−9, 2011, http://www1.eere.energy.gov/hydrogenandfuelcells/wkshp_alkaline_membrane.html (accessed Jun 1, 2018).
(64) Piana, M.; Boccia, M.; Filpi, A.; Flammia, E.; Miller, H. A.; Orsini, M.; Salusti, F.; Santiccioli, S.; Ciardelli, F.; Pucci, A. H2/air alkaline membrane fuel cell performance and durability, using novel ionomer and non-platinum group metal cathode catalyst. *J. Power Sources* **2010**, *195*, 5875−5881.
(65) Gottesfeld, S. *CellEra Perspective on AMFCs: Breaking the Fuel Cell Barrier*, Presented at Alkaline Membrane Fuel Cell Workshop [Online], Washington, DC, May 8−9, 2011, http://www1.eere.energy.gov/hydrogenandfuelcells/wkshp_alkaline_membrane.html (accessed Jun 1, 2018).
(66) He, Q.; Li, Q.; Khene, S.; Ren, X.; López-Suárez, F. E.; Lozano-Castelló, D.; Bueno-López, A.; Wu, G. High-Loading Cobalt Oxide Coupled with Nitrogen-Doped Graphene for Oxygen Reduction in Anion-Exchange-Membrane Alkaline Fuel Cells. *J. Phys. Chem. C* **2013**, *117*, 8697−8707.
(67) Wu, G.; More, K. L.; Johnston, C. M.; Zelenay, P. High-performance electrocatalysts for oxygen reduction derived from polyaniline, iron, and cobalt. *Science* **2011**, *332*, 443−447.
(68) Lefevre, M.; Proietti, E.; Jaouen, F.; Dodelet, J.-P. Iron-Based Catalysts with Improved Oxygen Reduction Activity in Polymer Electrolyte Fuel Cells. *Science* **2009**, *324*, 71−74.
(69) Proietti, E.; Jaouen, F.; Lefevre, M.; Larouche, N.; Tian, J.; Herranz, J.; Dodelet, J.-P. Iron-based cathode catalyst with enhanced power density in polymer electrolyte membrane fuel cells. *Nat. Commun.* **2011**, *2*, 416.
(70) Pivovar, B. *Alkaline Membrane Fuel Cell Workshop Summary Report*, Presented at U.S. Department of Energy (DOE) - Fuel Cell Technologies Office (FCTO) [Online], Phoenix, AZ, April 1, 2016. https://energy.gov/sites/prod/files/2016/10/f33/fcto_2016_amfcw_report.pdf (accessed Jun 1, 2018).
(71) Holdcroft, S. Fuel Cell Catalyst Layers: A Polymer Science Perspective. *Chem. Mater.* **2014**, *26*, 381−393.
(72) Alesker, M.; Page, M.; Shviro, M.; Paska, Y.; Gershinsky, G.; Dekel, D. R.; Zitoun, D. Palladium/nickel bifunctional electrocatalyst for hydrogen oxidation reaction in alkaline membrane fuel cell. *J. Power Sources* **2016**, *304*, 332−339.
(73) Park, J.-S.; Park, S.-H.; Yim, S.-D.; Yoon, Y.-G.; Lee, W.-Y.; Kim, C.-S. Performance of solid alkaline fuel cells employing anion-exchange membranes. *J. Power Sources* **2008**, *178*, 620−626.
(74) Maurya, S.; Noh, S.; Matanovic, I.; Park, E. J.; Narvaez Villarrubia, C.; Martinez, U.; Han, J.; Bae, C.; Kim, Y. S. Rational design of polyaromatic ionomers for alkaline membrane fuel cells with > 1 W cm−2 power density. *Energy Environ. Sci.* **2018**, *11*, 3283−3291.
(75) Poynton, S. D.; Kizewski, J. P.; Slade, R. C. T.; Varcoe, J. R. Novel electrolyte membranes and non-Pt catalysts for low temperature fuel cells. *Solid State Ionics* **2010**, *181*, 219−222.
(76) Poynton, S. D.; Slade, R. C. T.; Omasta, T. J.; Mustain, W. E.; Escudero-Cid, R.; Ocón, P.; Varcoe, J. R. Preparation of radiation-grafted powders for use as anion exchange ionomers in alkaline polymer electrolyte fuel cells. *J. Mater. Chem. A* **2014**, *2*, 5124−5130.
(77) Luo, Y.; Guo, J.; Wang, C.; Chu, D. Tunable High-Molecular-Weight Anion-Exchange Membranes for Alkaline Fuel Cells. *Macromol. Chem. Phys.* **2011**, *212*, 2094−2102.
(78) Luo, Y.; Guo, J.; Wang, C.; Chu, D. An Acrylate-Polymer-Based Electrolyte Membrane for Alkaline Fuel Cell Applications. *ChemSusChem* **2011**, *4*, 1557−1560.
(79) Cao, Y.-C.; Wang, X.; Mamlouk, M.; Scott, K. Preparation of alkaline anion exchange polymer membrane from methylated melamine grafted poly(vinylbenzyl chloride) and its fuel cell performance. *J. Mater. Chem.* **2011**, *21*, 12910−12916.
(80) Gu, S.; Cai, R.; Luo, T.; Chen, Z.; Sun, M.; Liu, Y.; He, G.; Yan, Y. A Soluble and Highly Conductive Ionomer for High-Performance Hydroxide Exchange Membrane Fuel Cells. *Angew. Chem., Int. Ed.* **2009**, *48*, 6499−6502.
(81) Zhao, Y.; Yu, H.; Yang, D.; Li, J.; Shao, Z.; Yi, B. High-performance alkaline fuel cells using crosslinked composite anion exchange membrane. *J. Power Sources* **2013**, *221*, 247−251.
(82) Kim, Y. S. *DOE Hydrogen and Fuel Cells Program Review*; Department of Energy: Washinton, DC, 2011.
(83) Lu, S.; Pan, J.; Huang, A.; Zhuang, L.; Lu, J. Alkaline polymer electrolyte fuel cells completely free from noble metal catalysts. *Proc. Natl. Acad. Sci. U. S. A.* **2008**, *105*, 20611.
(84) Gu, S.; Sheng, W.; Cai, R.; Alia, S. M.; Song, S.; Jensen, K. O.; Yan, Y. An efficient Ag−ionomer interface for hydroxide exchange membrane fuel cells. *Chem. Commun.* **2013**, *49*, 131−133.
(85) Varcoe, J. R.; Atanassov, P.; Dekel, D. R.; Herring, A. M.; Hickner, M. A.; Kohl, P. A.; Kucernak, A. R.; Mustain, W. E.; Nijmeijer,

DOI: 10.1021/acs.chemrev.9b00157
Chem. Rev. XXXX, XXX, XXX−XXX

K.; Scott, K.; et al. Anion-exchange membranes in electrochemical energy systems. *Energy Environ. Sci.* **2014**, *7*, 3135−3191.
(86) Zhang, H. W.; Chen, D. Z.; Xianze, Y.; Yin, S. B. Anion-Exchange Membranes for Fuel Cells: Synthesis Strategies, Properties and Perspectives. *Fuel Cells* **2015**, *15*, 761−780.
(87) Grew, K. N.; Chiu, W. K. S. A Dusty Fluid Model for Predicting Hydroxyl Anion Conductivity in Alkaline Anion Exchange Membranes. *J. Electrochem. Soc.* **2010**, *157*, B327−B337.
(88) Raamat, E.; Kaupmees, K.; Ovsjannikov, G.; Trummal, A.; Kütt, A.; Saame, J.; Koppel, I.; Kaljurand, I.; Lipping, L.; Rodima, T.; et al. Acidities of strong neutral Brønsted acids in different media. *J. Phys. Org. Chem.* **2013**, *26*, 162−170.
(89) Kreuer, K. D. On the development of proton conducting polymer membranes for hydrogen and methanol fuel cells. *J. Membr. Sci.* **2001**, *185*, 29−39.
(90) Marino, M. G.; Melchior, J. P.; Wohlfarth, A.; Kreuer, K. D. Hydroxide, halide and water transport in a model anion exchange membrane. *J. Membr. Sci.* **2014**, *464*, 61−71.
(91) Varcoe, J. R.; Slade, R. C. T.; Lam How Yee, E.; Poynton, S. D.; Driscoll, D. J.; Apperley, D. C. Poly(ethylene-co-tetrafluoroethylene)-Derived Radiation-Grafted Anion-Exchange Membrane with Properties Specifically Tailored for Application in Metal-Cation-Free Alkaline Polymer Electrolyte Fuel Cells. *Chem. Mater.* **2007**, *19*, 2686−2693.
(92) Zhou, J.; Guo, J.; Chu, D.; Chen, R. Impacts of anion-exchange-membranes with various ionic exchange capacities on the performance of H2/O2 fuel cells. *J. Power Sources* **2012**, *219*, 272−279.
(93) Janarthanan, R.; Horan, J. L.; Caire, B. R.; Ziegler, Z. C.; Yang, Y.; Zuo, X.; Liberatore, M. W.; Hibbs, M. R.; Herring, A. M. Understanding anion transport in an aminated trimethyl polyphenylene with high anionic conductivity. *J. Polym. Sci., Part B: Polym. Phys.* **2013**, *51*, 1743−1750.
(94) Fujimoto, C.; Kim, D.-S.; Hibbs, M.; Wrobleski, D.; Kim, Y. S. Backbone stability of quaternized polyaromatics for alkaline membrane fuel cells. *J. Membr. Sci.* **2012**, *423*−*424*, 438−449.
(95) Zhang, M.; Kim, H. K.; Chalkova, E.; Mark, F.; Lvov, S. N.; Chung, T. C. M. New Polyethylene Based Anion Exchange Membranes (PE−AEMs) with High Ionic Conductivity. *Macromolecules* **2011**, *44*, 5937−5946.
(96) Pan, J.; Chen, C.; Li, Y.; Wang, L.; Tan, L.; Li, G.; Tang, X.; Xiao, L.; Lu, J.; Zhuang, L. Constructing ionic highway in alkaline polymer electrolytes. *Energy Environ. Sci.* **2014**, *7*, 354−360.
(97) Neagu, V.; Bunia, I.; Plesca, I. Ionic polymers VI. Chemical stability of strong base anion exchangers in aggressive media. *Polym. Degrad. Stab.* **2000**, *70*, 463−468.
(98) Coms, F. D. The Chemistry of Fuel Cell Membrane Chemical Degradation. *ECS Trans* **2008**, *16*, 235−255.
(99) Pivovar, B. *Alkaline Membrane Fuel Cell Workshop Report*, Presented at U.S. Department of Energy (DOE) - Fuel Cell Technologies Office (FCTO) [Online], Arlington, VA, May 8−9, 2011, http://www1.eere.energy.gov/hydrogenandfuelcells/pdfs/amfc_may2011_workshop_report.pdf (accessed January 6th, 2013).
(100) Ran, J.; Wu, L.; Varcoe, J. R.; Ong, A. L.; Poynton, S. D.; Xu, T. Development of imidazolium-type alkaline anion exchange membranes for fuel cell application. *J. Membr. Sci.* **2012**, *415*−*416*, 242−249.
(101) Zhang, F.; Zhang, H.; Qu, C. Imidazolium functionalized polysulfone anion exchange membrane for fuel cell application. *J. Mater. Chem.* **2011**, *21*, 12744−12752.
(102) Qiu, B.; Lin, B.; Qiu, L.; Yan, F. Alkaline imidazolium- and quaternary ammonium-functionalized anion exchange membranes for alkaline fuel cell applications. *J. Mater. Chem.* **2012**, *22*, 1040−1045.
(103) Deavin, O. I.; Murphy, S.; Ong, A. L.; Poynton, S. D.; Zeng, R.; Herman, H.; Varcoe, J. R. Anion-exchange membranes for alkaline polymer electrolyte fuel cells: comparison of pendent benzyltrimethylammonium- and benzylmethylimidazolium-head-groups. *Energy Environ. Sci.* **2012**, *5*, 8584−8597.
(104) Chen, D.; Hickner, M. A. Degradation of Imidazolium- and Quaternary Ammonium-Functionalized Poly(fluorenyl ether ketone sulfone) Anion Exchange Membranes. *ACS Appl. Mater. Interfaces* **2012**, *4*, 5775−5781.
(105) Ye, Y.; Elabd, Y. A. Relative Chemical Stability of Imidazolium-Based Alkaline Anion Exchange Polymerized Ionic Liquids. *Macromolecules* **2011**, *44*, 8494−8503.
(106) Jiang, L.; Lin, X.; Ran, J.; Li, C.; Wu, L.; Xu, T. Synthesis and Properties of Quaternary Phosphonium-based Anion Exchange Membrane for Fuel Cells. *Chin. J. Chem.* **2012**, *30*, 2241−2246.
(107) Gu, S.; Cai, R.; Yan, Y. Self-crosslinking for dimensionally stable and solvent-resistant quaternary phosphonium based hydroxide exchange membranes. *Chem. Commun.* **2011**, *47*, 2856−2858.
(108) Zhang, Q.; Li, S.; Zhang, S. A novel guanidinium grafted poly(aryl ether sulfone) for high-performance hydroxide exchange membranes. *Chem. Commun.* **2010**, *46*, 7495−7497.
(109) Zhang, B.; Gu, S.; Wang, J.; Liu, Y.; Herring, A. M.; Yan, Y. Tertiary sulfonium as a cationic functional group for hydroxide exchange membranes. *RSC Adv.* **2012**, *2*, 12683−12685.
(110) Gu, S.; Wang, J.; Kaspar, R. B.; Fang, Q.; Zhang, B.; Bryan Coughlin, E.; Yan, Y. Permethyl Cobaltocenium (Cp*2Co+) as an Ultra-Stable Cation for Polymer Hydroxide-Exchange Membranes. *Sci. Rep.* **2015**, *5*, 11668.
(111) Zha, Y.; Disabb-Miller, M. L.; Johnson, Z. D.; Hickner, M. A.; Tew, G. N. Metal-Cation-Based Anion Exchange Membranes. *J. Am. Chem. Soc.* **2012**, *134*, 4493−4496.
(112) Wang, J.; Gu, S.; Kaspar, R. B.; Zhang, B.; Yan, Y. Stabilizing the Imidazolium Cation in Hydroxide-Exchange Membranes for Fuel Cells. *ChemSusChem* **2013**, *6*, 2079−2082.
(113) Page, O. M. M.; Poynton, S. D.; Murphy, S.; Lien Ong, A.; Hillman, D. M.; Hancock, C. A.; Hale, M. G.; Apperley, D. C.; Varcoe, J. R. The alkali stability of radiation-grafted anion-exchange membranes containing pendent 1-benzyl-2,3-dimethylimidazolium head-groups. *RSC Adv.* **2013**, *3*, 579−587.
(114) Varcoe, J. R.; Slade, R. C. T.; Lam How Yee, E. An alkaline polymer electrochemical interface: a breakthrough in application of alkaline anion-exchange membranes in fuel cells. *Chem. Commun.* **2006**, 1428−1429.
(115) Ohma, A.; Mashio, T.; Sato, K.; Iden, H.; Ono, Y.; Sakai, K.; Akizuki, K.; Takaichi, S.; Shinohara, K. Analysis of proton exchange membrane fuel cell catalyst layers for reduction of platinum loading at Nissan. *Electrochim. Acta* **2011**, *56*, 10832−10841.
(116) Greszler, T. A.; Caulk, D.; Sinha, P. The Impact of Platinum Loading on Oxygen Transport Resistance. *J. Electrochem. Soc.* **2012**, *159*, F831−F840.
(117) Jomori, S.; Komatsubara, K.; Nonoyama, N.; Kato, M.; Yoshida, T. An Experimental Study of the Effects of Operational History on Activity Changes in a PEMFC. *J. Electrochem. Soc.* **2013**, *160*, F1067−F1073.
(118) Yanagi, H.; Fukuta, K. Anion Exchange Membrane and Ionomer for Alkaline Membrane Fuel Cells (AMFCs). *ECS Trans* **2008**, *16*, 257−262.
(119) Fukuta, K.; Inoue, H.; Watanabe, S.; Yanagi, H. In-situ Observation of CO2 through the Self-purging in Alkaline Membrane Fuel Cell (AMFC). *ECS Trans.* **2009**, *19*, 23−27.
(120) Varcoe, J. R.; Slade, R. C. T. An electron-beam-grafted ETFE alkaline anion-exchange membrane in metal-cation-free solid-state alkaline fuel cells. *Electrochem. Commun.* **2006**, *8*, 839−843.
(121) Clark, T. J.; Robertson, N. J.; Kostalik, H. A., IV; Lobkovsky, E. B.; Mutolo, P. F.; Abruña, H. c. D.; Coates, G. W. A Ring-Opening Metathesis Polymerization Route to Alkaline Anion Exchange Membranes: Development of Hydroxide-Conducting Thin Films from an Ammonium-Functionalized Monomer. *J. Am. Chem. Soc.* **2009**, *131*, 12888−12889.
(122) Zhu, S.; Hu, X.; Zhang, L.; Shao, M. Impacts of Perchloric Acid, Nafion, and Alkali Metal Ions on Oxygen Reduction Reaction Kinetics in Acidic and Alkaline Solutions. *J. Phys. Chem. C* **2016**, *120*, 27452−27461.
(123) Subbaraman, R.; Danilovic, N.; Lopes, P. P.; Tripkovic, D.; Strmcnik, D.; Stamenkovic, V. R.; Markovic, N. M. Origin of Anomalous Activities for Electrocatalysts in Alkaline Electrolytes. *J. Phys. Chem. C* **2012**, *116*, 22231−22237.

DOI: 10.1021/acs.chemrev.9b00157
Chem. Rev. XXXX, XXX, XXX−XXX

(124) Hoare, J. P. Oxygen. In *Standard Potentials in Aqueous Solution*; Bard, A. J., Parsons, R., Jordan, J., Eds.; CRC Press: New York, 1985; pp 49−60.
(125) Yang, H.-H.; McCreery, R. L. Elucidation of the mechanism of dioxygen reduction on metal-free carbon electrodes. *J. Electrochem. Soc.* **2000**, *147*, 3420−3428.
(126) Blizanac, B. B.; Ross, P. N.; Markovic, N. M. Oxygen electroreduction on Ag(111): The pH effect. *Electrochim. Acta* **2007**, *52*, 2264−2271.
(127) Schmidt, T. J.; Ross, P. N.; Markovic, N. M. Temperature dependent surface electrochemistry on Pt single crystals in alkaline electrolytes Part 2. The hydrogen evolution/oxidation reaction. *J. Electroanal. Chem.* **2002**, *524*−*525*, 252−260.
(128) Davydova, E. S.; Mukerjee, S.; Jaouen, F.; Dekel, D. R. Electrocatalysts for Hydrogen Oxidation Reaction in Alkaline Electrolytes. *ACS Catal.* **2018**, *8*, 6665−6690.
(129) Woodroof, M. D.; Wittkopf, J. A.; Gu, S.; Yan, Y. S. Exchange current density of the hydrogen oxidation reaction on Pt/C in polymer solid base electrolyte. *Electrochem. Commun.* **2015**, *61*, 57−60.
(130) Breiter, M. W. Reaction mechanisms of the H2 oxidation/evolution reaction. In *Handbook of Fuel Cells*; John Wiley & Sons, Ltd: 2010.
(131) Krischer, K.; Savinova, E. R. Special catalytic systems: electrocatalysis: fundamental of electrocatalysis. *Handbook of Heterogeneous Catalysis*; Wiley, 2008; Vol. *4*, pp 1873−1905.
(132) Conway, B. E.; Tilak, B. V. Interfacial processes involving electrocatalytic evolution and oxidation of H2, and the role of chemisorbed. *Electrochim. Acta* **2002**, *47*, 3571−3594.
(133) Skúlason, E.; Tripkovic, V.; Björketun, M. E.; Gudmundsdóttir, S.; Karlberg, G.; Rossmeisl, J.; Bligaard, T.; Jónsson, H.; Nørskov, J. K. Modeling the Electrochemical Hydrogen Oxidation and Evolution Reactions on the Basis of Density Functional Theory Calculations. *J. Phys. Chem. C* **2010**, *114*, 18182−18197.
(134) Zhang, T.; Anderson, A. B. Hydrogen Oxidation and Evolution on Platinum Electrodes in Base: Theoretical Study. *J. Phys. Chem. C* **2007**, *111*, 8644−8648.
(135) Elbert, K.; Hu, J.; Ma, Z.; Zhang, Y.; Chen, G.; An, W.; Liu, P.; Isaacs, H. S.; Adzic, R. R.; Wang, J. X. Elucidating Hydrogen Oxidation/Evolution Kinetics in Base and Acid by Enhanced Activities at the Optimized Pt Shell Thickness on the Ru Core. *ACS Catal.* **2015**, *5*, 6764−6772.
(136) Rheinländer, P. J.; Herranz, J.; Durst, J.; Gasteiger, H. A. Kinetics of the Hydrogen Oxidation/Evolution Reaction on Polycrystalline Platinum in Alkaline Electrolyte Reaction Order with Respect to Hydrogen Pressure. *J. Electrochem. Soc.* **2014**, *161*, F1448−F1457.
(137) Alia, S. M.; Pivovar, B. S.; Yan, Y. Platinum-Coated Copper Nanowires with High Activity for Hydrogen Oxidation Reaction in Base. *J. Am. Chem. Soc.* **2013**, *135*, 13473−13478.
(138) Zheng, J.; Zhuang, Z.; Xu, B.; Yan, Y. Correlating Hydrogen Oxidation/Evolution Reaction Activity with the Minority Weak Hydrogen-Binding Sites on Ir/C Catalysts. *ACS Catal.* **2015**, *5*, 4449−4455.
(139) St. John, S.; Atkinson, R. W.; Unocic, R. R.; Zawodzinski, T. A.; Papandrew, A. B. Ruthenium-Alloy Electrocatalysts with Tunable Hydrogen Oxidation Kinetics in Alkaline Electrolyte. *J. Phys. Chem. C* **2015**, *119*, 13481−13487.
(140) Zheng, J.; Sheng, W.; Zhuang, Z.; Xu, B.; Yan, Y. Universal dependence of hydrogen oxidation and evolution reaction activity of platinum-group metals on pH and hydrogen binding energy. *Sci. Adv.* **2016**, *2*, No. e1501602.
(141) Schwämmlein, J. N.; El-Sayed, H. A.; Stühmeier, B. M.; Wagenbauer, K. F.; Dietz, H.; Gasteiger, H. A. Origin of Superior Activity of Ru@Pt Core-Shell Nanoparticles towards Hydrogen Oxidation in Alkaline Media. *ECS Trans.* **2016**, *75*, 971−982.
(142) Rossmeisl, J.; Chan, K.; Ahmed, R.; Tripkovic, V.; Bjorketun, M. E. pH in atomic scale simulations of electrochemical interfaces. *Phys. Chem. Chem. Phys.* **2013**, *15*, 10321−10325.
(143) Cai, Y.; Anderson, A. B. The Reversible Hydrogen Electrode: Potential-Dependent Activation Energies over Platinum from Quantum Theory. *J. Phys. Chem. B* **2004**, *108*, 9829−9833.
(144) Anderson, A. B.; Sidik, R. A.; Narayanasamy, J.; Shiller, P. Theoretical Calculation of Activation Energies for Pt + H+(aq.) + e-(U) .tautm. Pt-H: Activation Energy-Based Symmetry Factors in the Marcus Normal and Inverted Regions. *J. Phys. Chem. B* **2003**, *107*, 4618−4623.
(145) Subbaraman, R.; Tripkovic, D.; Strmcnik, D.; Chang, K.-C.; Uchimura, M.; Paulikas, A. P.; Stamenkovic, V.; Markovic, N. M. Enhancing Hydrogen Evolution Activity in Water Splitting by Tailoring Li+-Ni(OH)2-Pt Interfaces. *Science* **2011**, *334*, 1256−1260.
(146) St. John, S.; Atkinson, R. W.; Unocic, K. A.; Unocic, R. R.; Zawodzinski, T. A.; Papandrew, A. B. Platinum and Palladium Overlayers Dramatically Enhance the Activity of Ruthenium Nanotubes for Alkaline Hydrogen Oxidation. *ACS Catal.* **2015**, *5*, 7015−7023.
(147) Miller, H. A.; Vizza, F.; Marelli, M.; Zadick, A.; Dubau, L.; Chatenet, M.; Geiger, S.; Cherevko, S.; Doan, H.; Pavlicek, R. K.; et al. Highly active nanostructured palladium-ceria electrocatalysts for the hydrogen oxidation reaction in alkaline medium. *Nano Energy* **2017**, *33*, 293−305.
(148) Bakos, I.; Paszternák, A.; Zitoun, D. Pd/Ni Synergestic Activity for Hydrogen Oxidation Reaction in Alkaline Conditions. *Electrochim. Acta* **2015**, *176*, 1074−1082.
(149) Jervis, R.; Mansor, N.; Gibbs, C.; Murray, C. A.; Tang, C. C.; Shearing, P. R.; Brett, D. J. L. Hydrogen Oxidation on PdIr/C Catalysts in Alkaline Media. *J. Electrochem. Soc.* **2014**, *161*, F458−F463.
(150) McBreen, J.; Mukerjee, S. In Situ X-Ray Absorption Studies of a Pt-Ru Electrocatalyst. *J. Electrochem. Soc.* **1995**, *142*, 3399−3404.
(151) Krausa, M.; Vielstich, W. Study of the electrocatalytic influence of Pt/Ru and Ru on the oxidation of residues of small organic molecules. *J. Electroanal. Chem.* **1994**, *379*, 307−314.
(152) Nørskov, J. K.; Bligaard, T.; Logadottir, A.; Kitchin, J. R.; Chen, J. G.; Pandelov, S.; Stimming, U. Trends in the Exchange Current for Hydrogen Evolution. *J. Electrochem. Soc.* **2005**, *152*, J23−J26.
(153) Sheng, W.; Myint, M.; Chen, J. G.; Yan, Y. Correlating the hydrogen evolution reaction activity in alkaline electrolytes with the hydrogen binding energy on monometallic surfaces. *Energy Environ. Sci.* **2013**, *6*, 1509−1512.
(154) Ohyama, J.; Sato, T.; Yamamoto, Y.; Arai, S.; Satsuma, A. Size Specifically High Activity of Ru Nanoparticles for Hydrogen Oxidation Reaction in Alkaline Electrolyte. *J. Am. Chem. Soc.* **2013**, *135*, 8016−8021.
(155) Lasia, A. Hydrogen evolution reaction. In *Handbook of Fuel Cells*; John Wiley & Sons, Ltd, 2010.
(156) McKone, J. R.; Sadtler, B. F.; Werlang, C. A.; Lewis, N. S.; Gray, H. B. Ni−Mo Nanopowders for Efficient Electrochemical Hydrogen Evolution. *ACS Catal.* **2013**, *3*, 166−169.
(157) Oshchepkov, A. G.; Bonnefont, A.; Saveleva, V. A.; Papaefthimiou, V.; Zafeiratos, S.; Pronkin, S. N.; Parmon, V. N.; Savinova, E. R. Exploring the Influence of the Nickel Oxide Species on the Kinetics of Hydrogen Electrode Reactions in Alkaline Media. *Top. Catal.* **2016**, *59*, 1319−1331.
(158) Sheng, W.; Bivens, A. P.; Myint, M.; Zhuang, Z.; Forest, R. V.; Fang, Q.; Chen, J. G.; Yan, Y. Non-precious metal electrocatalysts with high activity for hydrogen oxidation reaction in alkaline electrolytes. *Energy Environ. Sci.* **2014**, *7*, 1719−1724.
(159) Zhuang, Z.; Giles, S. A.; Zheng, J.; Jenness, G. R.; Caratzoulas, S.; Vlachos, D. G.; Yan, Y. Nickel supported on nitrogen-doped carbon nanotubes as hydrogen oxidation reaction catalyst in alkaline electrolyte. *Nat. Commun.* **2016**, *7*, 1−8.
(160) Ge, X.; Sumboja, A.; Wuu, D.; An, T.; Li, B.; Goh, F. W. T.; Hor, T. S. A.; Zong, Y.; Liu, Z. Oxygen Reduction in Alkaline Media: From Mechanisms to Recent Advances of Catalysts. *ACS Catal.* **2015**, *5*, 4643−4667.
(161) Shao, M.; Chang, Q.; Dodelet, J.-P.; Chenitz, R. Recent Advances in Electrocatalysts for Oxygen Reduction Reaction. *Chem. Rev.* **2016**, *116*, 3594−3657.

DOI: 10.1021/acs.chemrev.9b00157
Chem. Rev. XXXX, XXX, XXX−XXX

(162) He, Q.; Cairns, E. J. Review—Recent Progress in Electrocatalysts for Oxygen Reduction Suitable for Alkaline Anion Exchange Membrane Fuel Cells. *J. Electrochem. Soc.* **2015**, *162*, F1504−F1539.
(163) Xu, Y.; Shao, M.; Mavrikakis, M.; Adzic, R. R. Recent Developments in the Electrocatalysis of the O_2 Reduction Reaction. In *Fuel Cell Catalysis A Surface Science Approach*; Koper, M. T. M., Ed.; John Wiley & Sons, Inc., 2009.
(164) Mukerjee, S. In-situ x-ray absorption spectroscopy of carbon-supported Pt and Pt-alloy electrocatalysts: correlation of electrocatalytic activity with particle size and alloying. *Catalysis and Electrocatalysis at Nanoparticle Surfaces* **2003**, 501−530.
(165) Strasser, P.; Koh, S.; Anniyev, T.; Greeley, J.; More, K.; Yu, C.; Liu, Z.; Kaya, S.; Nordlund, D.; Ogasawara, H.; et al. Lattice-strain control of the activity in dealloyed core−shell fuel cell catalysts. *Nat. Chem.* **2010**, *2*, 454−460.
(166) Markovic, N. M.; Ross, P. N. Surface science studies of model fuel cell electrocatalysts. *Surf. Sci. Rep.* **2002**, *45*, 117−229.
(167) Quaino, P.; Luque, N. B.; Nazmutdinov, R.; Santos, E.; Schmickler, W. Why is Gold such a Good Catalyst for Oxygen Reduction in Alkaline Media? *Angew. Chem., Int. Ed.* **2012**, *51*, 12997−13000.
(168) Christensen, P. A.; Hamnett, A.; Linares-Moya, D. Oxygen reduction and fuel oxidation in alkaline solution. *Phys. Chem. Chem. Phys.* **2011**, *13*, 5206−5214.
(169) Damjanovic, A.; Genshaw, M. A.; Bockris, J. O. M. Mechanism of oxygen reduction at platinum in alkaline solutions with special reference to hydrogen peroxide. *J. Electrochem. Soc.* **1967**, *114*, 1107−1112.
(170) Adzic, R. Recent advances in the kinetics of oxygen reduction. In *Electrocatalysis*; Lipkowski, J., Ross, P. N., Eds.; Wiley-VCH: 1998; pp 197−242.
(171) Sepa, D. B.; Vojnovic, M. V.; Damjanovic, A. Kinetics and mechanism of O2 reduction at Pt IN alkaline solutions. *Electrochim. Acta* **1980**, *25*, 1491−1496.
(172) Yeager, E.; Razaq, M.; Gervasio, D.; Razaq, A.; Tryk, D. *The electrolyte factor in oxygen reduction electrocatalysis*; Technical Report for Office of Naval Research: Cleveland, OH, April 1993.
(173) Markovic, N. M.; Gasteiger, H. A.; Ross, P. N., Jr. Oxygen reduction on platinum low-index single-crystal surfaces in alkaline solution: rotating ring diskPt(hkl) studies. *J. Phys. Chem.* **1996**, *100*, 6715−6721.
(174) Shao, M.-H.; Liu, P.; Adzic, R. R. Superoxide Anion is the Intermediate in the Oxygen Reduction Reaction on Platinum Electrodes. *J. Am. Chem. Soc.* **2006**, *128*, 7408−7409.
(175) Li, X.; Gewirth, A. A. Oxygen Electroreduction through a Superoxide Intermediate on Bi-Modified Au Surfaces. *J. Am. Chem. Soc.* **2005**, *127*, 5252−5260.
(176) Shao, M. H.; Adzic, R. R. Spectroscopic Identification of the Reaction Intermediates in Oxygen Reduction on Gold in Alkaline Solutions. *J. Phys. Chem. B* **2005**, *109*, 16563−16566.
(177) Damjanovic, A.; Dey, A.; Bockris, J. O. M. Kinetics of oxygen evolution and dissolution on platinum electrodes. *Electrochim. Acta* **1966**, *11*, 791−814.
(178) Sepa, D. B.; Vojnovic, M. V.; Damjanovic, A. Kinetics and mechanism of oxygen reduction at platinum in alkaline solutions. *Electrochim. Acta* **1980**, *25*, 1491−1496.
(179) Sepa, D. B.; Vojnovic, M. V.; Vracar, L. M.; Damjanovic, A. Different views regarding the kinetics and mechanisms of oxygen reduction at platinum and palladium electrodes. *Electrochim. Acta* **1987**, *32*, 129−134.
(180) Liu, S.; White, M. G.; Liu, P. Mechanism of Oxygen Reduction Reaction on Pt(111) in Alkaline Solution: Importance of Chemisorbed Water on Surface. *J. Phys. Chem. C* **2016**, *120*, 15288−15298.
(181) Li, R.; Li, H.; Xu, S.; Liu, J. Theoretical investigation of the effect of OH− ions on O2 adsorption on low-index Pt surfaces in alkaline solution. *Appl. Surf. Sci.* **2015**, *351*, 853−861.
(182) Bard, A. J. Inner-Sphere Heterogeneous Electrode Reactions. Electrocatalysis and Photocatalysis: The Challenge. *J. Am. Chem. Soc.* **2010**, *132*, 7559−7567.
(183) Fischer, P.; Heitbaum, J. Mechanistic aspects of cathodic oxygen reduction. *J. Electroanal. Chem. Interfacial Electrochem.* **1980**, *112*, 231−238.
(184) Park, S. M.; Ho, S.; Aruliah, S.; Weber, M. F.; Ward, C. A.; Venter, R. D.; Srinivasan, S. Electrochemical Reduction of Oxygen at Platinum Electrodes in KOH Solutions - Temperature and Concentration Effects. *J. Electrochem. Soc.* **1986**, *133*, 1641−1649.
(185) Striebel, K. A.; McLarnon, F. R.; Cairns, E. J. Oxygen Reduction on Pt in Aqueous K 2 CO 3 and KOH . *J. Electrochem. Soc.* **1990**, *137*, 3351−3359.
(186) Zinola, C. F.; Castro Luna, A. M.; Triaca, W. E.; Arvia, A. J. Kinetics and mechanism of the electrochemical reduction of molecular oxygen on platinum in KOH: influence of preferred crystallographic orientation. *J. Appl. Electrochem.* **1994**, *24*, 531−541.
(187) Tarasevich, M. R.; Sadkowski, A.; Yeager, E. Oxygen Electrochemistry. In *Comprehensive Treatise of Electrochemistry*; Conway, B. E., Bockris, J. O. M., Yeager, E., Eds.; Plenum Press: New York, 1983; Vol. 7, p 301.
(188) Strbac, S. The effect of pH on oxygen and hydrogen peroxide reduction on polycrystalline Pt electrode. *Electrochim. Acta* **2011**, *56*, 1597−1604.
(189) Murthi, V. S.; Urian, R. C.; Mukerjee, S. Oxygen Reduction Kinetics in Low and Medium Temperature Acid Environment: Correlation of Water Activation and Surface Properties in Supported Pt and Pt Alloy Electrocatalysts. *J. Phys. Chem. B* **2004**, *108*, 11011−11023.
(190) Kar, T.; Devivaraprasad, R.; Bera, B.; Ramesh, R.; Neergat, M. Investigation on the reduction of the oxides of Pd and graphite in alkaline medium and the simultaneous evolution of oxygen reduction reaction and peroxide generation features. *Electrochim. Acta* **2016**, *191*, 81−89.
(191) Ramaswamy, N.; Allen, R. J.; Mukerjee, S. Electrochemical Kinetics and X-ray Absorption Spectroscopic Investigations of Oxygen Reduction on Chalcogen-Modified Ruthenium Catalysts in Alkaline Media. *J. Phys. Chem. C* **2011**, *115*, 12650−12664.
(192) Shao, M.; Odell, J.; Humbert, M.; Yu, T.; Xia, Y. Electrocatalysis on Shape-Controlled Palladium Nanocrystals: Oxygen Reduction Reaction and Formic Acid Oxidation. *J. Phys. Chem. C* **2013**, *117*, 4172−4180.
(193) Coleman, E. J.; Co, A. C. The Complex Inhibiting Role of Surface Oxide in the Oxygen Reduction Reaction. *ACS Catal.* **2015**, *5*, 7299−7311.
(194) Janin, E.; von Schenck, H.; Gothelid, M.; Karlsson, U. O.; Svensson, M. Bridge-bonded atomic oxygen on Pt(110). *Phys. Rev. B: Condens. Matter Mater. Phys.* **2000**, *61*, 13144−13149.
(195) Zhang, C.; Fan, F.-R. F.; Bard, A. J. Electrochemistry of Oxygen in Concentrated NaOH Solutions: Solubility, Diffusion Coefficients, and Superoxide Formation. *J. Am. Chem. Soc.* **2009**, *131*, 177−181.
(196) Jerkiewicz, G.; Vatankhah, G.; Lessard, J.; Soriaga, M. P.; Park, Y.-S. Surface-oxide growth at platinum electrodes in aqueous H2SO4. Reexamination of its mechanism through combined cyclic-voltammetry, electrochemical quartz-crystal nanobalance, and Auger electron spectroscopy measurements. *Electrochim. Acta* **2004**, *49*, 1451−1459.
(197) Haas, T. W. *Kinetics of the uncatalyzed, alkaline decomposition of hydrogen peroxide*. Ph.D. Thesis, Iowa State University, 1960.
(198) Goldstein, J. R.; Tseung, A. C. C. The kinetics of hydrogen peroxide decomposition catalyzed by cobalt-iron oxides. *J. Catal.* **1974**, *32*, 452−465.
(199) McKee, D. W. Catalytic decomposition of hydrogen peroxide by metals and alloys of the platinum group. *J. Catal.* **1969**, *14*, 355−364.
(200) Petri, B. G.; Watts, R. J.; Teel, A. L.; Huling, S. G.; Brown, R. A. Fundamentals of ISCO Using Hydrogen Peroxide. In *In Situ Chemical Oxidation for Groundwater Remediation*; Siegrist, R. L., Crimi, M., Simpkin, T. J., Eds.; Springer New York: New York, NY, 2011; pp 33−88.
(201) Abbot, J.; Brown, D. G. Kinetics of Iron-catalyzed decomposition of hydrogen peroxide in alkaline solution. *Int. J. Chem. Kinet.* **1990**, *22*, 963−974.

DOI: 10.1021/acs.chemrev.9b00157
Chem. Rev. XXXX, XXX, XXX−XXX

(202) Kehrer, J. P. The Haber−Weiss reaction and mechanisms of toxicity. *Toxicology* **2000**, *149*, 43−50.
(203) Rigo, A.; Stevanato, R.; Finazzi-Agro, A.; Rotilio, G. An attempt to evaluate the rate of the haber-weiss reaction by using ·OH radical scavengers. *FEBS Lett.* **1977**, *80*, 130−132.
(204) Nicoll, W. D.; Smith, A. F. Stability of Dilute Alkaline Solutions of Hydrogen Peroxide. *Ind. Eng. Chem.* **1955**, *47*, 2548−2554.
(205) Spalek, O.; Balej, J.; Paseka, I. Kinetics of the decomposition of hydrogen peroxide in alkaline solutions. *J. Chem. Soc., Faraday Trans. 1* **1982**, *78*, 2349−2359.
(206) Lousada, C. M.; Yang, M.; Nilsson, K.; Jonsson, M. Catalytic decomposition of hydrogen peroxide on transition metal and lanthanide oxides. *J. Mol. Catal. A: Chem.* **2013**, *379*, 178−184.
(207) Broughton, D. B.; Wentworth, R. L. Mechanism of Decomposition of Hydrogen Peroxide Solutions with Manganese Dioxide. *J. Am. Chem. Soc.* **1947**, *69*, 741−744.
(208) Broughton, D. B.; Wentworth, R. L.; Laing, M. E. Mechanism of Decomposition of Hydrogen Peroxide Solutions with Manganese Dioxide. II. *J. Am. Chem. Soc.* **1947**, *69*, 744−747.
(209) Hasan, M. A.; Zaki, M. I.; Pasupulety, L.; Kumari, K. Promotion of the hydrogen peroxide decomposition activity of manganese oxide catalysts. *Appl. Catal., A* **1999**, *181*, 171−179.
(210) Mao, L.; Zhang, D.; Sotomura, T.; Nakatsu, K.; Koshiba, N.; Ohsaka, T. Mechanistic study of the reduction of oxygen in air electrode with manganese oxides as electrocatalysts. *Electrochim. Acta* **2003**, *48*, 1015−1021.
(211) Lima, F. H. B.; Calegaro, M. L.; Ticianelli, E. A. Electrocatalytic activity of manganese oxides prepared by thermal decomposition for oxygen reduction. *Electrochim. Acta* **2007**, *52*, 3732−3738.
(212) Roy, C. B. Catalytic decomposition of hydrogen peroxide on some oxide catalysts. *J. Catal.* **1968**, *12*, 129−133.
(213) Cota, H. M.; Katan, T.; Chin, M.; Schoenweis, F. J. Decomposition of Dilute Hydrogen Peroxide in Alkaline Solutions. *Nature* **1964**, *203*, 1281−12810000.
(214) Sánchez-Sánchez, C. M.; Bard, A. J. Hydrogen Peroxide Production in the Oxygen Reduction Reaction at Different Electrocatalysts as Quantified by Scanning Electrochemical Microscopy. *Anal. Chem.* **2009**, *81*, 8094−8100.
(215) Maldonado, S.; Stevenson, K. J. Influence of Nitrogen Doping on Oxygen Reduction Electrocatalysis at Carbon Nanofiber Electrodes. *J. Phys. Chem. B* **2005**, *109*, 4707−4716.
(216) Slanac, D. A.; Hardin, W. G.; Johnston, K. P.; Stevenson, K. J. Atomic Ensemble and Electronic Effects in Ag-Rich AgPd Nanoalloy Catalysts for Oxygen Reduction in Alkaline Media. *J. Am. Chem. Soc.* **2012**, *134*, 9812−9819.
(217) Wiggins-Camacho, J. D.; Stevenson, K. J. Mechanistic discussion of the oxygen reduction reaction at nitrogen-doped carbon nanotubes. *J. Phys. Chem. C* **2011**, *115*, 20002−20010.
(218) Lee, Y. N.; Lago, R. M.; Fierro, J. L. G.; González, J. Hydrogen peroxide decomposition over Ln1−xAxMnO3 (Ln = La or Nd and A = K or Sr) perovskites. *Appl. Catal., A* **2001**, *215*, 245−256.
(219) Shimizu, Y.; Uemura, K.; Matsuda, H.; Miura, N.; Yamazoe, N. Bi-functional oxygen electrode using large surface area lanthanum calcium cobalt oxide (La1-xCaxCoO3) for rechargeable metal-air battery. *J. Electrochem. Soc.* **1990**, *137*, 3430−3433.
(220) Carbonio, R. E.; Fierro, C.; Tryk, D.; Scherson, D.; Yeager, E. Perovskite-type oxides: oxygen electrocatalysis and bulk structure. *J. Power Sources* **1988**, *22*, 387−398.
(221) Bursell, M.; Pirjamali, M.; Kiros, Y. La0.6Ca0.4CoO3, La0.1Ca0.9MnO3 and LaNiO3 as bifunctional oxygen electrodes. *Electrochim. Acta* **2002**, *47*, 1651−1660.
(222) Hermann, V.; Dutriat, D.; Müller, S.; Comninellis, C. Mechanistic studies of oxygen reduction at La0.6Ca0.4CoO3-activated carbon electrodes in a channel flow cell. *Electrochim. Acta* **2000**, *46*, 365−372.
(223) Venkatachalapathy, R.; Davila, G. P.; Prakash, J. Catalytic decomposition of hydrogen peroxide in alkaline solutions. *Electrochem. Commun.* **1999**, *1*, 614−617.
(224) Appleby, A. J.; Savy, M. Kinetics of oxygen reduction reactions involving catalytic decomposition of hydrogen peroxide. *J. Electroanal. Chem. Interfacial Electrochem.* **1978**, *92*, 15−30.
(225) Noël, J.-M.; Latus, A.; Lagrost, C.; Volanschi, E.; Hapiot, P. Evidence for OH Radical Production during Electrocatalysis of Oxygen Reduction on Pt Surfaces: Consequences and Application. *J. Am. Chem. Soc.* **2012**, *134*, 2835−2841.
(226) Suntivich, J.; Gasteiger, H. A.; Yabuuchi, N.; Nakanishi, H.; Goodenough, J. B.; Shao-Horn, Y. Design principles for oxygen-reduction activity on perovskite oxide catalysts for fuel cells and metal−air batteries. *Nat. Chem.* **2011**, *3*, 546−550.
(227) Li, X.; Zhang, H.-J.; Li, H.; Deng, C.; Yang, J. Evaluation of Loading Influence on Catalytic Performance of Co-Based Catalyst for Oxygen Reduction. *ECS Electrochem. Lett.* **2014**, *3*, H33−H37.
(228) Pan, F.; Zhao, Q.; Wang, J.; Zhang, J. High-Performance Fe−N-Doped Graphene Electrocatalysts with pH-Dependent Active Sites for the Oxygen Reduction Reaction. *ChemElectroChem* **2015**, *2*, 2032−2040.
(229) Thorum, M. S.; Yadav, J.; Gewirth, A. A. Oxygen Reduction Activity of a Copper Complex of 3,5-Diamino-1,2,4-triazole Supported on Carbon Black. *Angew. Chem., Int. Ed.* **2009**, *48*, 165−167.
(230) Wang, J.; Wang, K.; Wang, F.-B.; Xia, X.-H. Bioinspired copper catalyst effective for both reduction and evolution of oxygen. *Nat. Commun.* **2014**, *5*, 5285.
(231) Holewinski, A.; Idrobo, J.-C.; Linic, S. High-performance Ag−Co alloy catalysts for electrochemical oxygen reduction. *Nat. Chem.* **2014**, *6*, 828−834.
(232) Wang, J.; Wang, H.-S.; Wang, K.; Wang, F.-B.; Xia, X.-H. Ice crystals growth driving assembly of porous nitrogen-doped graphene for catalyzing oxygen reduction probed by in situ fluorescence electrochemistry. *Sci. Rep.* **2015**, *4*, 6723.
(233) Gorlin, Y.; Chung, C.-J.; Nordlund, D.; Clemens, B. M.; Jaramillo, T. F. Mn3O4 Supported on Glassy Carbon: An Active Non-Precious Metal Catalyst for the Oxygen Reduction Reaction. *ACS Catal.* **2012**, *2*, 2687−2694.
(234) Wu, H.; Chen, W. Copper Nitride Nanocubes: Size-Controlled Synthesis and Application as Cathode Catalyst in Alkaline Fuel Cells. *J. Am. Chem. Soc.* **2011**, *133*, 15236−15239.
(235) Alia, S. M.; Duong, K.; Liu, T.; Jensen, K.; Yan, Y. Supportless Silver Nanowires as Oxygen Reduction Reaction Catalysts for Hydroxide-Exchange Membrane Fuel Cells. *ChemSusChem* **2012**, *5*, 1619−1624.
(236) Zhou, X.; Bai, Z.; Wu, M.; Qiao, J.; Chen, Z. 3-Dimensional porous N-doped graphene foam as a non-precious catalyst for the oxygen reduction reaction. *J. Mater. Chem. A* **2015**, *3*, 3343−3350.
(237) Gong, K.; Du, F.; Xia, Z.; Durstock, M.; Dai, L. Nitrogen-Doped Carbon Nanotube Arrays with High Electrocatalytic Activity for Oxygen Reduction. *Science (Washington, DC, U. S.)* **2009**, *323*, 760−764.
(238) Wu, Z.-S.; Yang, S.; Sun, Y.; Parvez, K.; Feng, X.; Müllen, K. 3D Nitrogen-Doped Graphene Aerogel-Supported Fe3O4 Nanoparticles as Efficient Electrocatalysts for the Oxygen Reduction Reaction. *J. Am. Chem. Soc.* **2012**, *134*, 9082−9085.
(239) Sa, Y. J.; Seo, D.-J.; Woo, J.; Lim, J. T.; Cheon, J. Y.; Yang, S. Y.; Lee, J. M.; Kang, D.; Shin, T. J.; Shin, H. S.; et al. A General Approach to Preferential Formation of Active Fe−Nx Sites in Fe−N/C Electrocatalysts for Efficient Oxygen Reduction Reaction. *J. Am. Chem. Soc.* **2016**, *138*, 15046−15056.
(240) Huang, D.; Luo, Y.; Li, S.; Zhang, B.; Shen, Y.; Wang, M. Active catalysts based on cobalt oxide@cobalt/N-C nanocomposites for oxygen reduction reaction in alkaline solutions. *Nano Res.* **2014**, *7*, 1054−1064.
(241) Kreek, K.; Sarapuu, A.; Samolberg, L.; Joost, U.; Mikli, V.; Koel, M.; Tammeveski, K. Cobalt-Containing Nitrogen-Doped Carbon Aerogels as Efficient Electrocatalysts for the Oxygen Reduction Reaction. *ChemElectroChem* **2015**, *2*, 2079−2088.
(242) Strickland, K.; Miner, E.; Jia, Q.; Tylus, U.; Ramaswamy, N.; Liang, W.; Sougrati, M.-T.; Jaouen, F.; Mukerjee, S. Highly active

DOI: 10.1021/acs.chemrev.9b00157
Chem. Rev. XXXX, XXX, XXX−XXX

oxygen reduction non-platinum group metal electrocatalyst without direct metal−nitrogen coordination. *Nat. Commun.* **2015**, *6*, 7343.
(243) Gokhale, R.; Chen, Y.; Serov, A.; Artyushkova, K.; Atanassov, P. Direct synthesis of platinum group metal-free Fe-N-C catalyst for oxygen reduction reaction in alkaline media. *Electrochem. Commun.* **2016**, *72*, 140−143.
(244) Yang, W.; Fellinger, T.-P.; Antonietti, M. Efficient Metal-Free Oxygen Reduction in Alkaline Medium on High-Surface-Area Mesoporous Nitrogen-Doped Carbons Made from Ionic Liquids and Nucleobases. *J. Am. Chem. Soc.* **2011**, *133*, 206−209.
(245) Wang, Y.; Kong, A.; Chen, X.; Lin, Q.; Feng, P. Efficient Oxygen Electroreduction: Hierarchical Porous Fe−N-doped Hollow Carbon Nanoshells. *ACS Catal.* **2015**, *5*, 3887−3893.
(246) Jahan, M.; Bao, Q.; Loh, K. P. Electrocatalytically Active Graphene−Porphyrin MOF Composite for Oxygen Reduction Reaction. *J. Am. Chem. Soc.* **2012**, *134*, 6707−6713.
(247) Zhao, P.; Xu, W.; Hua, X.; Luo, W.; Chen, S.; Cheng, G. Facile Synthesis of a N-Doped Fe3C@CNT/Porous Carbon Hybrid for an Advanced Oxygen Reduction and Water Oxidation Electrocatalyst. *J. Phys. Chem. C* **2016**, *120*, 11006−11013.
(248) Vezzù, K.; Bach Delpeuch, A.; Negro, E.; Polizzi, S.; Nawn, G.; Bertasi, F.; Pagot, G.; Artyushkova, K.; Atanassov, P.; Di Noto, V. Fe-carbon nitride "Core-shell" electrocatalysts for the oxygen reduction reaction. *Electrochim. Acta* **2016**, *222*, 1778.
(249) Qiu, K.; Chai, G.; Jiang, C.; Ling, M.; Tang, J.; Guo, Z. Highly Efficient Oxygen Reduction Catalysts by Rational Synthesis of Nanoconfined Maghemite in a Nitrogen-Doped Graphene Framework. *ACS Catal.* **2016**, *6*, 3558−3568.
(250) Li, S.; Wu, D.; Liang, H.; Wang, J.; Zhuang, X.; Mai, Y.; Su, Y.; Feng, X. Metal−Nitrogen Doping of Mesoporous Carbon/Graphene Nanosheets by Self-Templating for Oxygen Reduction Electrocatalysts. *ChemSusChem* **2014**, *7*, 3002−3006.
(251) Ranjbar Sahraie, N.; Paraknowitsch, J. P.; Göbel, C.; Thomas, A.; Strasser, P. Noble-Metal-Free Electrocatalysts with Enhanced ORR Performance by Task-Specific Functionalization of Carbon using Ionic Liquid Precursor Systems. *J. Am. Chem. Soc.* **2014**, *136*, 14486−14497.
(252) Higgins, D. C.; Hoque, M. A.; Hassan, F.; Choi, J.-Y.; Kim, B.; Chen, Z. Oxygen Reduction on Graphene−Carbon Nanotube Composites Doped Sequentially with Nitrogen and Sulfur. *ACS Catal.* **2014**, *4*, 2734−2740.
(253) Yang, D.-S.; Bhattacharjya, D.; Inamdar, S.; Park, J.; Yu, J.-S. Phosphorus-Doped Ordered Mesoporous Carbons with Different Lengths as Efficient Metal-Free Electrocatalysts for Oxygen Reduction Reaction in Alkaline Media. *J. Am. Chem. Soc.* **2012**, *134*, 16127−16130.
(254) Yu, Q.; Xu, J.; Wu, C.; Guan, L. Strong-coupled Co-g-C3N4/SWCNTs composites as high-performance electrocatalysts for oxygen reduction reaction. *RSC Adv.* **2015**, *5*, 65303−65307.
(255) Jiang, W.-J.; Gu, L.; Li, L.; Zhang, Y.; Zhang, X.; Zhang, L.-J.; Wang, J.-Q.; Hu, J.-S.; Wei, Z.; Wan, L.-J. Understanding the High Activity of Fe−N−C Electrocatalysts in Oxygen Reduction: Fe/Fe3C Nanoparticles Boost the Activity of Fe−Nx. *J. Am. Chem. Soc.* **2016**, *138*, 3570−3578.
(256) Guo, J.; Zhou, J.; Chu, D.; Chen, R. Tuning the Electrochemical Interface of Ag/C Electrodes in Alkaline Media with Metal-lophthalocyanine Molecules. *J. Phys. Chem. C* **2013**, *117*, 4006−4017.
(257) Roche, I.; Chaînet, E.; Chatenet, M.; Vondrák, J. Carbon-Supported Manganese Oxide Nanoparticles as Electrocatalysts for the Oxygen Reduction Reaction (ORR) in Alkaline Medium: Physical Characterizations and ORR Mechanism. *J. Phys. Chem. C* **2007**, *111*, 1434−1443.
(258) Gorlin, Y.; Jaramillo, T. F. A Bifunctional Nonprecious Metal Catalyst for Oxygen Reduction and Water Oxidation. *J. Am. Chem. Soc.* **2010**, *132*, 13612−13614.
(259) Stoerzinger, K. A.; Risch, M.; Han, B.; Shao-Horn, Y. Recent Insights into Manganese Oxides in Catalyzing Oxygen Reduction Kinetics. *ACS Catal.* **2015**, *5*, 6021−6031.
(260) Gorlin, Y.; Lassalle-Kaiser, B.; Benck, J. D.; Gul, S.; Webb, S. M.; Yachandra, V. K.; Yano, J.; Jaramillo, T. F. In Situ X-ray Absorption Spectroscopy Investigation of a Bifunctional Manganese Oxide Catalyst with High Activity for Electrochemical Water Oxidation and Oxygen Reduction. *J. Am. Chem. Soc.* **2013**, *135*, 8525−8534.
(261) Bikkarolla, S. K.; Yu, F.; Zhou, W.; Joseph, P.; Cumpson, P.; Papakonstantinou, P. A three-dimensional Mn3O4 network supported on a nitrogenated graphene electrocatalyst for efficient oxygen reduction reaction in alkaline media. *J. Mater. Chem. A* **2014**, *2*, 14493−14501.
(262) Valim, R. B.; Santos, M. C.; Lanza, M. R. V.; Machado, S. A. S.; Lima, F. H. B.; Calegaro, M. L. Oxygen reduction reaction catalyzed by ε-MnO2: Influence of the crystalline structure on the reaction mechanism. *Electrochim. Acta* **2012**, *85*, 423−431.
(263) Zakaria, M. B.; Li, C.; Pramanik, M.; Tsujimoto, Y.; Hu, M.; Malgras, V.; Tominaka, S.; Yamauchi, Y. Nanoporous Mn-based electrocatalysts through thermal conversion of cyano-bridged coordination polymers toward ultra-high efficiency hydrogen peroxide production. *J. Mater. Chem. A* **2016**, *4*, 9266−9274.
(264) Meng, Y.; Song, W.; Huang, H.; Ren, Z.; Chen, S.-Y.; Suib, S. L. Structure−Property Relationship of Bifunctional MnO2 Nanostructures: Highly Efficient, Ultra-Stable Electrochemical Water Oxidation and Oxygen Reduction Reaction Catalysts Identified in Alkaline Media. *J. Am. Chem. Soc.* **2014**, *136*, 11452−11464.
(265) Liang, Y.; Li, Y.; Wang, H.; Zhou, J.; Wang, J.; Regier, T.; Dai, H. Co3O4 nanocrystals on graphene as a synergistic catalyst for oxygen reduction reaction. *Nat. Mater.* **2011**, *10*, 780−786.
(266) Wang, C.-H.; Yang, C.-W.; Lin, Y.-C.; Chang, S.-T.; Chang, S. L. Y. Cobalt−iron(II,III) oxide hybrid catalysis with enhanced catalytic activities for oxygen reduction in anion exchange membrane fuel cell. *J. Power Sources* **2015**, *277*, 147−154.
(267) Farjami, E.; Deiner, L. J. Kinetic Study of the Oxygen Reduction Reaction on α-Ni(OH)2 and α-Ni(OH)2 Supported on Graphene Oxide. *J. Electrochem. Soc.* **2015**, *162*, H571−H578.
(268) Wang, Y.; Zhang, D.; Liu, H. A study of the catalysis of cobalt hydroxide towards the oxygen reduction in alkaline media. *J. Power Sources* **2010**, *195*, 3135−3139.
(269) Yuasa, M.; Shimanoe, K.; Teraoka, Y.; Yamazoe, N. High-Performance Oxygen Reduction Catalyst Using Carbon-Supported La-Mn-Based Perovskite-Type Oxide. *Electrochem. Solid-State Lett.* **2011**, *14*, A67−A69.
(270) Meadowcroft, D. B. Low-cost oxygen electrode material. *Nature* **1970**, *226*, 847−848.
(271) Fabbri, E.; Mohamed, R.; Levecque, P.; Conrad, O.; Kötz, R.; Schmidt, T. J. Composite Electrode Boosts the Activity of $Ba_{0.5}Sr_{0.5}Co_{0.8}Fe_{0.2}O_{3-\delta}$ Perovskite and Carbon toward Oxygen Reduction in Alkaline Media. *ACS Catal.* **2014**, *4*, 1061−1070.
(272) Takeguchi, T.; Yamanaka, T.; Takahashi, H.; Watanabe, H.; Kuroki, T.; Nakanishi, H.; Orikasa, Y.; Uchimoto, Y.; Takano, H.; Ohguri, N.; et al. Layered Perovskite Oxide: A Reversible Air Electrode for Oxygen Evolution/Reduction in Rechargeable Metal-Air Batteries. *J. Am. Chem. Soc.* **2013**, *135*, 11125−11130.
(273) Su, H.-Y.; Gorlin, Y.; Man, I. C.; Calle-Vallejo, F.; Norskov, J. K.; Jaramillo, T. F.; Rossmeisl, J. Identifying active surface phases for metal oxide electrocatalysts: a study of manganese oxide bi-functional catalysts for oxygen reduction and water oxidation catalysis. *Phys. Chem. Chem. Phys.* **2012**, *14*, 14010−14022.
(274) Sunarso, J.; Torriero, A. A. J.; Zhou, W.; Howlett, P. C.; Forsyth, M. Oxygen Reduction Reaction Activity of La-Based Perovskite Oxides in Alkaline Medium: A Thin-Film Rotating Ring-Disk Electrode Study. *J. Phys. Chem. C* **2012**, *116*, 5827−5834.
(275) Matsumoto, Y.; Yoneyama, H.; Tamura, H. Catalytic activity for electrochemical reduction of oxygen of lanthanum nickel oxide and related oxides. *J. Electroanal. Chem. Interfacial Electrochem.* **1977**, *79*, 319−326.
(276) Cheng, F.; Shen, J.; Peng, B.; Pan, Y.; Tao, Z.; Chen, J. Rapid room-temperature synthesis of nanocrystalline spinels as oxygen reduction and evolution electrocatalysts. *Nat. Chem.* **2011**, *3*, 79−84.
(277) Liang, Y.; Wang, H.; Zhou, J.; Li, Y.; Wang, J.; Regier, T.; Dai, H. Covalent Hybrid of Spinel Manganese−Cobalt Oxide and Graphene as Advanced Oxygen Reduction Electrocatalysts. *J. Am. Chem. Soc.* **2012**, *134*, 3517−3523.

DOI: 10.1021/acs.chemrev.9b00157
Chem. Rev. XXXX, XXX, XXX−XXX

(278) Adzic, R. R.; Markovic, N. M. Structural effects in electrocatalysis: oxygen and hydrogen peroxide reduction on single crystal gold electrodes and the effects of lead ad-atoms. *J. Electroanal. Chem. Interfacial Electrochem.* **1982**, *138*, 443−447.
(279) Adic, R.R.; Markovic, N.M.; Vesovic, V.B. Structural effects in electrocatalysis. Oxygen reduction on the gold(100) single crystal electrode. *J. Electroanal. Chem. Interfacial Electrochem.* **1984**, *165*, 105−120.
(280) Adzic, R. R.; Strbac, S.; Anastasijevic, N. Electrocatalysis of oxygen on single crystal gold electrodes. *Mater. Chem. Phys.* **1989**, *22*, 349−375.
(281) Taylor, E. J.; Vilambi, N. R. K.; Gelb, A. The nature of the catalytic peak for oxygen reduction in alkaline electrolyte on the gold(100) surface. *J. Electrochem. Soc.* **1989**, *136*, 1939−1944.
(282) Markovic, N. M.; Tidswell, I. M.; Ross, P. N. Oxygen and hydrogen peroxide reduction on the gold(100) surface in alkaline electrolyte: the roles of surface structure and hydroxide adsorption. *Langmuir* **1994**, *10*, 1−4.
(283) Strbac, S.; Adzic, R. R. The influence of pH on reaction pathways for O2 reduction on the Au(100) face. *Electrochim. Acta* **1996**, *41*, 2903−2908.
(284) Falcon, H.; Carbonio, R. E. Study of the heterogeneous decomposition of hydrogen peroxide: its application to the development of catalysts for carbon-based oxygen cathodes. *J. Electroanal. Chem.* **1992**, *339*, 69−83.
(285) Yeager, E. Electrocatalysts for molecular oxygen reduction. *Electrochim. Acta* **1984**, *29*, 1527−1537.
(286) Geniès, L.; Faure, R.; Durand, R. Electrochemical reduction of oxygen on platinum nanoparticles in alkaline media. *Electrochim. Acta* **1998**, *44*, 1317−1327.
(287) Lee, S. Y.; Chung, D. Y.; Lee, M. J.; Kang, Y. S.; Shin, H.; Kim, M.-J.; Bielawski, C. W.; Sung, Y.-E. Charting the Outer Helmholtz Plane and the Role of Nitrogen Doping in the Oxygen Reduction Reaction Conducted in Alkaline Media Using Nonprecious Metal Catalysts. *J. Phys. Chem. C* **2016**, *120*, 24511−24520.
(288) Choi, C. H.; Lim, H.-K.; Chung, M. W.; Park, J. C.; Shin, H.; Kim, H.; Woo, S. I. Long-Range Electron Transfer over Graphene-Based Catalyst for High-Performing Oxygen Reduction Reactions: Importance of Size, N-doping, and Metallic Impurities. *J. Am. Chem. Soc.* **2014**, *136*, 9070−9077.
(289) Olson, T. S.; Pylypenko, S.; Atanassov, P.; Asazawa, K.; Yamada, K.; Tanaka, H. Anion-Exchange Membrane Fuel Cells: Dual-Site Mechanism of Oxygen Reduction Reaction in Alkaline Media on Cobalt-Polypyrrole Electrocatalysts. *J. Phys. Chem. C* **2010**, *114*, 5049−5059.
(290) Wan, K.; Yu, Z.-p.; Li, X.-h.; Liu, M.-y.; Yang, G.; Piao, J.-h.; Liang, Z.-x. pH Effect on Electrochemistry of Nitrogen-Doped Carbon Catalyst for Oxygen Reduction Reaction. *ACS Catal.* **2015**, *5*, 4325−4332.
(291) Kordesch, K.; Hacker, V.; Gsellmann, J.; Cifrain, M.; Faleschini, G.; Enzinger, P.; Fankhauser, R.; Ortner, M.; Muhr, M.; Aronson, R. R. Alkaline fuel cells applications. *J. Power Sources* **2000**, *86*, 162−165.
(292) Penner, S. S. *Assessment of Research Needs for Advanced Fuel Cells*; Technical Report for U.S. Department of Energy: Washington, D.C., 1986.
(293) Brushett, F. R.; Naughton, M. S.; Ng, J. W. D.; Yin, L.; Kenis, P. J. A. Analysis of Pt/C electrode performance in a flowing-electrolyte alkaline fuel cell. *Int. J. Hydrogen Energy* **2012**, *37*, 2559−2570.
(294) Grew, K. N.; Ren, X.; Chu, D. Effects of Temperature and Carbon Dioxide on Anion Exchange Membrane Conductivity. *Electrochem. Solid-State Lett.* **2011**, *14*, B127−B131.
(295) Watanabe, S.; Fukuta, K.; Yanagi, H. Determination of Carbonate Ion in MEA during the Alkaline Membrane Fuel Cell (AMFC) Operation. *ECS Trans.* **2010**, *33*, 1837−1845.
(296) Yu, C.-H.; Huang, C.-H.; Tan, C.-S. A Review of CO2 Capture by Absorption and Adsorption. *Aerosol Air Qual. Res.* **2012**, *12*, 745−769.
(297) Siroma, Z.; Watanabe, S.; Yasuda, K.; Fukuta, K.; Yanagi, H. Mathematical Modeling of the Concentration Profile of Carbonate Ions in an Anion Exchange Membrane Fuel Cell. *J. Electrochem. Soc.* **2011**, *158*, B682−B689.
(298) Kimura, T.; Yamazaki, Y. Effects of CO_2 Concentration and Electric Current on the Ionic Conductivity of Anion Exchange Membranes for Fuel Cells. *Electrochemistry* **2011**, *79*, 94−97.
(299) Matsui, Y.; Saito, M.; Tasaka, A.; Inaba, M. Influence of Carbon Dioxide on the Performance of Anion-Exchange Membrane Fuel Cells. *ECS Trans.* **2009**, *25*, 105−110.
(300) Vega, J. A.; Smith, S.; Mustain, W. E. Hydrogen and Methanol Oxidation Reaction in Hydroxide and Carbonate Alkaline Media. *J. Electrochem. Soc.* **2011**, *158*, B349−B354.
(301) Gunasekara, I.; Lee, M.; Abbott, D.; Mukerjee, S. Mass Transport and Oxygen Reduction Kinetics at an Anion Exchange Membrane Interface: Microelectrode Studies on Effect of Carbonate Exchange. *ECS Electrochem. Lett.* **2012**, *1*, F16−F19.
(302) Vega, J. A.; Mustain, W. E. Effect of CO2, HCO3− and CO3−2 on oxygen reduction in anion exchange membrane fuel cells. *Electrochim. Acta* **2010**, *55*, 1638−1644.
(303) Kienitz, B. L.; Baskaran, H.; Zawodzinski, T. A., Jr Modeling the steady-state effects of cationic contamination on polymer electrolyte membranes. *Electrochim. Acta* **2009**, *54*, 1671−1679.
(304) Gottesfeld, S. Systems and Methods of Securing Immunity to Air CO2 in Alkaline Fuel Cells. U.S. Patent 9,368,819, June 14, 2016.
(305) Goeppert, A.; Czaun, M.; May, R. B.; Prakash, G. K. S.; Olah, G. A.; Narayanan, S. R. Carbon Dioxide Capture from the Air Using a Polyamine Based Regenerable Solid Adsorbent. *J. Am. Chem. Soc.* **2011**, *133*, 20164−20167.
(306) Isomura, T.; Fukuta, K.; Yanagi, H.; Ge, S.; Wang, C.-Y. Alkaline Membrane Fuel Cell Operated at Elevated Temperatures. *ECS Meeting Abstracts* **2010**, *MA2010−02*, 751.
(307) Adams, L. A.; Poynton, S. D.; Tamain, C.; Slade, R. C. T.; Varcoe, J. R. A Carbon Dioxide Tolerant Aqueous-Electrolyte-Free Anion-Exchange Membrane Alkaline Fuel Cell. *ChemSusChem* **2008**, *1*, 79−81.
(308) Vega, J. A.; Shrestha, S.; Ignatowich, M.; Mustain, W. E. Carbonate Selective Ca2Ru2O7-y Pyrochlore Enabling Room Temperature Carbonate Fuel Cells: I. Synthesis and Physical Characterization. *J. Electrochem. Soc.* **2011**, *159*, B12−B17.
(309) Vega, J. A.; Spinner, N.; Catanese, M.; Mustain, W. E. Carbonate Selective Ca2Ru2O7−y Pyrochlore Enabling Room Temperature Carbonate Fuel Cells I. Synthesis and Physical Characterization: II. Verification of Carbonate Cycle and Electrochemical Performance. *J. Electrochem. Soc.* **2011**, *159*, B18−B23.
(310) Katayama, Y.; Yamauchi, K.; Hayashi, K.; Okanishi, T.; Muroyama, H.; Matsui, T.; Kikkawa, Y.; Negishi, T.; Watanabe, S.; Isomura, T.; et al. Anion-Exchange Membrane Fuel Cells with Improved CO2 Tolerance: Impact of Chemically Induced Bicarbonate Ion Consumption. *ACS Appl. Mater. Interfaces* **2017**, *9*, 28650−28658.
(311) Li, Y. S.; Zhao, T. S.; Xu, J. B.; Shen, S. Y.; Yang, W. W. Effect of cathode micro-porous layer on performance of anion-exchange membrane direct ethanol fuel cells. *J. Power Sources* **2011**, *196*, 1802−1807.
(312) Demarconnay, L.; Brimaud, S.; Coutanceau, C.; Leger, J. M. Ethylene glycol electrooxidation in alkaline medium at multi-metallic Pt based catalysts. *J. Electroanal. Chem.* **2007**, *601*, 169−180.
(313) Matsuoka, K.; Iriyama, Y.; Abe, T.; Matsuoka, M.; Ogumi, Z. Alkaline direct alcohol fuel cells using an anion exchange membrane. *J. Power Sources* **2005**, *150*, 27−31.
(314) Li, Y. S.; Zhao, T. S.; Liang, Z. X. Performance of alkaline electrolyte-membrane based direct ethanol fuel cells. *J. Power Sources* **2009**, *187*, 387−392.
(315) Fujiwara, N.; Siroma, Z.; Yamazaki, S.-i.; Ioroi, T.; Senoh, H.; Yasuda, K. Direct ethanol fuel cells using an anion exchange membrane. *J. Power Sources* **2008**, *185*, 621−626.
(316) Prabhuram, J.; Manoharan, R. Investigation of methanol oxidation on unsupported platinum electrodes in strong alkali and strong acid. *J. Power Sources* **1998**, *74*, 54−61.
(317) Yu, E. H.; Scott, K.; Reeve, R. W.; Yang, L.; Allen, R. G. Characterisation of platinised Ti mesh electrodes using electrochemical

DOI: 10.1021/acs.chemrev.9b00157
Chem. Rev. XXXX, XXX, XXX−XXX

methods: methanol oxidation in sodium hydroxide solutions. *Electrochim. Acta* **2004**, *49*, 2443−2452.
(318) Kim, H.; Zhou, J.; Ünlü, M.; Anestis-Richard, I.; Joseph, K.; Kohl, P. A. The effect of hydrophobicity in alkaline electrodes for passive DMFC. *Electrochim. Acta* **2011**, *56*, 3085−3090.
(319) Li, Y. S.; Zhao, T. S.; Liang, Z. X. Effect of polymer binders in anode catalyst layer on performance of alkaline direct ethanol fuel cells. *J. Power Sources* **2009**, *190*, 223−229.
(320) Anson, F. C. Patterns of Ionic and Molecular Adsorption at Electrodes. *Acc. Chem. Res.* **1975**, *8*, 400−406.
(321) Gierst, L.; Tondeur, J.; Nicolas, E. Double Couche Electrochimique Et Cinetique Des Reactions Delectrode - Elucidation Du Mode Daction Des Cations Tetraalkylammonium. *J. Electroanal. Chem.* **1965**, *10*, 397−415.
(322) Bard, A. J.; Faulkner, L. *Electrochemical Methods*; Wiley: New York, 2001; pp 534−560.
(323) Breiter, M.; Kleinerman, M.; Delahay, P. Structure of the Double Layer and Electrode Processes. *J. Am. Chem. Soc.* **1958**, *80*, 5111−5117.
(324) Devanathan, M. A. V.; Fernando, M. J. Specific adsorption of tetra-alkyl-ammonium iodides at the mercury-water interface and the structure of the electrical double layer. *Trans. Faraday Soc.* **1962**, *58*, 368−381.
(325) Ong, A. L.; Whelligan, D. K.; Fox, M. L.; Varcoe, J. R. Impact of 1 mmol dm-3 concentrations of small molecules containing nitrogen-based cationic groups on the oxygen reduction reaction on polycrystalline platinum in aqueous KOH (1 mol dm-3). *Phys. Chem. Chem. Phys.* **2013**, *15*, 18992−19000.
(326) Lemke, A. J.; O'Toole, A. W.; Phillips, R. S.; Eisenbraun, E. T. The effect of high anionomer loading with silver nanowire catalysts on the oxygen reduction reaction in alkaline environment. *J. Power Sources* **2014**, *256*, 319−323.
(327) Lu, W.; Shao, Z.-G.; Zhang, G.; Zhao, Y.; Li, J.; Yi, B. Preparation and characterization of imidazolium-functionalized poly (ether sulfone) as anion exchange membrane and ionomer for fuel cell application. *Int. J. Hydrogen Energy* **2013**, *38*, 9285−9296.
(328) Chen, X.; McCrum, I. T.; Schwarz, K. A.; Janik, M. J.; Koper, M. T. M. Co-adsorption of Cations as the Cause of the Apparent pH Dependence of Hydrogen Adsorption on a Stepped Platinum Single-Crystal Electrode. *Angew. Chem., Int. Ed.* **2017**, *56*, 15025−15029.
(329) Chung, H. T.; Martinez, U.; Matanovic, I.; Kim, Y. S. Cation−Hydroxide−Water Coadsorption Inhibits the Alkaline Hydrogen Oxidation Reaction. *J. Phys. Chem. Lett.* **2016**, *7*, 4464−4469.
(330) McCrum, I. T.; Janik, M. J. pH and Alkali Cation Effects on the Pt Cyclic Voltammogram Explained Using Density Functional Theory. *J. Phys. Chem. C* **2016**, *120*, 457−471.
(331) Matsumoto, T.; Sadakiyo, M.; Ooi, M. L.; Kitano, S.; Yamamoto, T.; Matsumura, S.; Kato, K.; Takeguchi, T.; Yamauchi, M. CO_2-Free Power Generation on an Iron Group Nanoalloy Catalyst via Selective Oxidation of Ethylene Glycol to Oxalic Acid in Alkaline Media. *Sci. Rep.* **2015**, *4*, 1−6.
(332) Yu, E. H.; Wang, X.; Krewer, U.; Li, L.; Scott, K. Direct oxidation alkaline fuel cells: from materials to systems. *Energy Environ. Sci.* **2012**, *5*, 5668−5680.
(333) Ene, N.; Ileana Ionita, M.; C Zecasin, S. Electrochemical behaviour of dimethyl ether in alkaline solutions at 298 K. *Revue Roumaine de Chimie* **2006**, *51*, 293−297.
(334) Verma, A.; Basu, S. Direct Alcohol and Borohydride Alkaline Fuel Cells. In *Recent Trends in Fuel Cell Science and Technology*; Basu, S., Ed.; Springer: New York, NY, 2007; pp 157−187.
(335) Adli, N. M.; Zhang, H.; Mukherjee, S.; Wu, G. Review—Ammonia Oxidation Electrocatalysis for Hydrogen Generation and Fuel Cells. *J. Electrochem. Soc.* **2018**, *165*, J3130−J3147.
(336) Serov, A.; Kwak, C. Direct hydrazine fuel cells: A review. *Appl. Catal., B* **2010**, *98*, 1−9.
(337) Rees, N. V.; Compton, R. G. Carbon-free energy: a review of ammonia- and hydrazine-based electrochemical fuel cells. *Energy Environ. Sci.* **2011**, *4*, 1255−1260.
(338) Tanaka, H.; Asazawa, K.; Sakamoto, T. Automotive Applications of Alkaline Membrane Fuel Cells. In *Non-Noble Metal Fuel Cell Catalysts*; Wiley-VCH: 2014; pp 389−422.
(339) Asazawa, K.; Yamada, K.; Tanaka, H.; Oka, A.; Taniguchi, M.; Kobayashi, T. A Platinum-Free Zero-Carbon-Emission Easy Fuelling Direct Hydrazine Fuel Cell for Vehicles. *Angew. Chem., Int. Ed.* **2007**, *46*, 8024−8027.
(340) Sanabria-Chinchilla, J.; Asazawa, K.; Sakamoto, T.; Yamada, K.; Tanaka, H.; Strasser, P. Noble Metal-Free Hydrazine Fuel Cell Catalysts: EPOC Effect in Competing Chemical and Electrochemical Reaction Pathways. *J. Am. Chem. Soc.* **2011**, *133*, 5425−5431.
(341) Álvarez-Ruiz, B.; Gómez, R.; Orts, J. M.; Feliu, J. M. Role of the Metal and Surface Structure in the Electro-oxidation of Hydrazine in Acidic Media. *J. Electrochem. Soc.* **2002**, *149*, D35−D45.
(342) Aldous, L.; Compton, R. G. The mechanism of hydrazine electro-oxidation revealed by platinum microelectrodes: role of residual oxides. *Phys. Chem. Chem. Phys.* **2011**, *13*, 5279−5287.
(343) Rosca, V.; Koper, M. T. M. Electrocatalytic oxidation of hydrazine on platinum electrodes in alkaline solutions. *Electrochim. Acta* **2008**, *53*, 5199−5205.
(344) Asazawa, K.; Yamada, K.; Tanaka, H.; Taniguchi, M.; Oguro, K. Electrochemical oxidation of hydrazine and its derivatives on the surface of metal electrodes in alkaline media. *J. Power Sources* **2009**, *191*, 362−365.
(345) Dantas, L. M. F.; Reis, A. P. d.; Tanaka, S. M. C. N.; Zagal, J. H.; Chen, Y.-Y.; Tanaka, A. A. Electrocatalytic oxidation of hydrazine in alkaline media promoted by iron tetrapyridinoporphyrazine adsorbed on graphite surface. *J. Braz. Chem. Soc.* **2008**, *19*, 720−726.
(346) Yamazaki, S.-i.; Ioroi, T.; Tanimoto, K.; Yasuda, K.; Asazawa, K.; Yamaguchi, S.; Tanaka, H. Electrochemical oxidation of hydrazine derivatives by carbon-supported metalloporphyrins. *J. Power Sources* **2012**, *204*, 79−84.
(347) Sakamoto, T.; Asazawa, K.; Martinez, U.; Halevi, B.; Suzuki, T.; Arai, S.; Matsumura, D.; Nishihata, Y.; Atanassov, P.; Tanaka, H. Electrooxidation of hydrazine hydrate using Ni−La catalyst for anion exchange membrane fuel cells. *J. Power Sources* **2013**, *234*, 252−259.
(348) Karim-Nezhad, G.; Jafarloo, R.; Dorraji, P. S. Copper (hydr)oxide modified copper electrode for electrocatalytic oxidation of hydrazine in alkaline media. *Electrochim. Acta* **2009**, *54*, 5721−5726.
(349) Yamada, K.; Yasuda, K.; Fujiwara, N.; Siroma, Z.; Tanaka, H.; Miyazaki, Y.; Kobayashi, T. Potential application of anion-exchange membrane for hydrazine fuel cell electrolyte. *Electrochem. Commun.* **2003**, *5*, 892−896.
(350) Yin, W. X.; Li, Z. P.; Zhu, J. K.; Qin, H. Y. Effects of NaOH addition on performance of the direct hydrazine fuel cell. *J. Power Sources* **2008**, *182*, 520−523.

DOI: 10.1021/acs.chemrev.9b00157
Chem. Rev. XXXX, XXX, XXX−XXX